Integrierte Strömungs-berechnungen im Rahmen des EU-Projekts NURISP

Abschlussbericht

GRS - A - 3678

Gesellschaft für Anlagen- und Reaktorsicherheit (GRS) mbH

Abschlussbericht/
Final Report

Reaktorsicherheitsforschung-Vorhabens Nr.:/
Reactor Safety Research-Project No.:
RS1188

Vorhabenstitel / Project Title:

Integrierte Strömungsberechnungen im Rahmen des EU-Projekts NURISP

Integration of simulation tools into the NURESIM platform in order to perform coupled, multi-scalar calculations in nuclear reactors

Autor / Authors:
M.Scheuerer

Berichtszeitraum / Publication Date:
Juli 2012

Anmerkung:
Das diesem Bericht zugrunde liegende F&E-Vorhaben wurde im Auftrag des Bundesministeriums für Wirtschaft und Technologie (BMWi) unter dem Kennzeichen RS1188 durchgeführt.

GRS – A – 3678

Kurzfassung

Im Rahmen der Reaktorsicherheitsforschung des BMWi, Forschungsschwerpunkt "Transientenanalyse und Unfallabläufe" wurde das Vorhaben RS1188 mit dem Titel „Integrierte Strömungsberechnungen“ durchgeführt. Dieses Vorhaben ist Teilprojekt des EU-Projekts NURISP (Nuclear Reactor Integrated Simulation Project), das im 7. EURATOM-Rahmenprogramm auf Kostenteilungsbasis finanziert wurde. Die Ergebnisse des Projekts sind auf der NURISP-Webseite unter www.nurisp.eu veröffentlicht.

Die GRS beteiligte sich im Rahmen des Vorhabens RS1188 an den NURISP Teilprojekten Thermohydraulik (NURISP-SP2) und Multi-Physik (NURISP-SP3). Im Teilprojekt Thermohydraulik wurden Aufgaben zum Thema "Pressurized Thermal Shock" behandelt, die eine Verbesserung der Simulationsmodelle für den Impuls- und Energieaustausch an freien Oberflächen erfordern. Zu diesem Zweck führte die GRS einen Vergleich von CFD-Rechnungen mit ausgewählten ROSA Experimenten aus dem OECD/NEA Programm durch. Im Teilprojekt Multi-Physik wurde die Implementierung des Systemcode ATHLET in die SALOME- oder NURISP-Plattform vorbereitet. Der Systemcode ATHLET wurde in die SALOME Plattform implementiert und ein Einführungsseminar zur Unterstützung potentieller Anwender gehalten. Zur Kopplung des dreidimensionalen CFD-Programmen ANSYS CFX und des eindimensionalen Systemcode ATHLET wurden Kopplungschnittstellen programmiert und getestet. In einem weitern Schritt wurden gekoppelte ATHLET-CFX Rechnungen für einen ROSA Testfall validiert.

Abstract

The project RS1188 is part of the NURSIP project (Nuclear Reactor Integrated Simulation Project) which was financed in the 7th frame work programme of EURATOM. Its objective was the development of a European reference simulation platform for nuclear reactor applications relevant to reactor safety, operational support and optimal design, using beyond the state-of-the-art methods. The project results are made availabe via internet at www.nurisp.eu

In the framework of RS1188, GRS has participated in the NURISP sub-project "thermal-hydraulics" (NURISP-SP2) and “multi-physics” (NURISP-SP3). In sub-project thermal-hydraulics safety issues such as pressurised thermal shocks (PTS) were investigated. In particular, CFD models were validated which are required for mass, momentum and energy transfer at free surfaces. For this purpose, GRS has selected ROSA experiments from the OECD-NEA programme and performed validation calculations with the CFD code ANSYS CFX. In sub-project "multi-physics" the implementation of the system code ATHLET into the SALOME or NURISP platform was prepared. ATHLET was implemented into the platform and an introductory seminar for potential ATHLET users was organised. A generic interface for the coupling of the system code ATHLET and the CFD code ANSYS CFX was generated and validated with simple test cases. Finally, a coupled simulation of ATHLET and CFX was prepared and tested for selected ROSA experiments.

Inhaltsverzeichnis

1 Einleitung 1

2 Arbeitsprogramm 2

3 Durchgeführte Arbeiten 3

3.1 Thermohydraulik 3

3.2 Multi-Physik Kopplung 5

4 Zusammenfassung und Schlussfolgerung 7

5 Abbildungen 8

6 Referenzen 11

Anhang NURISP - CFD Calculations of OECD/NEA ROSA Test 1-1

NURISP - Two-Phase CFD Simulation of OECD/NEA ROSA Tst 1-1

NURISP - Coupled ATHLET

Verteiler

1 Einleitung

Im Rahmen der Reaktorsicherheitsforschung des Bundesministeriums für Wirtschaft und Technologie (BMWi), Forschungsschwerpunkt "Transientenanalyse und Unfallabläufe" wurde das Vorhaben RS1188 mit dem Titel „Untersuchung von PTS-relevanten Strömungsphänomenen“ durchgeführt. Dieses Vorhaben ist Teilprojekt eines Vorhabens der Europäischen Union auf Kostenteilungsbasis „NURISP, Nuclear Reactor Integrated Simulation Project“ im 7. EURATOM-Rahmenprogramm.

Im integrierten Projekt NURISP waren unter der Führung von Frankreich (CEA, EDF) Partner aus Belgien (UCL), Bulgarien (INRNE), Deutschland (FZR, GRS, Uni-Karlsruhe), England (Imperial College), Finnland (LUT, VTT), Italien (U-Pisa), Niederlande (TU-Delft), Schweden (KTH, Chalmers), Schweiz (PSI), Slowenien (JSI), Spanien (UPM), Tschechien (NRI), und Ungarn (KFKI) beteiligt. Die Vorhaben NURISP und RS1188 begannen am 01.06.2009 und sollten am 31.12.2011 enden. Das EU-Vorhaben NURISP wurde bis 30.06.2012 verlängert. Abweichend davon wurde das BMWi-Vorhaben RS1188 nicht verlängert, es endete am 31.12.2011. Zu den NURISP Teilprojekten sind die EU-Berichte der GRS in der vollständigen Originalversion beigelegt.

2 Arbeitsprogramm

Im Rahmen des Vorhabens NURISP-SP2/RS1188 wurden ausgewählte ROSA Experiment mit den Einzelprogrammen ANSYS CFX und ATHLET berechnet. Die numeriscnen Ergebnisse wurden durch einen Vergleich mit experimentellen Daten validiert. Der Beitrag der GRS und die Ergebnisse der ANSY CFX Rechnungen, sowie der Vergleich mit ausgewählten ROSA V Experimenten sind im Abschnitt 3.1 beschrieben.

Im Teilprojekt NURISP-SP3 wurde der Systemcode ATHLET in die SALOME Plattform implementiert und ein Einführungsseminar zur Unterstützung potentieller Anwender gehalten. Am Beispiel der Kopplung des Systemcodes ATHLET mit dem CFD-Programm ANSYS CFX wurden generische Schnittstellen zur Kopplung von ATHLET und CFX untersucht. Die Kopplung wurde zunächst durch Berechnung einfacher Testfälle validiert. Abschließend wurde eine gekoppelte Simulation von ATHLET und CFX für den einphasigen ersten Teil des ROSA Experiments Test 1-1 vorbereitet und getestet. Die Ergebnisse sind im Abschnitt 3.2 zusammengefasst.

3 Durchgeführte Arbeiten

3.1 Thermohydraulik

Im Teilprojekt NURESIM-SP2 führte die GRS CFD Berechnungen mit dem Programm ANSYS CFX durch. Die ausgewählten Experimente der OECD ROSA V Test 1-1 Versuche behandeln die thermische Stratifizierung während der Notkühleinspeisung in den kalten Strang eines Druckwasserreaktors bei Naturkonvektionsbedingungen. Zur Vermessung der Temperaturverteilung wurden in einem kalten Strang und im Ringraum der Large Scale Test Facility (LSTF)-Anlage zusätzliche Thermoelemente installiert /JAERI, 2003/.

Im ersten Schritt wurde die Einspeisung von kalten ECC-Wasser in die mit heißem Wasser gefüllte Hauptkühlmittelleitung untersucht /JAERI, 2008/. Für die numerische Simulation wurden Rechennetze nach Vorgabe der OECD/NEA Best Practice Guidelines /OECD BPD, 2007/ generiert und numerische Fehler systematisch analysiert. Die transiente Rechnung wurde gestartet, nachdem sich quasi stationäre Naturkonvektion eingestellt hatte. Die gemessenen Temperaturen und Massenströme wurden am Pumpenauslass und an der ECC-Einspeisestellle als Randbedingungen vorgegeben. Der Strömungsaustritt wurde im unteren Teil des Ringraums positionniert. Dort wurde eine Druckrandbedingung vorgegeben. Zur Untersuchung der Diskretisierungsverfahren und der Turbulenzmodelle (Shear Stress Transport und Reynolds Stess Modelle) wurde zunächst ein „halbes“ Rechennetz unter Vorgabe von Symmetriebedingungen entlang der Mittelachse im Ringraum benutzt. Für die endgültigen Rechnungen wurden ein vollständiges Modell des Ringraums mit den kalten Strängen A und B der LSTF Anlage verwendet, siehe Abbildung 1. Die Berechnung der einphasigen ECC-Einspeisung zeigte, dass die thermische Stratifizierung im kalten Strang und im Ringraum in guter Übereinstimmung mit den Messdaten ist. Das deutet darauf hin, dass auftriebsbehaftete, stratifizierte Strömungen mit ANSYS CFX genau berechnet werden können. Wie im Experiment beobachtet, liegt der berechnete Kaltwasserstrahl an der Aussenwand des Ringraums an. In der Nähe der Einspeisestelle wird jedoch die turbulente Vermischung unterschätzt. Eine Verbesserung der Übereinstimmung von Messung und Rechnung erfordert den Einsatz von komplexere Turbulenzmodellen im Bereich des Prallstrahls. Dieser Ansatz wurde in den anschließenden gekoppelten Berechnungen (siehe Abschnitt 3.2) verfolgt. Die

Berechnung des einphasigen ROSA V Testfalls wird ausführlich im EU-Deliverable /Scheuerer 2010/ beschrieben.

Nach der Berechnung des einphasigen ersten Teils des ROSA V Test 1-1 Experiments wurden die experimentellen Daten für den zweiten Teil analysiert, in dem nach 10 Minuten Stabilisierungszeit der Wasserstand auf 80 % des Inventars reduziert wurde. Vor Beginn der Einspeisung in den kalten Strang A, stellte sich eine stationäre Naturkonvektion der Wasser- und Dampfströmung bei Sättigungstemperatur ein (Abbildung 2). Die numerische Geometrie und das numerische Gitter wurden für eine Hälfte des Downcomers mit dem kalten Strang A und dem ECC-Einspeisestutzen modelliert, siehe Abbildung 1. Zur besseren Auflösung der stratifizierten Wasser-Dampfströmung wurde das Rechennetz an der Phasengrenze systematisch verfeinert, um numerische Diffusion zu reduzieren.

Die Berechnung der Wasser-Dampfströmung mit freier Oberfläche und Kondensation wurde mit einem homogenen Zweiphasenmodell durchgeführt, dabei wurden die Massen- und Impulserhaltungsgleichungen für eine Wasser-Dampfmischung berechnet. In den vorliegenden Berechnungen wurde angenommen, dass die Dampfphase isotherm ist und eine konstante Sättigungstemperatur hat. Deshalb wurden nur die Erhaltungsgleichungen für die Enthalpie von Wasser berechnet. Die CFD-Ergebnisse beschreiben in Übereinstimmung mit dem Experiment den Aufprall des Wasserstrahls auf die freie Oberfläche und den Mitriss von Dampfblasen in der Wasserschicht in Richtung Ringraum, siehe Abbildung 3. Die berechneten und gemessenen Temperaturen stimmen gut überein. Unterhalb der Einspeisestelle treten in der CFD-Rechnung jedoch sehr hohe Temperaturschwankungen auf. Da der Rechenauwand auf Grund der sehr kleinen Zeitschritte (0,0005 s bis 0.001 s) sehr hoch war, konnte nur der Beginn der Transienten bis 25 s simuliert werden. Der zweiphasige Testfall mit Kondensation ist im EU-Deliverable /Scheuerer 2012/ dokumentiert.

Weiterhin wurde ein detaillierter LSTF Datensatz für ATHLET erstellt und die komplette Transiente des ROSA V Test 1-1 berechnet. Dies umfasste die Notkühleinspeisung in den kalten Strang A und B bei einem Wasserfüllstand von 100 %, 80 %, 70 % und 50 %. In allen Phase stimmen Rechnungen und Messungen sehr gut überein.

3.2 Multi-Physik Kopplung

Im Teilprojekt NURISP-SP3 wurden Kopplungsverfahren für die in der SALOME Plattform implementierten Programme weiterentwickelt. Dazu gehören sowohl Programme aus dem Bereich der Themohydraulik als auch aus der Neutronenkinetik. Die GRS führte eine Literaturstudie zur Untersuchung von Neutronenkinetik- und Thermohydraulik-Kopplungsmethoden durch und leistete damit einen Beitrag zum EU-Bericht (Zerkak, 2010) über multi-physikalische Kopplungsverfahren und Vorschläge zur Verbesserung im Rahmen des NURISP Projekts.

Zur Kopplung des Thermhydraulk-Programmes ATHLET mit dem CFD-Programm ANSYS CFX wurden verschiedene Kopplungsschemata untersucht. Systemcodes wie ATHLET beruhen auf der Lösung eindimensionaler Modelgleichungen, wodurch die Möglichkeiten eingeschränkt sind, dreidimensionale Strömungs- und Vermischungs-vorgänge abzubilden, die für bestimmte Transienten und Störfallszenarien wichtig sind. Eine direkte Kopplung des eindimensional Systemcodes ATHLET mit dem dreidimen-sionalen CFD-Programm ANSYS CFX ermöglicht es, in ausgewählten Bereichen den Strömungs- und Wärmetransport dreidimensional abzubilden, während transiente Randbedingungen aus dem Systemberechnungen mit ATHLET direkt an das CFD-Programm in der laufenden Simulation übergeben werden. Durch diese Vorgehensweise kann der Rechenaufwand für de CFD-Verfahren reduziert werden, während gleichzeitig das Systemverhalten des Reaktors realistischer widergegeben wird. Deshalb wurden bei der GRS explizite und semi-explizite Verfahren zur Kopplung des Systemprogrammes ATHLET und des dreidimensionalen CFD-Programmes ANSYS CFX entwickelt.

Im Rahmen des NURISP-Projekts wurde das gekoppelte 1D-3D Codesystem ATHLET – ANSYS CFX weiterentwickelt und validiert. Als Demonstrationstestfall wurde das OECD ROSA V Test 1-1 Experiment mit dem gekoppelten Verfahren berechnet. Dafür wurde ein Teil des kalten Stranges A der Large Scale Test Facility als dreidimensionales Model mit Hilfe von ANSYS Workbench für die ANSYS CFX Berechnung dargestellt, siehe Abbildung 4. Die gekoppelte 1D-3D Simulationen wurden mit unterschiedlichen Turbulenzmodellen durchgeführt. Der ROSA Versuch 1-1 wurde sowohl mit Hilfe von Zwei-Gleichungs-Turbulenzmodellen (SST) als auch mit dem komplexeren Reynolds Spannungs- Turbulenzmodellen (BSL) nachgerechnet. Der Vergleich mit den Ergebnissen der stand-alone Programmen ATHLET und ANSYS CFX zeigte, dass die Ergebnisse sehr gut übereinstimmen /Papukchiev 2011/. Somit

konnte gezeigt werden, dass mit dem gekoppelten ATHLET-CFX nicht nur akademische Testfälle mit vereinfachten Geometrien sondern auch reale Versuchsanlagen simuliert werden können. Die gekoppelten Simulationen zu dem ROSA Versuch 1-1 für die einphasige Einspeisung in den kalten Strang A wurden dokumentiert und veröffentlicht /Papukchiev 2012/.

Schließlich wurde das ATHLET-Programm in die SALOME Plattform implementiert. ATHLET benutzt das SALOME Startmenue, und die ATHLET-Ergebniss können mit dem Postprocessing-Werkzeug von SALOME dargestellt werden. Es wurde ein Treiberprogramm erstellt, das das CFX-Programm nachahmt, indem es ATHLET aufruft, Zeitschrittweiten vorgibt, die Kopplungsfelder mit zeitlich sich ändernden Werten versorgt und die Rechnung abbricht. Dieses vereinfachte, gekoppelte System wurde erfolgreich als Black-Box in die SALOME-Plattform integriert. Das verwendete Simulationsbeispiel bestand aus einem Branch als „time dependent volume“, einem Pipe und einem weiteren Branch. Damit wurde die Ablauffähikeit des vereinfachten, gekoppelten Systems in der SALOME-Plattform demonstriert. Weiterhin wurde bei der GRS in Garching ein ATHLET-Seminar für die Teilnehmer des NURISP Projekts organisiert. Es nahmen 7 Telnehmer aus den Forschungszentren Karlsruhe (KIT), Rossendorf (HZDR), Atomenergie Ungarn (AEKI) und den Universitäten in Pisa und München (TUM/NTECH) teil.

4 Zusammenfassung und Schlussfolgerung

Im Rahmen des EU-Projekts NURISP wurden von der GRS Beiträge zu den Teilprojekten NURISP-SP2 und NURISP-SP3 geleistet. Im Teilprojekt NURISP-SP2 wurden PTS-relevante Strömungsphänome untersucht. Die GRS führte Rechnungen von ausgewählten OECD/ROSA V Experimenten durch. Mit einem detaillierten ATHLET Datensatz wurde die komplette Transiente des ROSA V Test 1-1 (100 % - 50 % Wasserfüllstand) berechnet. Dann wurden wurden mit ANSYS CFX Rechnungen durchgeführt, die die kaltseitige Notkühleinspeisung bei Naturkonvektion sowohl in der vollständig mit Wasser gefüllten, als auch in der mit 20 % Dampf gefüllten Hauptkühlmittelleitung simulierten. Der Vergleich lokaler, transienter Temperatur-verteilungen aus Rechnungen und Messungen zeigte gute Übereinstimmung, mit Ausnahme der Temperaturwerte unmittelbar an der Einspeisestelle.

Im Teilprojekt NURISP-SP3 wurde die Kopplung von ATHLET und ANSYS CFX weiterentwickelt und validiert. Als Demonstrationstestfall wurde das OECD ROSA V Test 1-1 Experiment bei einphasiger Notkühleinspeisung und Naturkonvektion mit dem gekoppelten Verfahren berechnet. Die gekoppelten Simulationen und die Ergebnisse der stand-alone Rechnung stimmen überein, womit gezeigt wurde, dass mit dem gekoppelte Verfahren auch reale Versuchsanlagen berechnet werden können.

Weiterhin wurde ATHLET in die SALOME Plattform implementiert und erste einfache Verifikationstest durchgeführt. In einem ATHLET Seminar bei der GRS wurden potentielle Nutzer im NURISP Projekt geschult.

5 Abbildungen

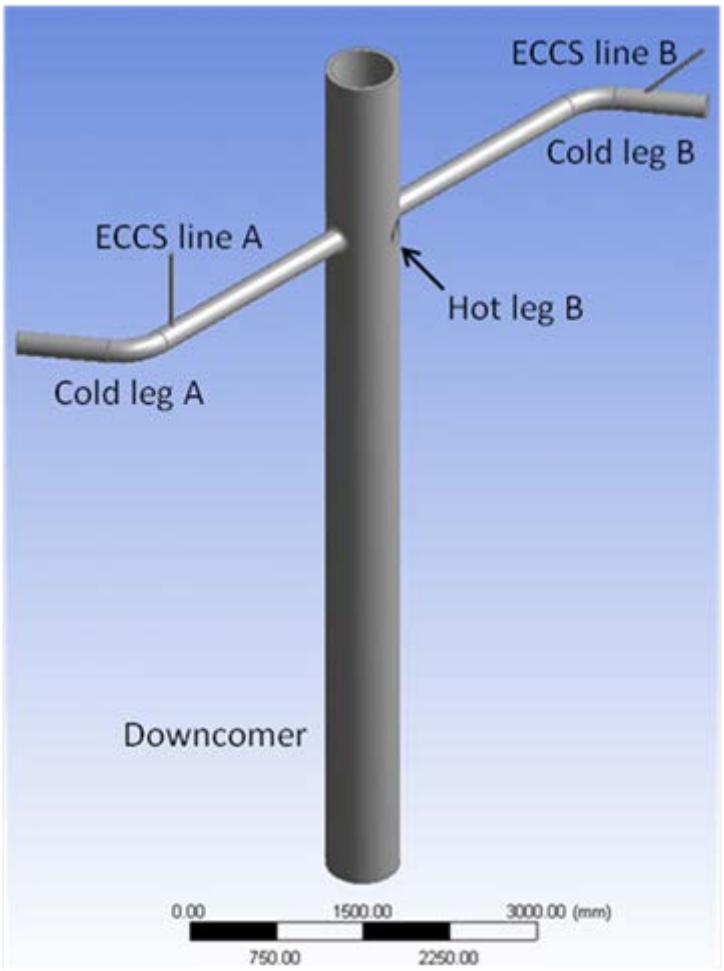

Abbildung 1: Geometrie LSTF Modell

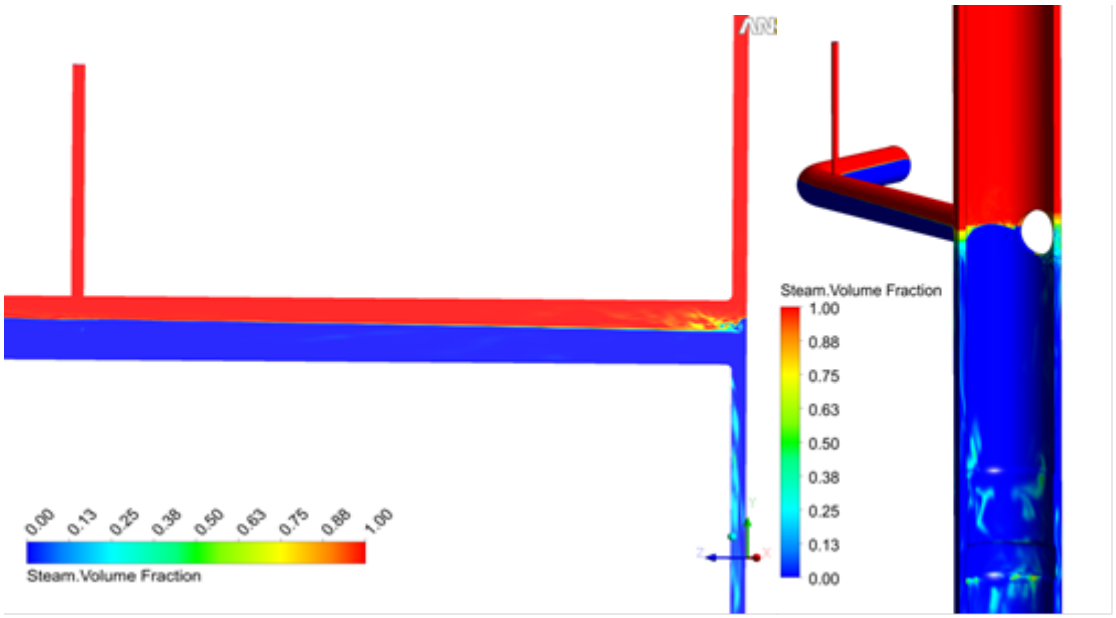

Abbildung 2: Anfangsbedingung ROSA Test 1-1 Wasser/Dampf-Naturkonvektion (Ansicht links: Mittlere Ebene & Ansicht rechts: Ringraum Innenwand)

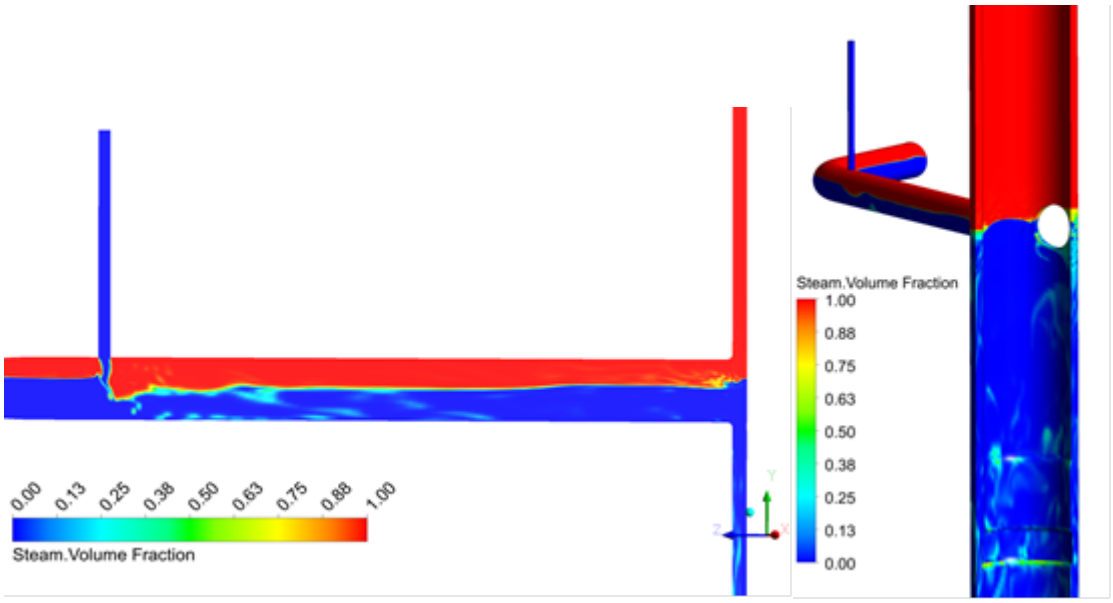

Abbildung 3: ECC-Einspeisung ROSA Test 1-1 Wasser/Dampf-Verteilung (Ansicht links: Mittlere Ebene & Ansicht rechts: Ringraum Innenwand)

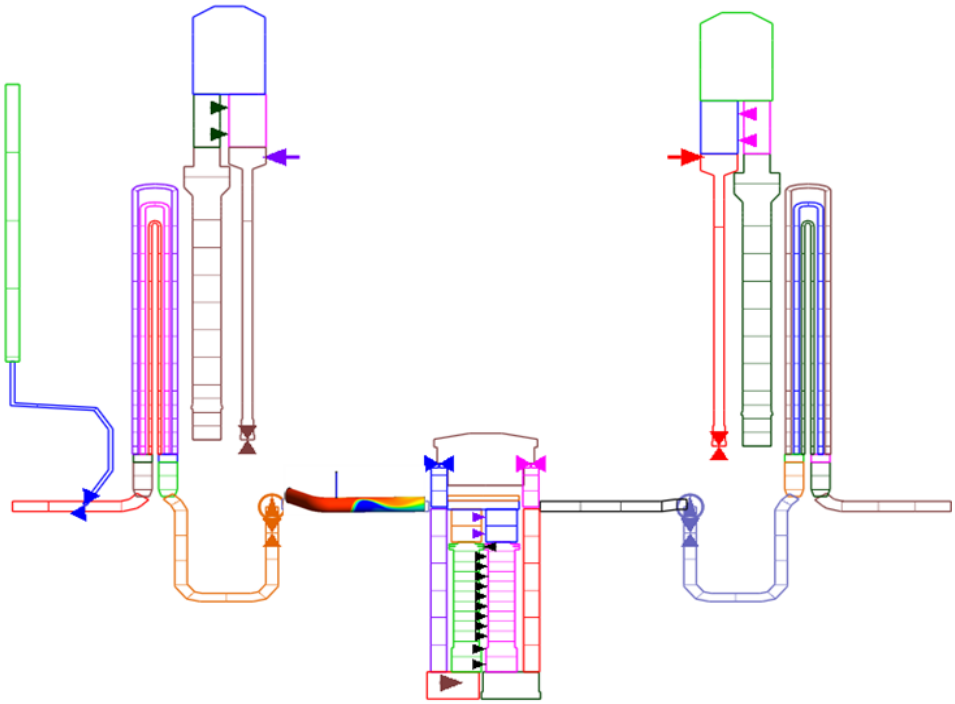

Abbildung 4: ATHLET – ANSYS CFX model of the LSTF RPV and loop A

6 Referenzen

Papukchiev, A., Lerchl, G., Scheuerer, M., „Coupled ATHLET – ANSYS CFX Calculations of the OECD/NEA Large Scale Test Facility ROSA V Test 1-1", NURISP report, EC-Deliverable NURISP D3.3.1.3 (2011)

Papukchiev, A., Lerchl, G., Weis, J., Scheuerer, M., „Multiscale Analysis of a Transient Pressurized Thermal Shock Experiment with the Coupled Code ATHLET- ANSYS CFX", International Journal for Nuclear Power – atw 6 (2012)

JAERI, "ROSA V Large Scale Test Facility (LSTF) System Description for the Third and Fourth Simulated Fuel Assemblies", Tokai Research Establishment, Japan Atomic Energy Research Institute (2003)

JAERI, "Final Data Report of OECD/NEA ROSA Project Test 1-1", Thermohydraulic Safety Research Group, Nuclear Safety Research Centre, Japan Atomic Energy Agency (2008)

Scheuerer, M., Weiss, J., "CFD Calculations of OECD/NEA ROSA Test 1-1", NURISP report, EC-Deliverable NURISP D2.1.2.4a (2010)

Scheuerer, M., "Two-Phase CFD Simulation of OECD/NEA ROSA Test 1-1", NURISP report, EC-Deliverable NURISP D2.1.2.4b (2012)

Zerkak, O., Manera, A., Gajev, I., Kozlowski, T., "Review of Multi-physics coupling techniques and suggestions of improvements in the context of NURISP", EC-Deliverable NURISP D3.2.1.1 (2010)

ANHANG

EUROPEAN COMMISSION

Community Research

EURATOM

NURISP

NUclear Reactor Integrated Simulation Project

Collaborative Project (Large – scale Integrating Project)

Seventh Framework Programme EURATOM

Contract Number: 232124

Start date: 01/01/2009 Duration: 36 Months

CFD Calculations of OECD/NEA ROSA Test 1-1

M. Scheuerer, J. Weis (GRS, Germany)

NURISP – Contract Number: 232124

NUclear Reactor Integrated Simulation Project

Document title	***CFD Simulation of OECD/NEA ROSA***
Author(s)	Martina Scheuerer, Johannes Weiss
Number of pages	31
Document type	Deliverable
Work Package	WPs-w
Document number	D 2.1.2.4a
Issued by	Gesellschaft für Anlagen- und Reaktorsicherheit mbH (GRS)
Date of completion	17/08/2010
Dissemination level	Public

Summary

This deliverable documents the CFD results obtained for the proposed validation experiment ROSA V Test 1-1. The test series was performed within the OECD ROSA V project in the Large Scale Test Facility LSTF. The test rig is a 1:48 volume scaled model of a four loop Westinghouse pressurized water reactor. The ROSA V test T1-1 investigates the temperature stratification under natural circulation conditions. Its main purpose is the validation of three dimensional CFD calculations. The experiments were performed in several steps. They started with emergency core cooling (ECC) injections into the cold legs at 15.5 MPa at 100 % primary inventory with a core power corresponding to 2 % of the scaled nominal power. In the next steps, after 10 minute intervals for re-stabilization, the water level was reduced to 80 %, 70 % and 50 % of the inventory. Multidimensional temperature distributions were measured by rakes of thermocouples in the cold legs located in three cross-sectional planes between injection nozzle and downcomer, containing 9 and 21 thermocouples, respectively. Below each cold leg, 18 thermocouples were installed.
The ANSYS CFD calculations were performed for single phase flow injection into loop A. Following the OECD/NEA Best Practice Guidelines for the use of in Nuclear Reactor Safety Applications (OECD BPG, 2007), three structured, hexahedral grids were generated. The coarse grid had 500 000 elements. The grids were scalable with a minimum grid angle of 32 degrees. Iteration and the discretisation errors in time and space were checked on each grid. The transient calculations were started from a steady-state solution of the natural circulation. At the pump positions and at the ECC line A, the measured mass flow rates and the measured temperature at the ECC-nozzle was used as inlet boundary condition. At the outlet, which was positioned at the lower part of the downcomer, a pressure boundary condition was prescribed. A number of calculations were performed applying symmetry boundary conditions in the downcomer. This half-model was used for checking the influence of the discretisation schemes and turbulence models (Shear Stress Transport and Reynolds Stress Model). The final transient calculations were obtained in a complete model of the downcomer with cold legs A and B of the LSTF facility. They are in good agreement with data.

Approval

Rev.	Date	First author	WP leader	SP or Project Coordinator
0	08/2010	M. Scheuerer, GRS 17/08/2010	D. Lucas FZD 23/08/2010	D. Bestion (CEA 23/08/2010

Distribution list

Name	Organisation	Comments
Michel HUGON	EC DG RTD	
All beneficiaries	NURISP	Through NIWS

Table of contents

1 Introduction 5
2 ROSA V EXPERIMENT 5
2.1 Upgrades for ROSA Test 1-1 10
2.2 Experimental Conditions and Procedures 14
2.3 ROSA V Test 1-1 14
3 CFD ANALYSIS 19
3.1 Geometry Generation 19
3.2 Grid Generation 20
3.2.1 Coarse Grid 21
3.2.2 Medium Grid 22
3.2.3 Fine Grid 23
3.3 Mathematical Models 23
3.4 Initial and Boundary Conditions 23
3.5 Numerical and Model Errors 24
3.6 Results and Comparison to Data 26
4 Conclusion 29
5 References 30
6 Annexes 31
6.1 Annex 1: Document approval by beneficiaries' internal QA 31

List of Figures:

Figure 1: Large Scale Test Facility and scheme of a W-type PWR 6
Figure 2: Primary Loop Dimensions (Plan View) 8
Figure 3: Comparison of PWR and LSTF pressure vessel dimension 9
Figure 4: Location of new thermocouples in cold legs and downcomer 10
Figure 5: Locations of new thermocouples in cold leg A 11
Figure 6: Thermocouples of group TE1 and ECC nozzle 11
Figure 7: Locations of new thermocouples of group TE2 and TE3 in CLA 12
Figure 8: Thermocouples in spool piece flange 12
Figure 9: Locations of thermocouples in downcomer 13
Figure 10: Frame structure of thermocouples of group TE4 and downcomer view from cold leg 13
Figure 11: Loop flow rates 15
Figure 12: Temperatures of the natural circulation and the ECC injection water 15
Figure 13: CLA temperature TE1A1 ~ TE1A3 (TE1174 ~ TE1176) 16
Figure 14: CLA temperature TE2A1 ~ TE2A7 (TE1177 ~ TE1183) 17
Figure 15: CLA temperature TE3A1 ~ TE3A7 (TE1198 ~ TE1204) 17
Figure 16: Downcomer temperature TE4A11 ~ TE4A23 (TE1219 ~ TE1224) 18
Figure 17: Geometry model and dimensions 19
Figure 18: Computational grids close to inlet of main pipe 20
Figure 19: Detailed pictures of the coarse mesh: ECC line attachment and CLA 21
Figure 20: Detailed pictures of the coarse mesh in the downcomer 22
Figure 21: Temperature as function of convergence criterion 25
Figure 22: Influence of spatial discretisation (TE1215) 25
Figure 23: Influence of discretisation scheme (TE1205) 25
Figure 24: Influence of initial time step size (TE1205) 26
Figure 25: Influence of turbulence model 26
Figure 26: Temperature stratification in Cold Leg A @ 80 s 27
Figure 27: Comparison of simulation and data in the downcomer (TE1225, TE1227) 27
Figure 28: Comparison of simulation and data in Cold Leg A (TE1187) 28
Figure 29: Comparison of simulations and data in Cold Leg A (TE1208) 28

List of Tables:

Table 1: Initial conditions of the ROSA project Test 1-1 14
Table 2: Chronology of major operations 14
Table 3: Summary of model dimensions 20
Table 4: Summary of numerical grids 23

1 Introduction

The focus of the NURISP thermo-hydraulic sub-project is on the investigation of Pressurized Thermal Shock (PTS) scenario. Pressurized thermal shocks are severely limiting the Reactor Pressure Vessel (RPV) life time. They occur when cold ECC-water is injected into the cold leg during a Loss of Coolant Accident (LOCA). The cold water jet mixes with the hot water in the cold leg and flows towards the downcomer where further mixing with the ambient fluid takes place. Thermal stratification may cause high thermal gradients in the structural components while the primary circuit pressurization is partially preserved. Therefore, the local fluid temperature must reliably be assessed to predict the thermal loads upon the RPV wall. The cold leg can either be in single-phase or in two-phase condition, depending on the leak size, its location, and on the operating conditions of the considered Nuclear Power Plant.

Because of their importance, PTS effects have been studied experimentally and numerically. The available investigations can be subdivided into separate-effect studies and combined-effect studies. The separate-effect studies deal only with a single aspect of PTS, like free surface flow or generic condensation (Scheuerer, 2002). The combined-effect studies are performed in realistic reactor configurations, and examine the interaction of all relevant effects. Because of their complexity and cost, only few data are available.

Combined-effect PTS data have been collected in the Upper Plenum Test Facility (UPTF). UPTF is a 1:1 model of a 1300 MWe Siemens/KWU PWR. In the UPTF Test 1, ECC injection into stagnant hot water at small-break LOCA conditions was investigated. The CFD simulation by Willemsen and Komen (2005) showed that buoyancy production terms have to be included in the applied eddy turbulence models in order to achieve a good representation of the temperature stratification in the cold leg.

The influence of density differences on the mixing of the primary loop inventory and ECC water in a PWR was analyzed at the Rossendorf Coolant Mixing (ROCOM) test facility. ROCOM is a 1:5-scaled model of a German PWR. It is equipped with instrumentation, which delivers high-resolution information for concentration fields. Experimental and numerical investigations by Höhne et al. (2005) show that buoyancy dominates slug propagation. ECC water reaching the downcomer flows in an almost vertical path and reaches the lower downcomer sensor directly below the inlet nozzle.

The ROSA V experiments which were performed in the Large Scale Test Facility LSTF (JAERI, 2003) belong also to the combined-effect category. In the ROSA V experiments, the three-dimensional temperature field was measured in the cold leg and downcomer under realistic reactor conditions. The test series performed within the OECD ROSA V project was selected as one of the validation cases in the NURISP project because of its detailed temperature data. In this paper, CFD simulations and data for the ROSA V Test 1-1 are compared and assessed. As the experimental data is proprietary, absolute temperature values can not be provided.

2 ROSA V EXPERIMENT

The Large Scale Test Facility (LSTF) was designed to simulate thermal-hydraulic phenomena which occur during to SBLOCAs and operational transients by having prototypical component elevation differences, large loop piping diameters, prototypical primary pressure levels, simulated system controls, and core power level

sufficient to simulate the core power decay starting from a few seconds after SCRAM (JAERI , 1985). The reference reactor for the LSTF is Tsungura-2, a 3423 MW_{th} (1100 MW_e) 4 loop Westinghouse-type pressurized water reactor. In Figure 1, there is a picture of the LSTF on the left side and in comparison a scheme of a W-type PWR to the right.

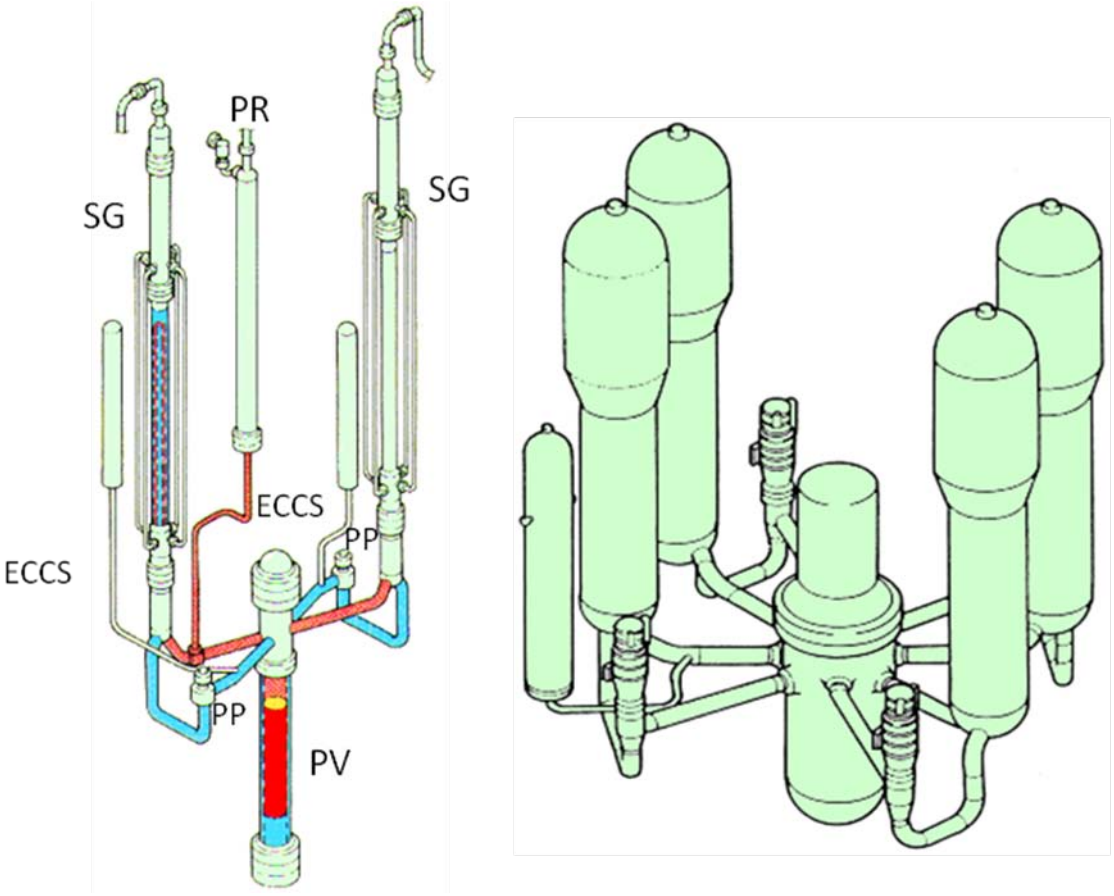

Figure 1: Large Scale Test Facility and scheme of a W-type PWR

The LSTF was constructed with two loops, including the steam generators (SG), the primary coolant pumps (PP), one hot and one cold leg in each loop. These two loops are nearly identical; the only difference is the attachment of the ECC line to the cold legs. In loop A, the ECC line is perpendicularly attached to the cold leg. This is related to the design in Russian PWRs. On the other side (loop side B) the ECC line is attached with an angle of 45° in the flow direction in the cold leg, which is similar to the design in European and American PWRs.

The LSTF is volumes scaled at 1/48 of its reference reactor, but it has the same heights which is about 30m. The pressure level which can be reached is also the same, about 16 MPa, and the pressure vessel is equipped with 1008 electrical heater rods with a thermal power of 10 MW. Approximately 2500 instruments are implemented in the LSTF to measure the different properties (Yonomoto, 2005).

Figure 2 shows the plan view of the pressure vessel and the two loops. In cold leg A (CLA) the coolant flows after the primary pumps (PP) through an elbow part before the straight part of the cold leg A is attached to the pressure vessel and the downcomer. The length and the diameter of the cold leg are the same in cold leg A and B. In cold leg

A, the ECC line is located behind the elbow part and is connected perpendicular to the cold leg, as already explained. In the B loop the ECC line is located between the primary pumps and the elbow junction. The location of the ECC line has an influence on the mixing behavior of the cold fluid and the hot water in the cold leg, as well as the difference in the connection angle.

Figure 3 shows a comparison between the dimensions of the pressure vessels of a real PWR and the LSTF. The heights of the pressure vessels are comparable (PWR: ~12.5m; LSTF: ~11m) and also the hot and cold legs are attached on the same heights level. However, the diameter of the LSTF pressure vessel is much smaller (inner diameter PWR: 4.4m; inner diameter LSTF: 0.6m), which lead to the ratio of 1/48 in volumetric scaling between the LSTF and its reference reactor.

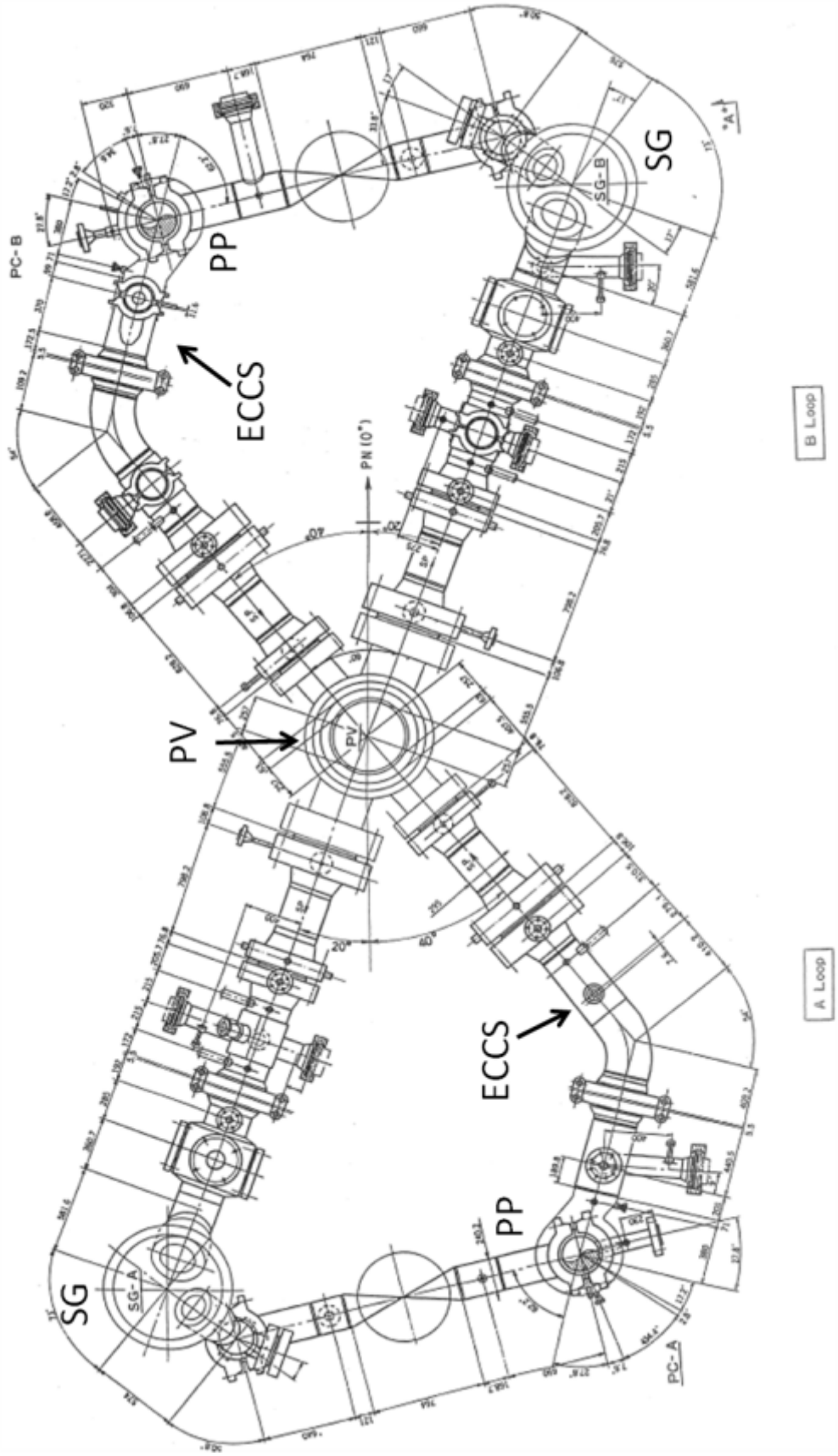

Figure 2: Primary Loop Dimensions (Plan View)

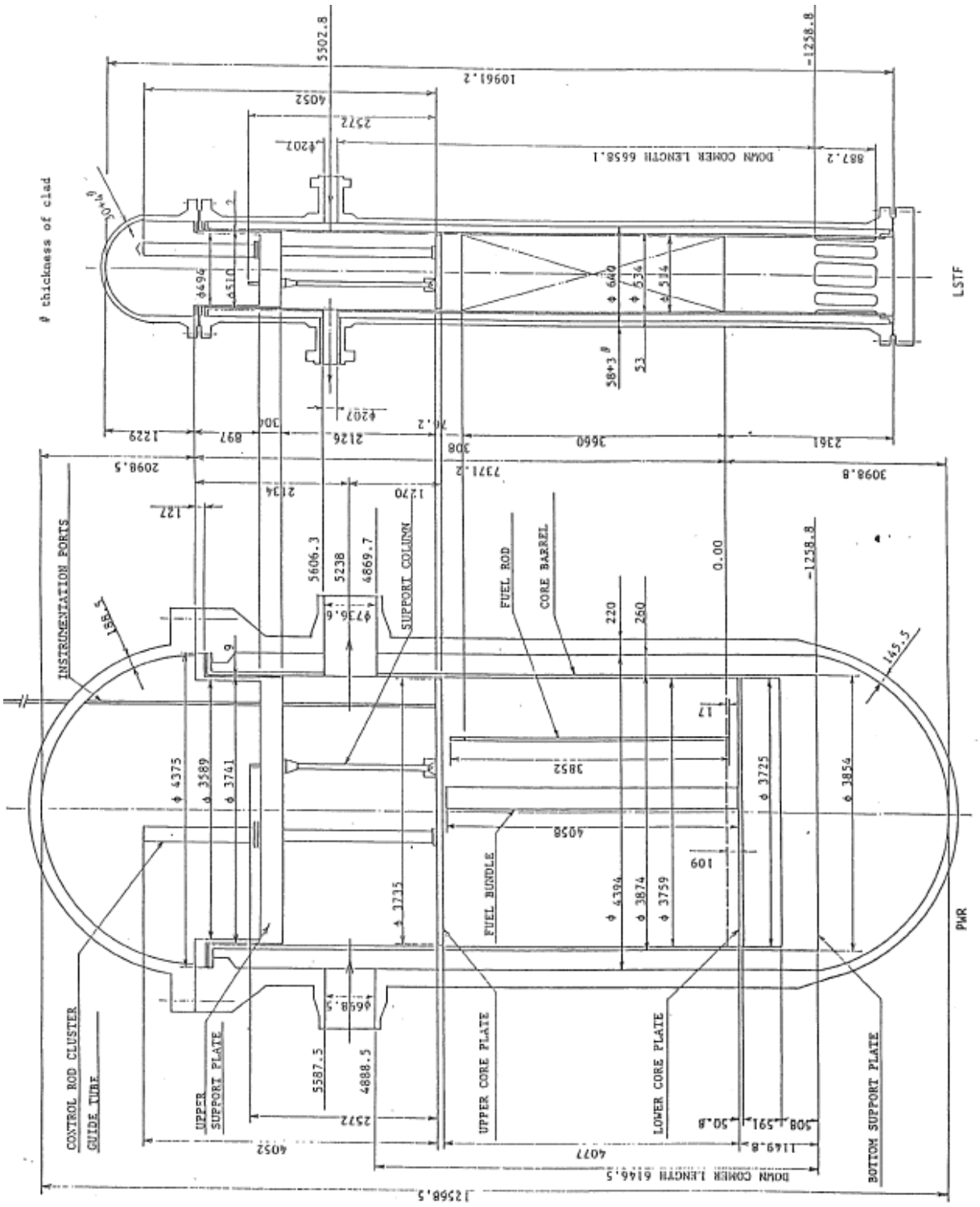

Figure 3: Comparison of PWR and LSTF pressure vessel dimension

2.1 Upgrades for ROSA Test 1-1

On October 26 and 27, 2006 the OECD/NEA ROSA Project Test 1-1 was conducted in the LSTF. The objective of this test was to obtain the multidimensional temperature distributions in cold legs and downcomer during ECC water injection for validation of computer codes and models (OECD/NEA 2008). To measure the stratified flow in the cold legs, the equipment of the LSTF had to be upgraded. The locations of the 144 new thermocouples, which were installed for this test, are explained in Figure 4:

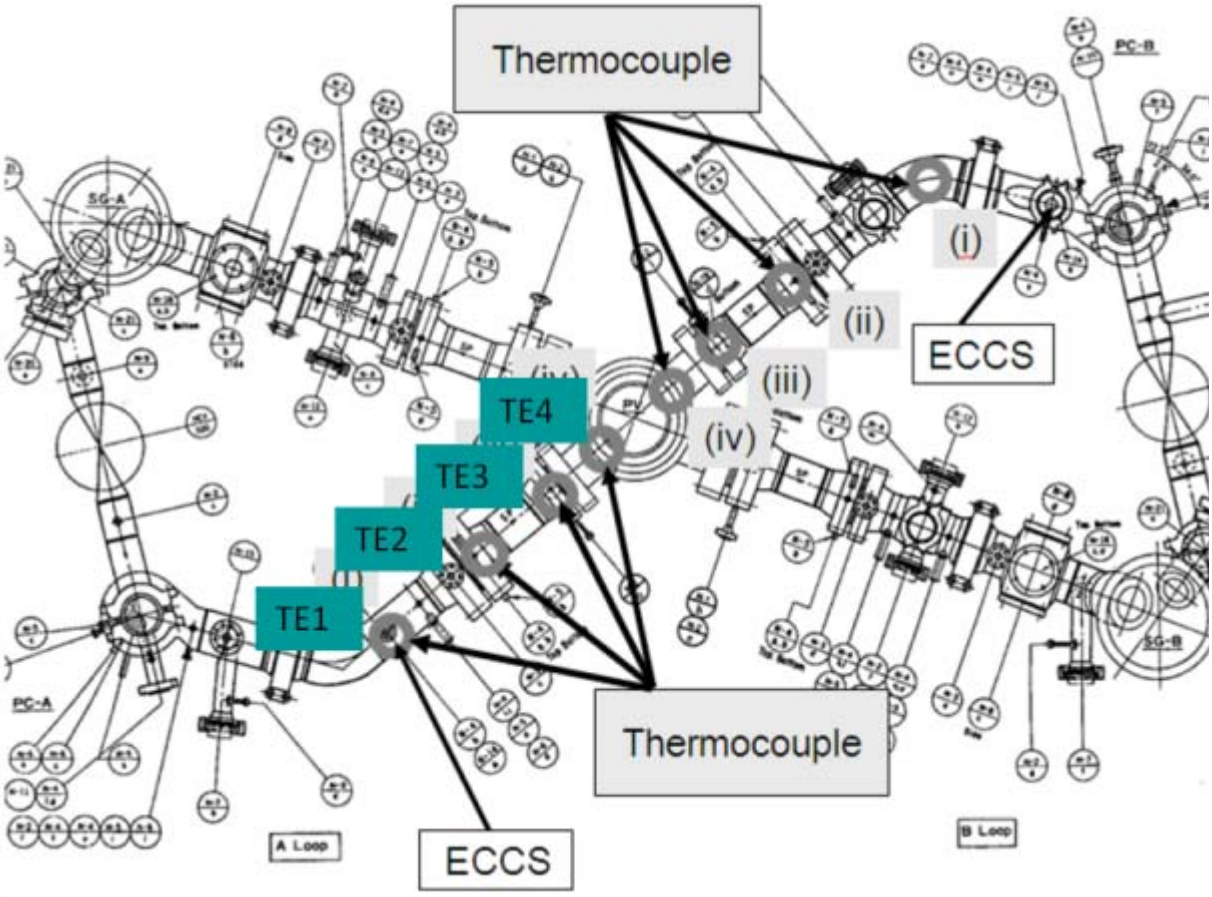

Figure 4: Location of new thermocouples in cold legs and downcomer

The newly installed thermocouples have an uncertainty of +/- 2.75 K and a range between 270 K and 720 K. There are 3 positions in cold leg A where a group of thermocouples is placed. The first group, which is called TE1, consists of 3 thermocouples which are located in the vertical center axis in the cross section perpendicular to the flow direction, see Figure 5:

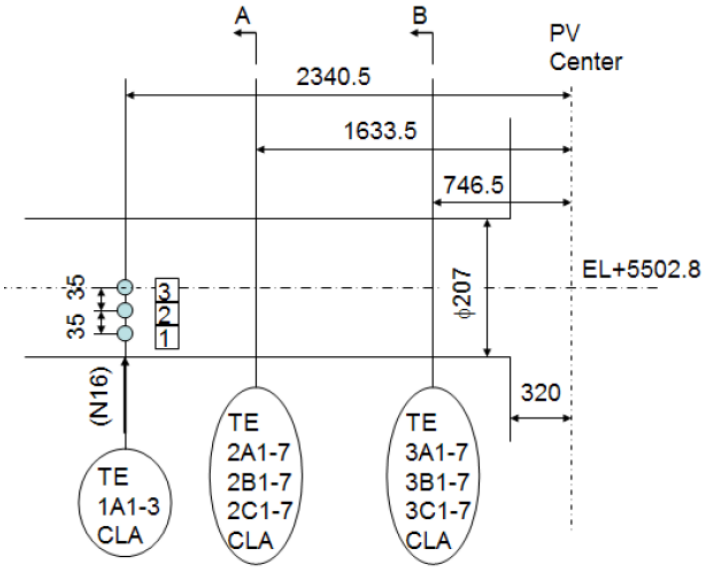

Figure 5: Locations of new thermocouples in cold leg A

It is located under the injection point of the ECC line which center is placed in a distance of 2329 mm to the center of the pressure vessel. The picture in Figure 6 shows the installed thermocouples of group TE1 in the cold leg and also the ECC nozzle is in evidence. The support rod for the TE1 thermocouples is 8 mm in diameter inserted from the bottom to the center of the cold leg A.

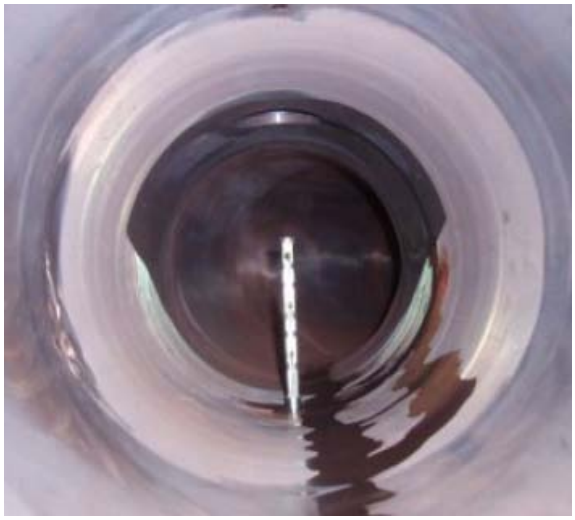

Figure 6: Thermocouples of group TE1 and ECC nozzle

The measuring points of group TE2 and group TE3 are located further downstream (TE2: 0.7m; TE3:1.6m, downstream of the ECC nozzle) in the cold leg and consist of 21 thermocouples each. The cross section A and B of Figure 5 is shown in Figure 7:

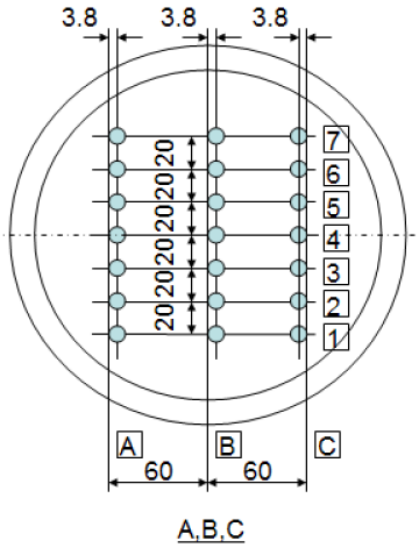

Figure 7: Locations of new thermocouples of group TE2 and TE3 in CLA

The thermocouples are distributed in three columns and seven rows and were placed at the ends of a spool piece flange which is shown in Figure 8:

Figure 8: Thermocouples in spool piece flange

The support rods for the thermocouples of group TE2 and TE3 are 6 mm x 13 mm in cross section inserted from the bottom to the top of the cold leg, and the 6mm side is faced to the main flow direction.
The thermocouples of group TE4 were installed in the downcomer. They consist of 18 thermocouples which are arranged as explained in Figure 9:

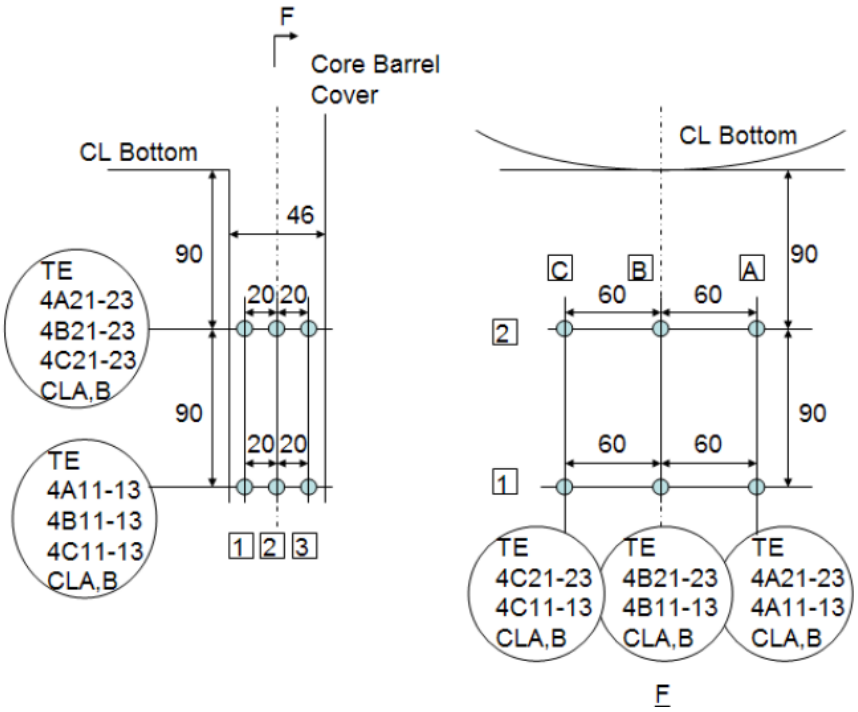

Figure 9: Locations of thermocouples in downcomer

The support rods of group TE4 are also 6mm x 13 mm in cross section, and fixed at the bottom of the cold leg as shown in the right part of Figure 10. The left side of Figure 10 shows the frame structure which was used to arrange the thermocouples of group TE4 and which was installed in the downcomer through the cold leg.

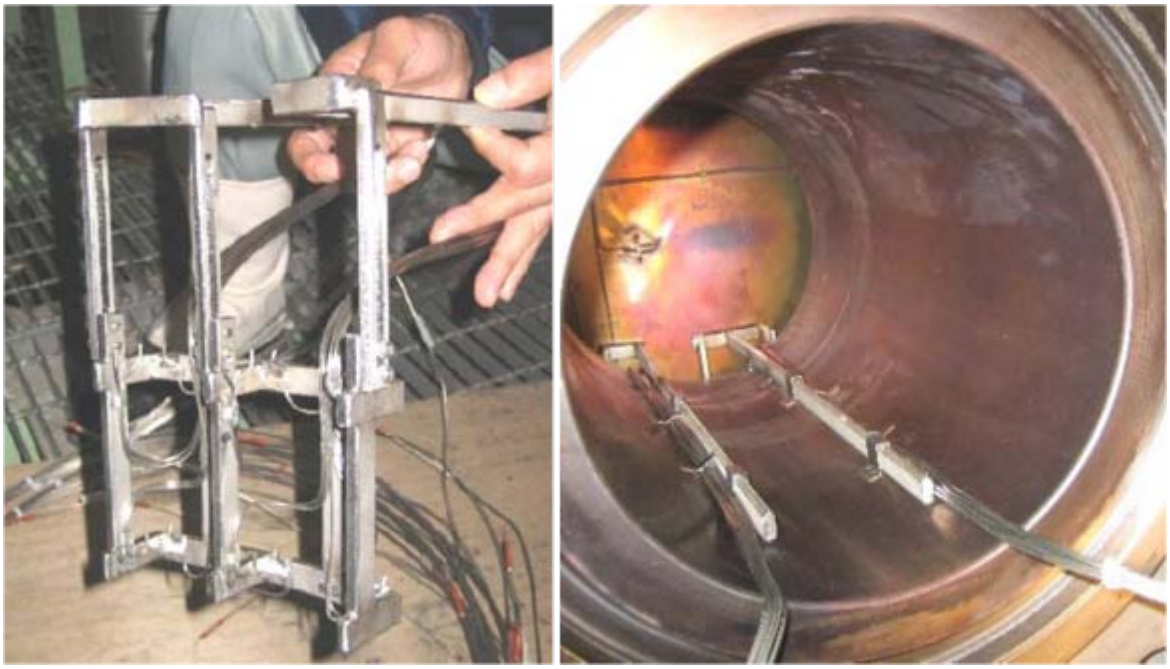

Figure 10: Frame structure of thermocouples of group TE4 and downcomer view from cold leg

2.2 Experimental Conditions and Procedures

The initial conditions for the experiment are steady-state operating conditions of the LSTF as explained in Table 1. These initial conditions correspond to small break LOCA experiments except for the core power. However, in these experiments temperature stratification phenomena at high pressure and high temperature are of interest (OECD/NEA 2008).

Table 1: Initial conditions of the ROSA project Test 1-1

Pressurizer pressure	15.5 Mpa
Pressurizer liquid level	7.2 m
Core Power	~6 MW
SG pressure	6.5 Mpa
SG secondary side liquid level	9.1 m
Primary loop flow rate	24.3 kg/s/loop
Primary coolant pump speed	800 rpm
Hot leg temperature	598.0 K
Cold leg temperature	562.0 K

After the initial condition is established, the core power is set to 1.4 MW, which corresponds to 2 % of the scaled nominal power, and the primary coolant pumps are stopped. Steady-state natural circulation is then established in the primary loop. A loop flow rate of 5.8 ~ 6.0 kg/s/loop was measured in the loop-seal section. This steady-state natural circulation is a single-phase natural circulation at 15.5 MPa with the primary inventory at 100 %. The ECC water is injected into the cold leg A and B one after another the injection flow rates are 0.3 kg/s and 1.0 kg/s. The flow rate of 0.3 kg/s corresponds to the actual injection flow rate for power plants, and 1.0 kg/s is almost the maximum flow rate at 15.5 MPa for the LSTF. The temperature of the ECC water is 300 K, and the duration of each injection lasts 80 s.

2.3 ROSA V Test 1-1

The ROSA Project Test 1-1 was realized on October 2006 and data CD-R was attached to the final report to extract the measured data and evaluate the results. An overview of the chronology of major operations is given in Table 2:

Table 2: Chronology of major operations

Time (s)	Event
-1901	Data record start
-1539	Core power was decreased from 7.11 MW to 1.44 MW
-1519	Primary coolant pump stopped
18 ~ 100	0.225 kg/s injection into cold leg A
275 ~ 314	Discharge
1128 ~ 1211	0.203 kg/s injection into cold leg B
1315 ~ 1349	Discharge
2097 ~ 2184	0.980 kg/s injection into cold leg A
2267 ~ 2421	Discharge
3192 ~ 3275	0.851 kg/s injection into cold leg B
3442 ~ 3600	Discharge

Figure 11 shows the flow rates of the first 120 s of the experiment. Due to the restrictions of publishing the experimental data, the scales at the y-axis are removed in all the charts of this chapter and the exact values are also not given in the text. The flow rate was measured every second, so that there are 120 measuring points for the displayed timeframe. The ECC flow rate is nearly constant for 82 s.

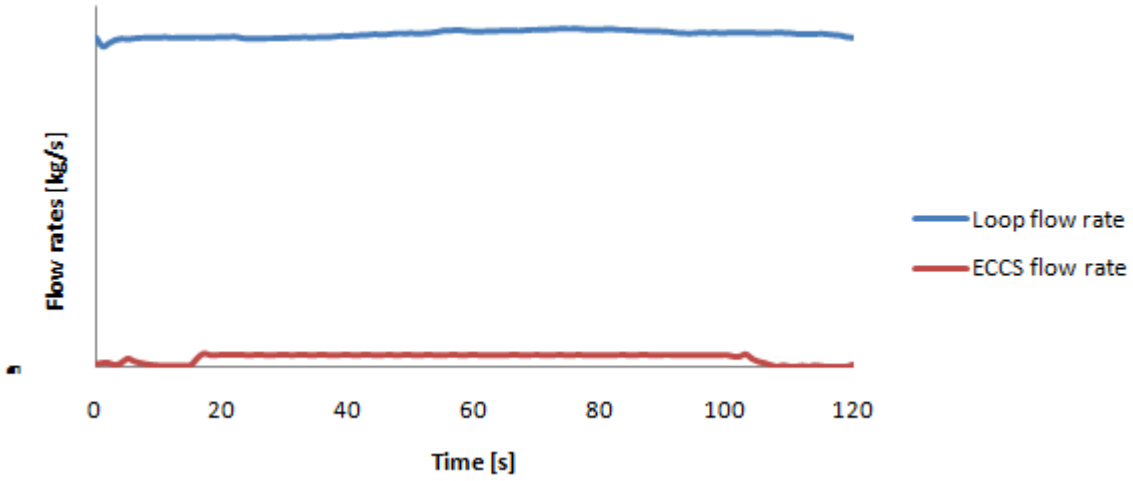

Figure 11: Loop flow rates

The temperatures of the ECC- water and the water in the loop are shown in Figure 12. All thermocouples in the experiment measure every 2.5 seconds the temperature, so there are 80 data points for the displayed timeframe.

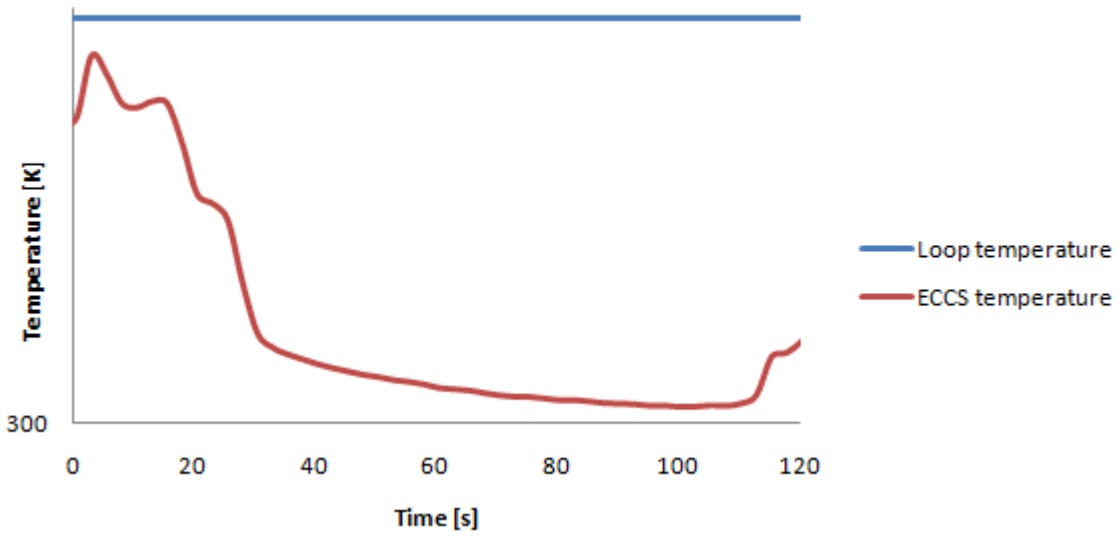

Figure 12: Temperatures of the natural circulation and the ECC injection water

In the following figures the experimental data of the new thermocouples in CLA during the first 120s of the experiment is shown. The newly installed thermocouples are continuously numbered from TE1174 to TE1236, starting from group TE1 to group TE4. Figure 13 shows the temperatures of group TE1 below the ECC injection nozzle. Here the temperatures are unchanged during the injection. This implies that the injected water did not reach these three thermocouples in the lower part of the pipe. It is also possible to

identify the stratification in the natural circulation flow. The temperature is decreasing from the top thermocouple TE1174 to the lowest installed thermocouple TE1176 at this position.

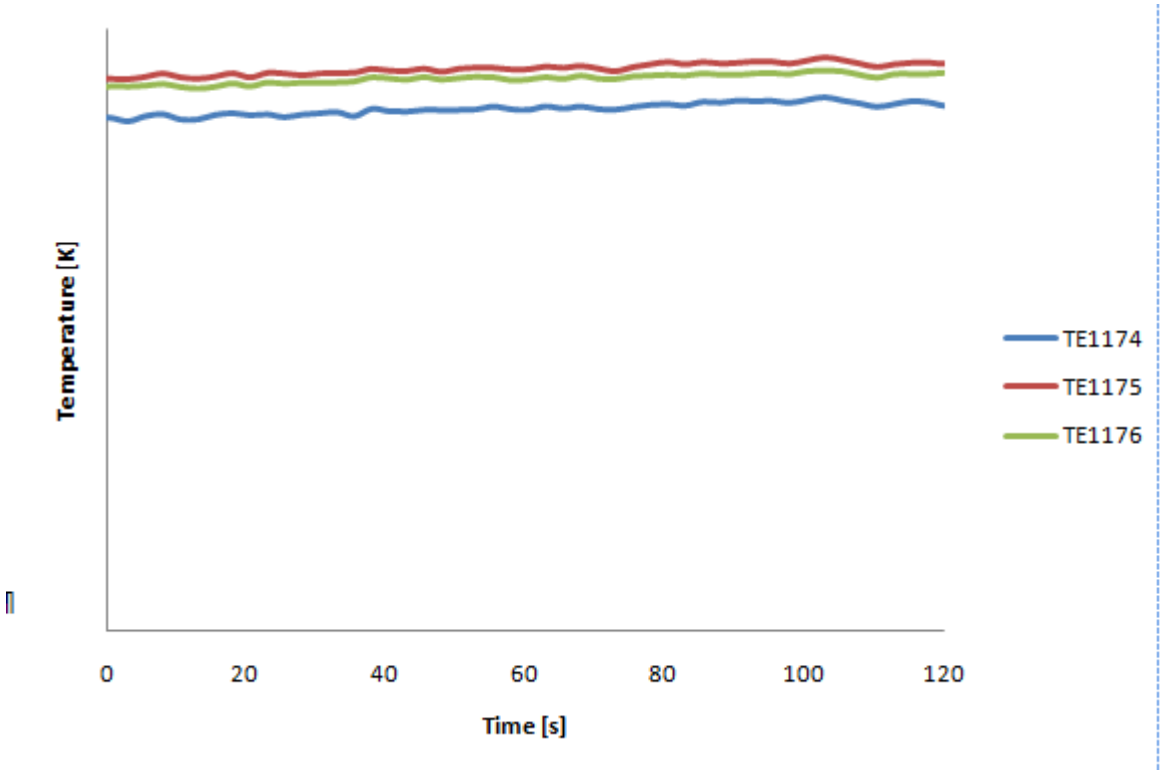

Figure 13: CLA temperature TE1A1 ~ TE1A3 (TE1174 ~ TE1176)

Figures 14 to 16 show, as an example, the temperature variations at the thermocouples in group TE2, TE3 and TE4.

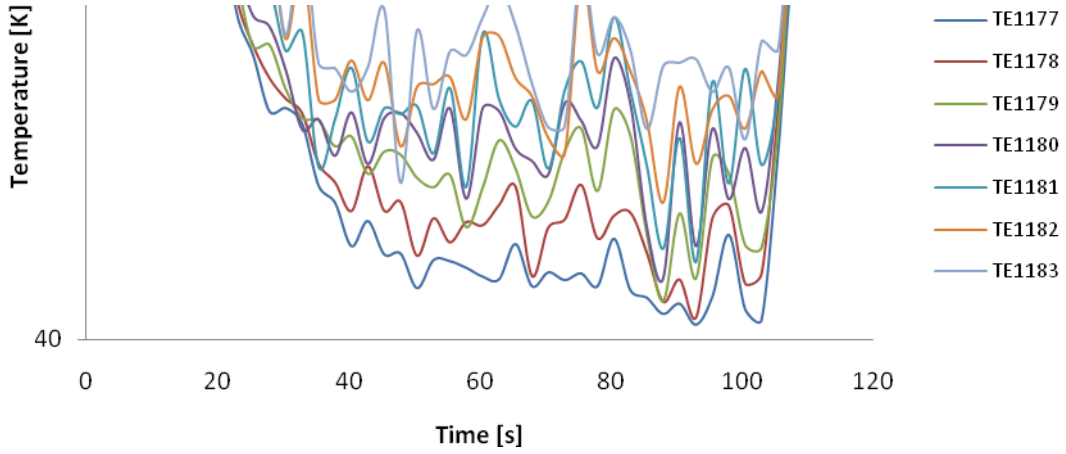

Figure 14: CLA temperature TE2A1 ~ TE2A7 (TE1177 ~ TE1183)

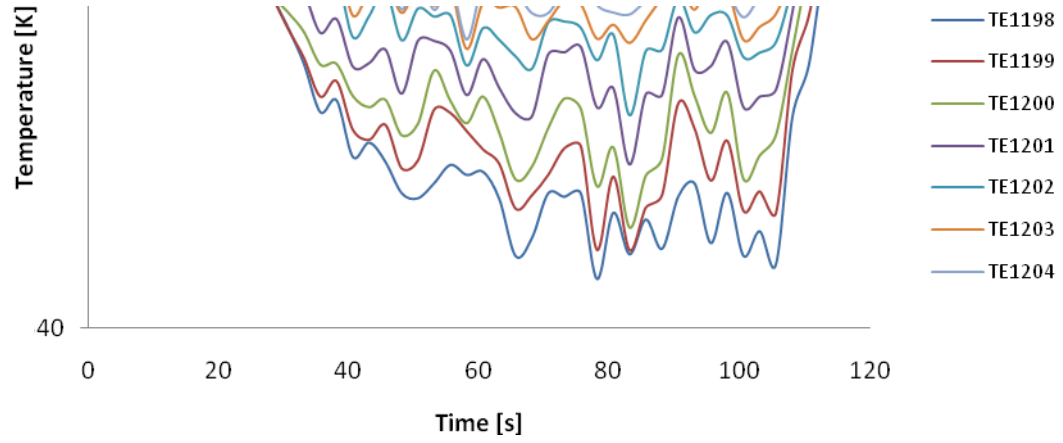

Figure 15: CLA temperature TE3A1 ~ TE3A7 (TE1198 ~ TE1204)

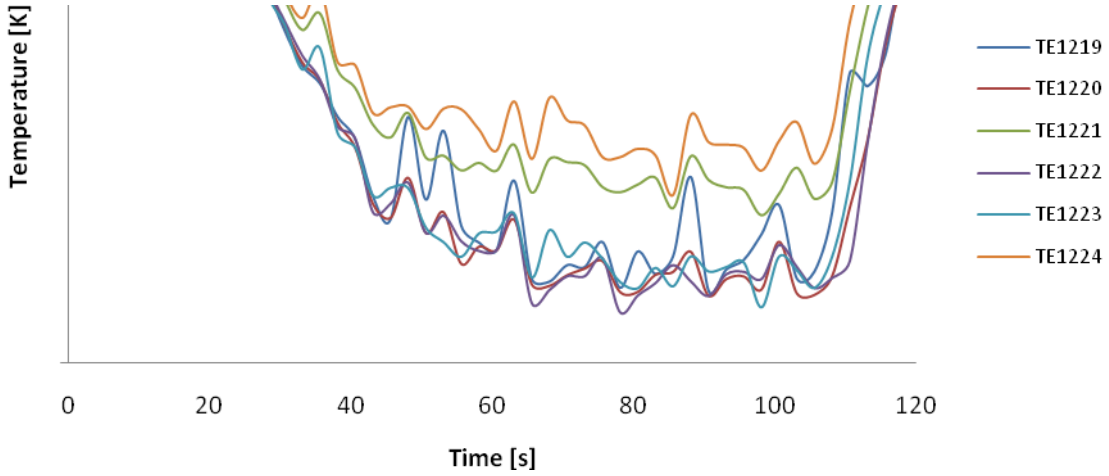

Figure 16: Downcomer temperature TE4A11 ~ TE4A23 (TE1219 ~ TE1224)

The measurement at group TE2, see in Figure 14, show a drop of the temperature between t = 25 s and t = 105 s. The temperature drop is delayed at the thermocouple groups TE3 and TE4 because the water needs some time to reach the end of the cold leg and the downcomer. After ECC injection the natural circulation stabilizes very fast and temperature stratification is established in the cold leg. However, a temperature decrease was not observed at the thermocouples installed directly below the ECC nozzle.

3 CFD ANALYSIS

The CFD analysis was performed for the first phase of Test 1-1 at 100 % primary inventory and single-phase flow injection into Loop A. The ANSYS CFD software was used for the simulation which consists of three major packages: ANSYS CFX-Pre, CFX-Solver and CFX-Post. ANSYS CFX-Pre is the physics definition pre-processor. It is used to import meshes produced in a mesh generation software packages and to select physical models for the CFD simulation. The CFX-Solver launches the calculations and monitors the calculation via the CFX-Solver Manager. With this tool the calculation are set up. CFX-Post is the post-processor for ANSYS CFX. It allows the visualization and quantitative post-processing of the results of simulations (ANSYS-CFX 2006).

3.1 Geometry Generation

A CAD model of the cold legs, the ECC lines, and the downcomer was generated on the basis of drawings (JAERI, 2003). The complete length of the downcomer was modelled to avoid feedback of boundary conditions on the flow in the section of interest. Following recommendations of Farkas et al. (2008), a rounded transition with a radius of 19 mm was used to connect the cold legs and the downcomer.

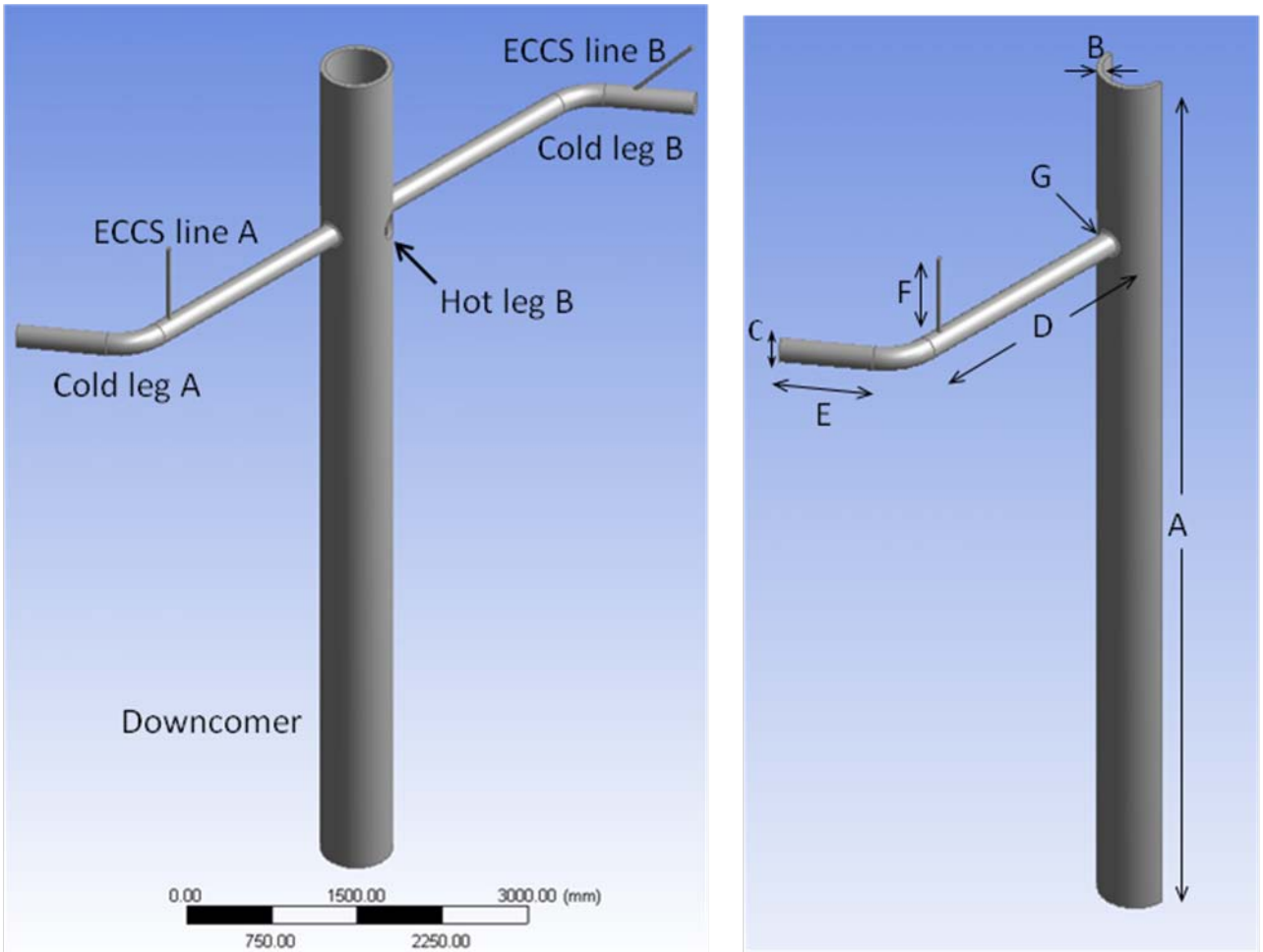

Figure 17: Geometry model and dimensions

Table 3: Summary of model dimensions

Token	Explanation	Value
A	Height of the downcomer	8410 mm
B	Thickness of the downcomer	39 – 53 mm
C	Diameter of the cold leg	207 mm
D	Length of the cold leg (till elbow part)	2739.2 mm
E	Length of the cold leg (after elbow part)	802 mm
F	Length of the ECC line	748.2 mm
G	Rounded Transition	Radius: 19 mm

A half model was used to investigate the numerical error according to the OECD/NEA CFD Best Practice Guidelines (Mahaffy, 2007). The final calculations were obtained in a complete model of the downcomer. The geometry is shown in Figure 17, the model dimensions are summarized in Table 3.

3.2 Grid Generation

Following the OECD/NEA Best Practice Guidelines (Mahaffy et al., 2007), three hexahedral grids with increasing resolution were generated to perform sensitivity studies, see Figure 18. In the first refinement step the number of elements was mainly increased in the cold leg. In the second step, the grid was additionally refined around the ECC nozzle. All generated grids were scalable with a minimum grid angle of 32º. Only 1 % of the control volumes have grid angles with less than 45º. The resulting grids are shown in Figure 18 for a cross section close to the inlet of the main pipe. The coarse grid has 1.0 million elements, the medium grid has 5.2 million elements, and the fine grid has 8.0 million elements for the complete geometry model.

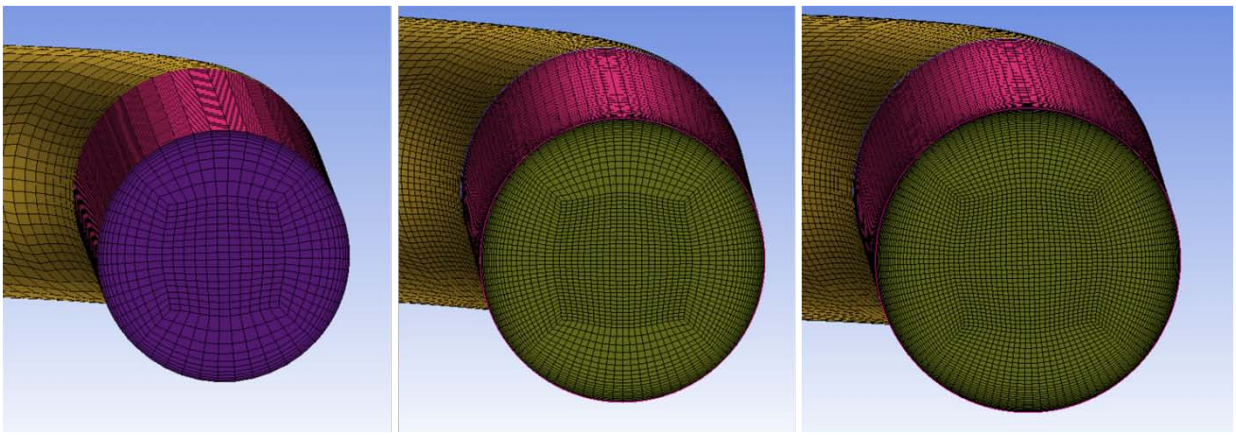

Figure 18: Computational grids close to inlet of main pipe

3.2.1 Coarse Grid

The coarse mesh consists of 495594 nodes and the total number of hexahedrons is 462941. In Figure 19 pictures of the coarse mesh show the ECC line attachment, the elbow part of the cold leg and the planar view on the main inlet of the cold leg. The first picture at the top left corner shows the O-grid of the ECC line and the second O-grid which is covering the O-grid in the mesh of the cold leg. In the last picture in the bottom right corner the O-grid of the cold leg is displayed. The refinement of the mesh towards the wall is leading to the situations that there is a jump in the grid size to the inner rectangular zone of the O-grid. This is a violation of the recommendations of the Best Practice Guidelines but without adding several more nodes this jump cannot be avoided. These extra nodes will lead to an increased number of volume elements in the whole mesh because this O-grid is continued through the whole cold leg. Due to the goal to keep the number of nodes of the coarse mesh below 500000, it was the compromise to accept such a jump in the grid and to improve this region in the next refinement.

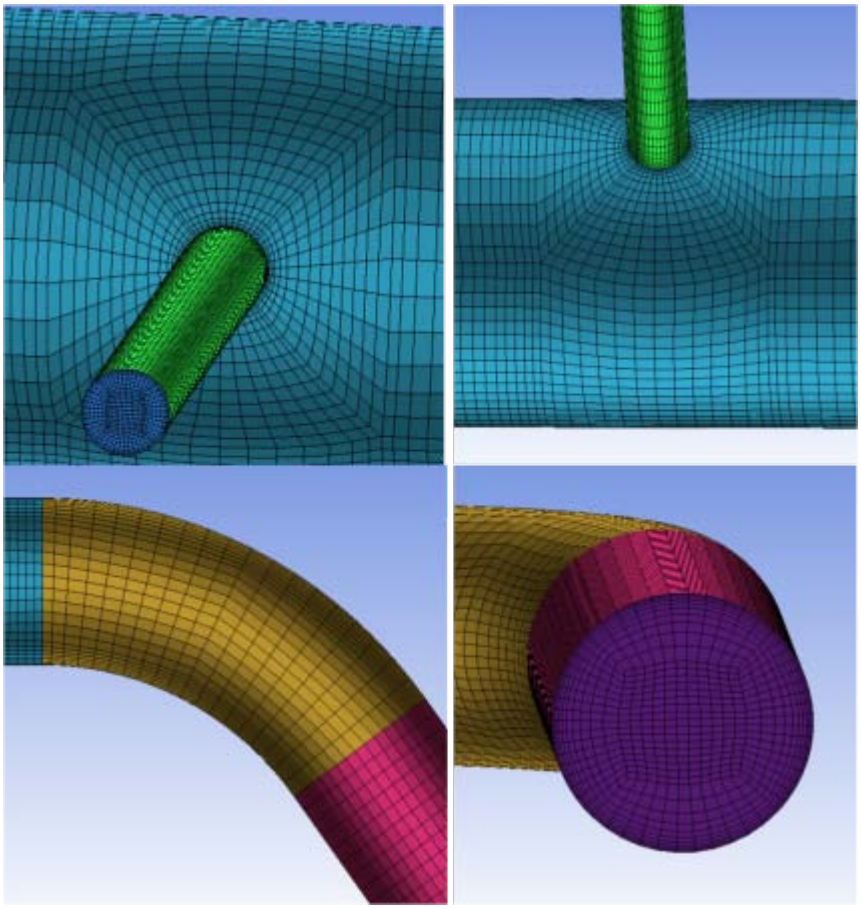

Figure 19: Detailed pictures of the coarse mesh: ECC line attachment and CLA

Detailed pictures of the grid in the downcomer are displayed in Figure 20.The top left picture is showing the top view of the downcomer. The mesh is refined towards the inner and outer wall of the downcomer. In the

top right picture, it is displayed how the change of the diameter in the fluid phase was realized by using one row of cells.

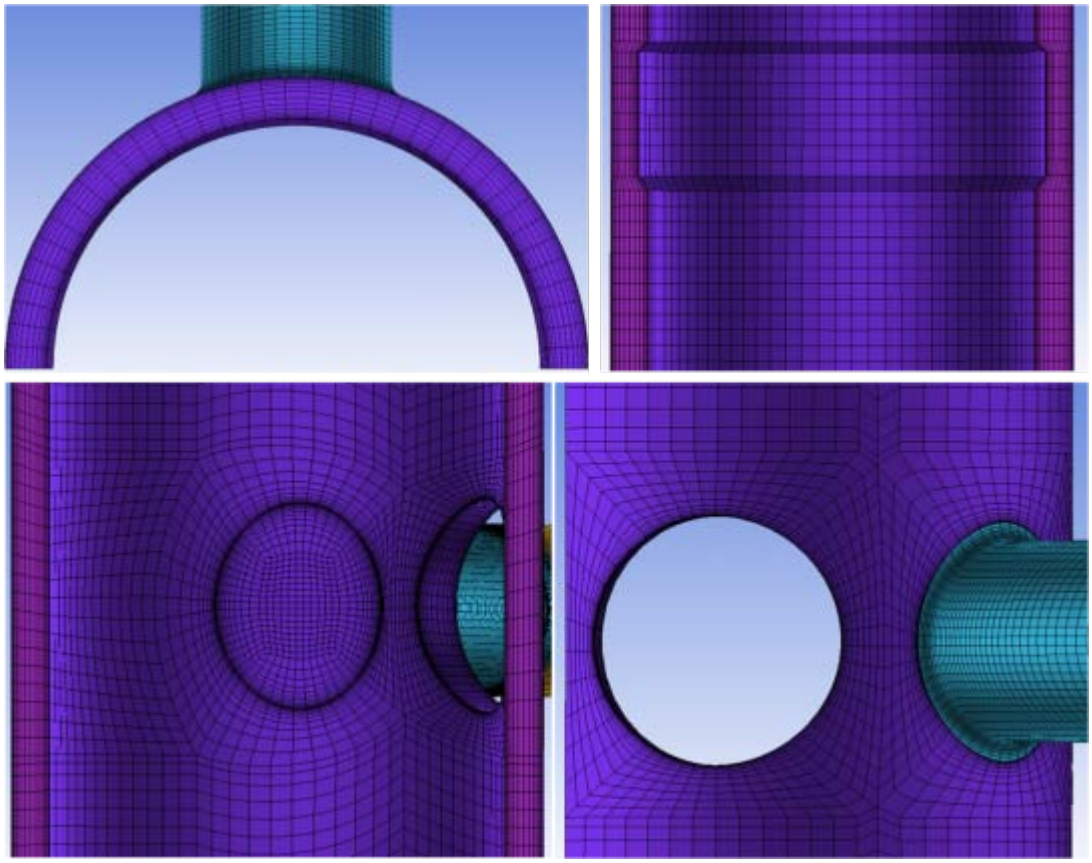

Figure 20: Detailed pictures of the coarse mesh in the downcomer

The two bottom pictures in Figure 20 show the attachment of the cold leg to the downcomer wall from the inside (left picture) and the outside (right picture) view. Both the cut out for the hot leg and the inner O-grid of the cold leg are surrounded by another O-grid. The O-grid which is covering the inner O-grid of the cold leg is necessary to avoid an extreme jump in the cell size as shown in the left picture how. It is used to decrease the refinement inside of the downcomer grid. Special care was given to the rounded transition at the end of the cold leg. A local refinement of the rounded part resolves the flow in this region in more detail.

3.2.2 Medium Grid

One of the big advantages of the structured grid is its scalability. That means the mesh can be refined without degrading the quality of the grid angles. To create the medium mesh the number of all the nodes along the edges was doubled in a first step. This can be done automatically for all the edges in the mesh and led to eight times more elements, because of the doubled number of elements in every direction. To reduce the number of around 4 million elements again, the grid was coarsened in a second step in the region of the upper and lower downcomer. The influence of these regions on the main flow was expected as not as important as the flow in the cold leg and the middle part of the downcomer. Also a local refinement towards the inlets of the cold leg, towards the ECC line and towards the outlet of the downcomer was realized to

improve the resolution of the mesh in the regions with the biggest influence on the behavior of the flow. The final result was a mesh with 2658134 nodes and 2579848 hexahedrons.

3.2.3 Fine Grid

The second refinement was a local grid refinement in the cold leg. The main focus of this refinement was directed towards the region between the ECC line and the downcomer. Therefore the number of nodes along the straight part of the cold leg was increased. On the other hand elements were removed in the region at the top and the end of the downcomer. The fine mesh consists of 4070008 nodes with 3986080 hexahedrons. Table 4 gives an overview of the numerical meshes:

Table 4: Summary of numerical grids

	Number of elements	**Smallest mesh angle**	**Description**
Coarse mesh	462941	31.6°	Base mesh to start first simulations
Medium mesh	2579848	31.6°	Refined mesh with higher resolution in the main parts of the geometry
Fine mesh	3986080	31.6°	Refined mesh in the cold leg

3.3 Mathematical Models

In the ROSA V Test 1-1 steady-state natural circulation is established in the primary loop and the main coolant pumps are stopped before ECC injection is started. The temperature difference between the hot water in the primary system and the cold ECC water is more than 200 K resulting in density differences of about 20 %. As a consequence, natural circulation is modelled in the CFD calculation by including buoyancy terms in the momentum equations, and in the production terms of the turbulence model equations. The buoyancy terms are driven by the density difference between the hot and cold water. Water density is calculated as a function of temperature on the basis of IAPWS-IF97 tables (Wagner and Kruse, 1998). The dynamic viscosity and conductivity of the fluid are also derived from the IAPWS-IF97 tables.

Two turbulence models were used in the simulation, the Shear Stress Transport (SST) model of Menter (1994) and a modification of the Reynolds stress model proposed by Launder et al. (1975). The modification of the Reynolds stress model concerns the length-scale equation. In contrast to the original proposal by Launder et al. (1995), a version using the turbulent vorticity as length-scale equation was used in this study. Both models were combined with ‘automatic’ wall functions in which the near-wall fluxes are derived from either linear or logarithmic wall laws, depending on the position of the wall-adjacent grid point.

3.4 Initial and Boundary Conditions

The transient calculations were started from a steady-state solution of the natural circulation. At the pump positions, and at the ECC injection nozzle A, the measured mass flow rates and temperatures were used as

inlet boundary conditions. At the pump position, the inlet temperature was set to a constant value of 553.8 K. The measured temperature at the ECC nozzle varied from 500 K to 300 K within 60 s.

At the outlet, which was positioned at the lower part of the downcomer, a pressure boundary condition was prescribed. At the walls no-slip boundary conditions for smooth surfaces were used. The energy transfer between the fluid and the downcomer walls was set to zero (adiabatic walls). This was the best approximation of the experimental conditions, given that no temperature or heat flux measurements were available. The approximation of adiabatic walls has also been used by other authors, e. g. Farkas and Toth (2008).

3.5 Numerical and Model Errors

A 180º-degree half model was used for the investigations of numerical and model errors in order to economize on computing resources. As a first step, iteration errors were checked on each grid at steady-state conditions. The purpose of this study was to determine a convergence criterion of the iterative CFD solver such that iteration errors became insignificant. Figure 21 shows temperatures at the measurement positions as a function of the convergence criterion. The temperatures did not change any more when the convergence criterion was reduced below 1×10^{-4}. As a consequence, a convergence criterion of 1×10^{-4} was set in the calculations.

Discretization errors in time and space were also checked on each grid. The influence of the spatial numerical grid was investigated by comparing temperature transients on the three grids at the measurement position TE 1215. As ROSA V data are proprietary, Figure 22 shows only temperature differences instead of absolute temperature values. Large differences are observed between the coarse and medium grids. On the other hand, temperature differences on the medium and fine grids amount to less than 1 K in the final part of the transient. This is less than the thermocouple uncertainty of ± 2.75 K. As a consequence, the medium-sized grid was chosen for the production calculations. It should be added that further grid refinement studies would be required to accurately quantify the solution errors as described by Mahaffy (2007). The comparison of calculations with first-order upwind and second-order high-resolution discretisation schemes is shown in Figures 23. As expected, the second-order scheme predicts more oscillatory flow behaviour. The absolute temperature differences between the two schemes were, however, not larger than 2 K.

In order to save CPU time and to optimize the time step size, adaptive time stepping was used in combination with an implicit first-order time discretisation scheme. The influence of the initial time step of the adaptive scheme is shown in Figure 24. The time step varied during the transient calculation between 0.01 and 1.0 s to achieve a convergence criterion of 1×10^{-4} for the normalized residuals in all time steps. On average 17 iterations per time step were necessary for convergence for the calculations starting with 0.01 s. The average influence of the time step size is around 8 K between 20 and 25 s, and amounts to around 4 K between 25 and 35 s. This corresponds to less than 2 % error considering absolute temperature values. Spatial and temporal grid convergence of the solutions would require further refinement of time steps and grid widths.

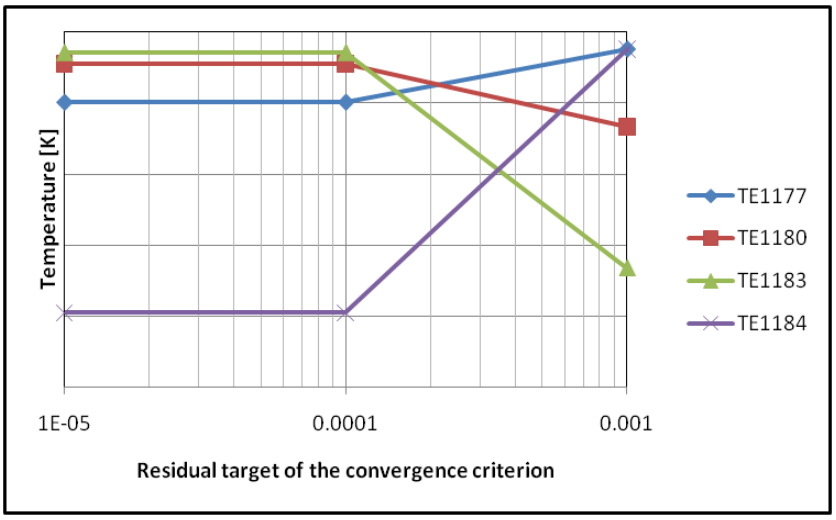

Figure 21: Temperature as function of convergence criterion

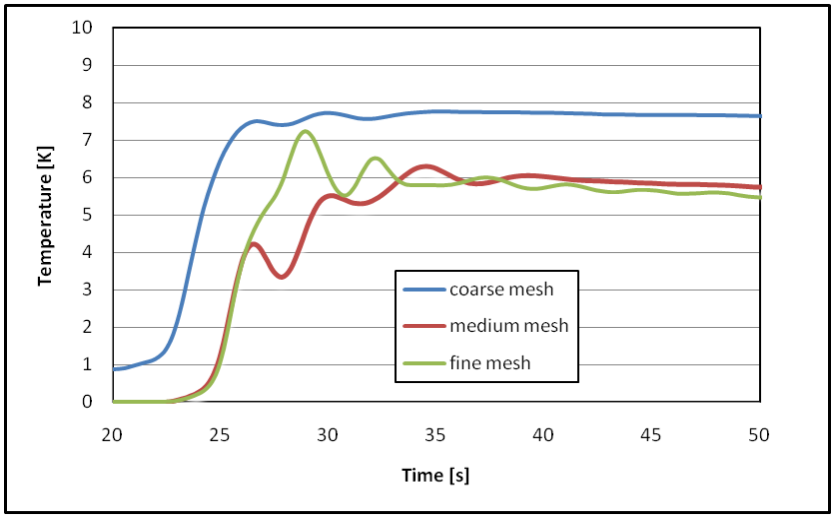

Figure 22: Influence of spatial discretisation (TE1215)

Figure 23: Influence of discretisation scheme (TE1205)

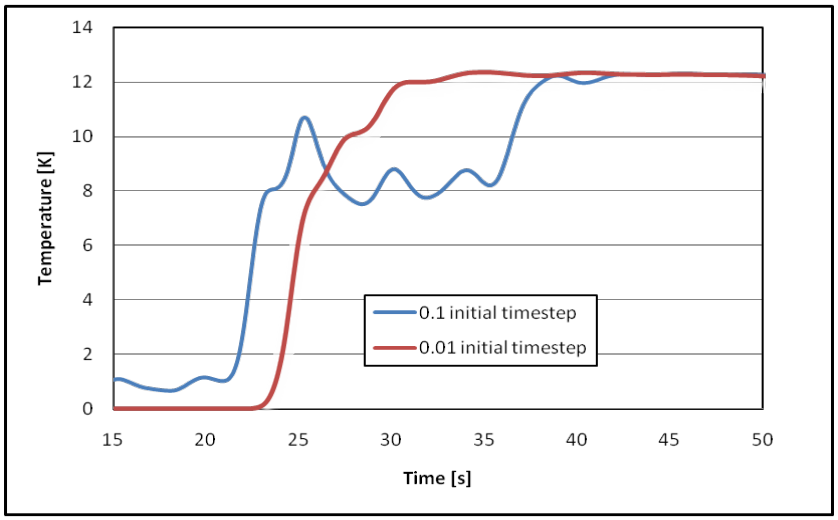

Figure 24: Influence of initial time step size (TE1205)

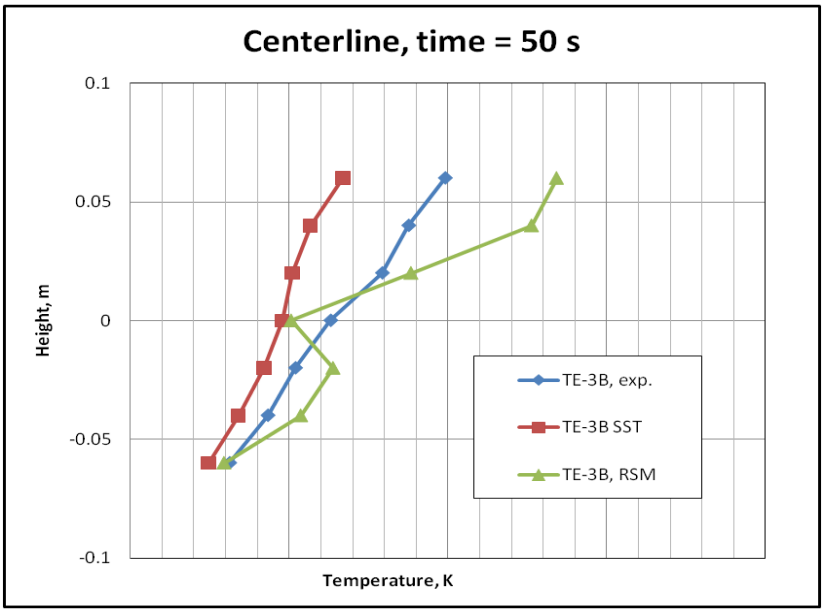

Figure 25: Influence of turbulence model

Finally, the influence of the physical models was investigated. To this end, the SST model, and the Reynolds stress model (RSM) were compared. Figure 25 shows as an example that there is no significant improvement from using the more complex RSM model, which took 1.4 times the calculation time of the SST model. Therefore, all further calculations were performed with the SST model.

3.6 Results and Comparison to Data

A 360º geometry model was used for the comparison of simulations and data. As the application of the Best Practice Guidelines in section 3.5 had shown that the medium-sized grid produced the best results in terms of accuracy and calculation time a corresponding 360º grid was generated for the production runs. This grid had 5.2 million elements. The calculations were performed with the ANSYS CFX software (Version 12) on a

Sun Galaxy with 16 processors at 2.6 GHz. The final calculations of 115 s transient time took approximately 2 days calculation time.

An impression of the temperature distribution in Cold Leg A, and in the downcomer during ECC injection is shown in Figure 26. The cold water in the cold leg shows stratification, and an oscillatory motion. The cold ECC water plume is transported downstream by the main flow and touches the bottom wall of the cold leg downstream of the injection nozzle. At this point, stratification is strongest. Downstream, the cold water plume is sloshing from side to side in the horizontal pipe and hot and cold water are mixed. As observed in the experiment, the cold water plume is entering the downcomer attached to the outer vessel wall.

A quantitative comparison of the temperature distribution in the downcomer is shown in Figure 27. Close to the vessel wall (TE1225) experiment and calculation are in good agreement. At the barrel wall (TE1227) the calculated temperatures are higher, while the data indicate stronger mixing of the cold water plume with the surrounding hot water. However, the experimental flow may be influenced by the relative large fixtures of the thermocouples which could not be included in the simulations because no geometry information was available.

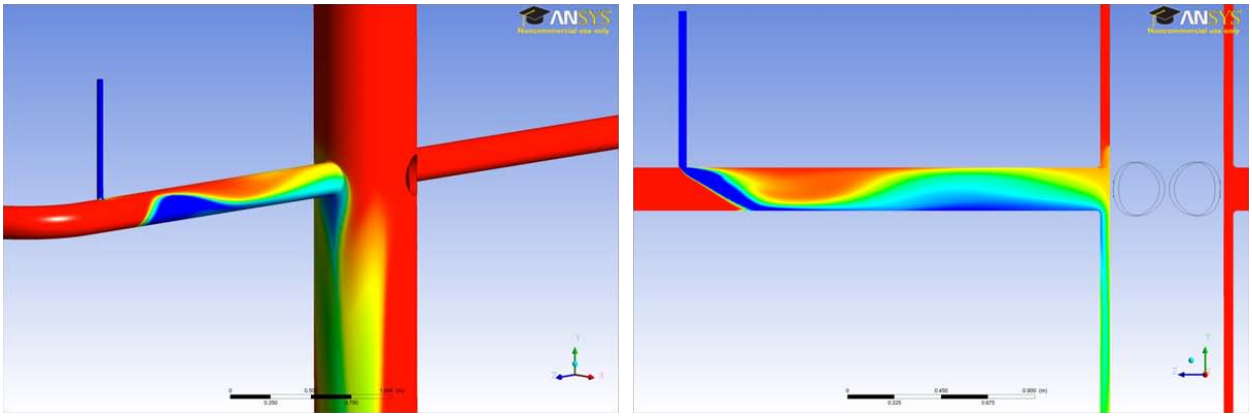

Figure 26: Temperature stratification in Cold Leg A @ 80 s

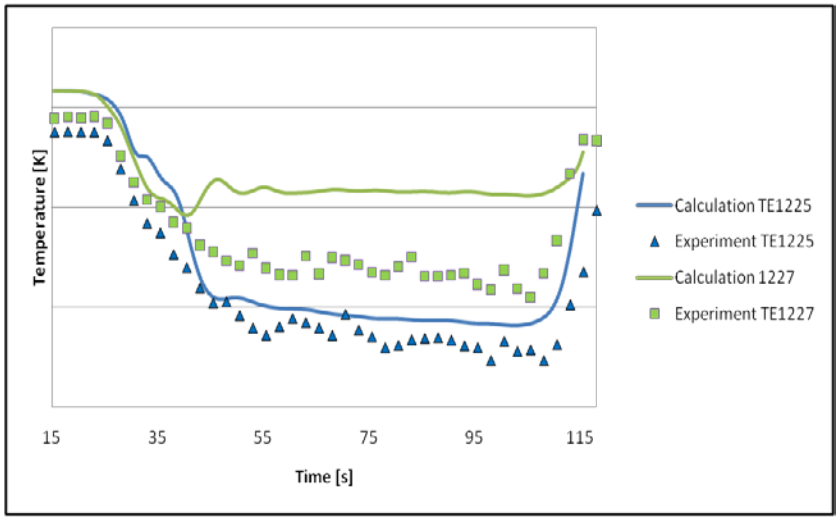

Figure 27: Comparison of simulation and data in the downcomer (TE1225, TE1227)

Figures 28 and 29 show the comparison to data at the central thermocouple position of rakes TE2 and TE3 in the cold leg, respectively. The red and black dashed lines show the measurement uncertainty of the thermocouples. At position TE2 (Figure 28), which is close to the inlet nozzle, the calculation under-predicts

mixing above the centreline of the horizontal pipe. The temperature in the upper part of the cold leg is therefore higher than in the experiment. At position TE3 (Figure 29), the simulation results are in good agreement with data.

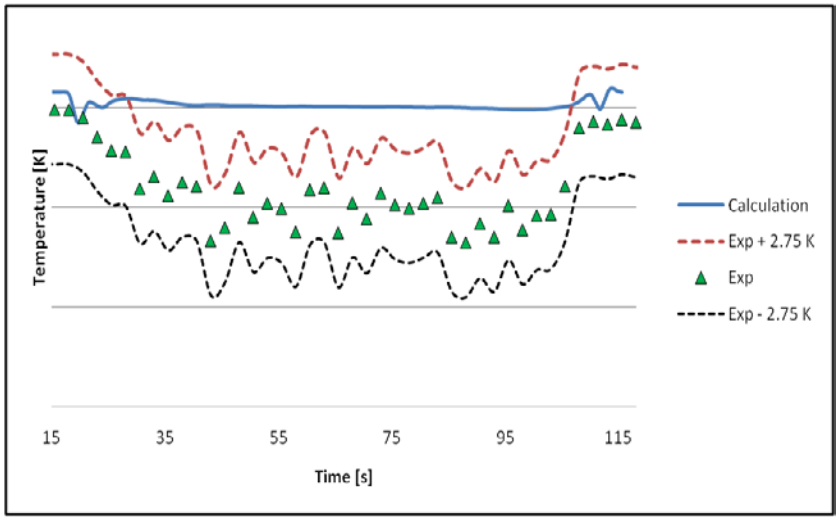

Figure 28: Comparison of simulation and data in Cold Leg A (TE1187)

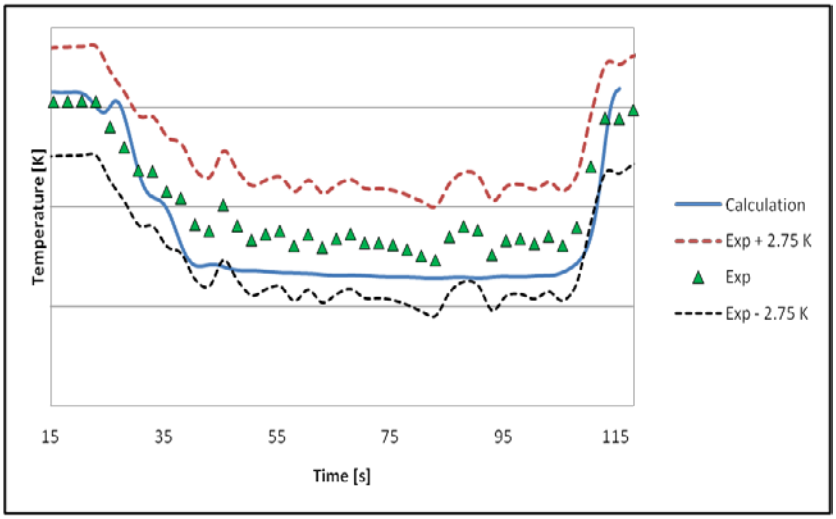

Figure 29: Comparison of simulations and data in Cold Leg A (TE1208)

4 Conclusion

A numerical analysis of the ROSA V Test 1-1 was performed with the ANSYS CFD software. The ROSA V experiment investigates thermal stratification at single-phase natural circulation conditions in the cold leg of a PWR. The numerical results were compared with temperature measurements at three rake positions in Cold Leg A, and at one position in the downcomer below the cold leg.

The numerical grid generation and error analysis was performed according to the OECD Best Practice Guidelines. After reduction of numerical errors, model errors were investigated by comparing different turbulence models. The final comparison with data showed good agreement. It leads to the following conclusions:

- Close to the ECC injection nozzle, turbulent mixing induced at the shear layer between the cold ECC-water and the hot water in the cold leg is under-predicted. In order to improve agreement between predictions and data use of a scale-resolving turbulence model may be necessary.
- Temperature stratification along the cold leg and in the downcomer is in good agreement with data which indicates that the buoyancy-driven stratification is accurately simulated.
- The attachment of the cold water plume to the outer wall of the pressure vessel in the downcomer is captured by the CFD simulation.

The calculations indicate the predominance of buoyancy effects caused by density difference between cold and hot water in the cold leg. The temperature measurements indicate that mixing effects are more dominant. It may be questioned to which extent this difference is influenced by the mixing effect of the thermocouple rakes and the video probe installed in the flow field. Further studies will concentrate on an increased resolution of the area around the ECC nozzle and the application of scale-resolving turbulence models.

5 References

ANSYS-CFX Users Manual; http//:www.ansys.com/cfx (2006)

T. Farkas, I. Tóth, “FLUENT Analysis of a ROSA Cold Leg Stratification Test”, Internal Report, Hungarian Academy of Sciences, KFKI, Atomic Energy Research Institute, Budapest (2008)

T. Höhne, S. Kliem, M. Scheuerer, “Experimental and Numerical Modelling of a Buoyancy-Driven Flow in a Reactor Pressure Vessel”, The 11th Int. Topical Meeting on Nuclear Reactor Thermal-Hydraulics (NURETH-11), Avignon, France, 2-6 October, Paper 480, (2005)

Japan Atomic Energy Research Institute (JAERI): ROSA IV, “Large Scale Test Facility (LSTF), System Description”, Tokai Research Establishment, (1985)

JAERI, “ROSA V Large Scale Test Facility (LSTF) System Description for the Third and Fourth Simulated Fuel Assemblies”, Tokai Research Establishment, Japan Atomic Energy Research Institute (2003)

JAERI, ”Final Data Report of OECD/NEA ROSA Project Test 1-1”, Thermohydraulic Safety Research Group, Nuclear Safety Research Centre, Japan Atomic Energy Agency (2008)

B. E. Launder, G. Reece, W. Rodi, “Progress in the development of a Reynolds stress turbulence closure”, J. Fluid Mech. 68:537-66 (1975)

J. Mahaffy, “Best Practice Guidelines for the Use of CFD in Nuclear Reactor Safety Applications”, NES/CSNI/R 5 (2007)

F. R. Menter, “Two-Equation Eddy-Viscosity Turbulence Models for Engineering Applications”, AIAA-Journal, Vol. 32, pp. 269 – 289 (1994)

M. Scheuerer, “Selection of PTS-Relevant Test Cases,” EVOL-ECORA-D05a (2002)

W. Wagner, and A. Kruse, The Industrial Standard IAPWS-IF97: Properties of Water and Steam, Springer-Verlag, Berlin (1998)

S. M. Willemsen, M. J. Komen, “Assessment of RANS CFD modelling for Pressurized Thermal Shock Analysis”, 11th Int. Topical Meeting on Nuclear Reactor Thermal-Hydraulics (NURETH-11), Avignon, France, Paper 121, (2005)

T. Yonomoto, “ROSA/LSTF Tests on PWR Natural Circulation and RELAP5 Validation”, Oregon State University, Corvallis, Oregon, (2005)

6 Annexes

6.1 Annex 1: Document approval by beneficiaries' internal QA

#	Name of beneficiary	Approved by	Function	Date
1	GRS	M. Scheuerer	Author	23-08-2010
2	GRS	J. Weis	Author	23-08-2010
3	FZD	D. Lucas	WP2.1 coordinator	23-08-2010
4	CEA	D. Bestion	SP2 coordinator	23-08-2010

EUROPEAN COMMISSION

Community Research

EURATOM

NURISP

NUclear Reactor Integrated Simulation Project

Collaborative Project (Large – scale Integrating Project)

Seventh Framework Programme EURATOM

Contract Number: 232124

Start date: 01/01/2009 Duration: 36 Months

Two-Phase CFD Simulation of OECD/NEA ROSA Test 1-1

M. Scheuerer (GRS, Germany)

NURISP – Contract Number: 232124
NUclear Reactor Integrated Simulation Project

Document title	***Two-Phase CFD Simulation of OECD/NEA ROSA***
Author(s)	Scheuerer, Martina (GRSmbH)
Number of pages	19
Document type	Deliverable
Work Package	WP2.1
Document number	D-2.1.2.4b – Revision 0
Issued by	Gesellschaft für Anlagen- und Reaktorsicherheit mbH (GRS)
Date of completion	28/03/2012
Dissemination level	Public

Summary

This document contains the continuation of the NURISP deliverable D2.1.2.4a (Scheuerer, 2010). The report describes the validation exercise with the ROSA V test 1-1 experiments. The OECD ROSA V test series were performed in the Large Scale Test Facility LSTF (JAERI, 2003) with the goal to validate Computational Fluid Dynamics (CFD) calculations. To this end, the three-dimensional temperature field was measured in the cold leg and downcomer. ANSYS CFX simulations at two-phase flow conditions and data for the ROSA V Test 1-1 are compared and assessed. As the experimental data is proprietary, absolute temperature values cannot be provided.

Approval

Rev.	Date	First author	WP leader	SP or Project Coordinator
0	03/2012	M. Scheuerer, GRS 28/03/2012	D. Lucas, HZDR 12/04/2012	D. Bestion, CEA 11/04/2012

Distribution list

Name	Organisation	Comments
Michel HUGON	EC DG RTD	
All beneficiaries	NURISP	Through NIWS
F. Name	organisation	

Table of contents

1. INTRODUCTION 5
2. ROSA V TEST 1-1 5
3. CFD ANALYSIS 10
   3.1 Geometry and Grid 10
   3.2 Mathematical Models 11
   3.3 Initial and boundary conditions 13
   3.4 Results and comparison to data 14
4. SUMMARY AND CONCLUSION 17
5. REFERENCES 18
6. ANNEX 1: DOCUMENT APPROVAL BY BENEFICIARIES' INTERNAL QA 19

List of Figures

Figure 1: Loop mass flow rate 6
Figure 2: Loop temperature 7
Figure 3: Transient ECC mass flow rate 7
Figure 4: Transient ECC temperature 8
Figure 5: Locations of thermocouples at TE2 and TE3 in CLA 8
Figure 6: CLA temperature TE1A1 to TE1A3 (TE1174 - TE1176) 9
Figure 7: CLA temperature TE2B1 to TE2B7 (TE1184 - TE1190) 9
Figure 8: CLA temperature TE3B1 to TE3B7 (TE1205 - TE1211) 10
Figure 9: Cross section of computational grid in cold leg A 11
Figure 10: Initial position of free surface (front view) 13
Figure 11: Initial natural circulation condition (left: center view & right: back view) 14
Figure 12: Transient temperature at TE1A1 – TE1A3 15
Figure 13: Transient temperature at TE-2B1 – TE-2B7 16
Figure 14: Transient temperature at TE-3B1 – TE-3B7 16
Figure 15: Void fraction distribution along center plane (left: center view & right: back view) 17

1. INTRODUCTION

In this report the validation exercise is continued which is described in the NURISP deliverable D2.1.2.4a (Scheuerer, 2010). The ROSA V test 1-1 experiments were selected as one of the validation cases in the NURISP project. The OECD ROSA V test series were performed in the Large Scale Test Facility (LSTF) (JAERI, 2003) with the goal to validate Computational Fluid Dynamics (CFD) calculations. To this end, the three-dimensional temperature field was measured in the cold leg and downcomer. In this report, CFD simulations at two-phase flow conditions and data for the ROSA V Test 1-1 are compared and assessed. As the experimental data is proprietary, absolute temperature values cannot be provided.

The ANSYS CFX analysis was performed with a structured mesh of 2.5 million nodes representing one half of the downcomer. A homogeneous two-phase flow model was used to simulate the free surface with condensation between steam and water. Before the start of ECC-injection, the free surface flow between steam and water at quasi steady-state natural circulation conditions was established. The CFD results describe correctly the jet impingement on the water surface, the entrainment of steam and its transport towards the downcomer in the water layer. Comparison with temperature measurements at the central positions of the thermocouple rakes in cold leg A show good agreement with data.

2. ROSA V TEST 1-1

The ROSA V experiments were performed in the Large Scale Test Facility LSTF. The Test 1-1 was performed in several steps. It started with emergency core cooling (ECC) injections into the cold legs at 15.5 MPa at 100 % primary inventory with a core power corresponding to 2 % of the scaled nominal power. In the next steps, after 10 minute intervals for re-stabilization, the water level was reduced to 80 %, 70 % and 50 % of the inventory. Local temperature distributions were measured by rakes of thermocouples in the cold legs located in three cross-sectional planes between injection nozzle and downcomer, containing 9 and 21 thermocouples, respectively. The test facility and the experimental set-up are described in detail in the NURISP deliverable D2.1.2.4a (NURISP, 2010). In Table 1 the major experimental operations are listed until the inventory is reduced to 70% of its initial value.

Table 1: Chronology of major operations

Time (s)	**Event**
-1901	Data record start
-1539	Core power was decreased from 7.11 MW to 1.44 MW
-1519	Primary coolant pump stopped
18 ~ 100	0.225 kg/s injection into cold leg A
275 ~ 314	Discharge
1128 ~ 1211	0.203 kg/s injection into cold leg B
1315 ~ 1349	Discharge

2097 ~ 2184	0.980 kg/s injection into cold leg A
2267 ~ 2421	Discharge
3192 ~ 3275	0.851 kg/s injection into cold leg B
3442 ~ 3600	Discharge
3822	Pressurizer isolation
4032 ~ 6107	Discharge: Primary inventory 100 → 80%
6929/6926 ~ 7004/7004	0.253/0.265 kg/s injection into cold leg A/B
7155 ~ 7281	Discharge
8237/8232 ~ 8318/8319	0.997/0.870 kg/s injection into cold leg A/B
8466 ~ 9229	Discharge: Primary inventory 100 → 70%

The time range relevant for the two-phase flow CFD simulation at 80% inventory is between 8220 s and 8340 s. The corresponding experimental transient mass flow rates and temperature are shown in Figure 1 to Figure 4. Due to the restrictions of publishing the experimental data, the scales of the y-axis are removed in all charts.

During the transient of 120 s the loop mass flow rate (Figure 1) varies between 7 kg/s and 11 kg/s and the loop temperature (Figure 2) varies between 551 K and 552 K.

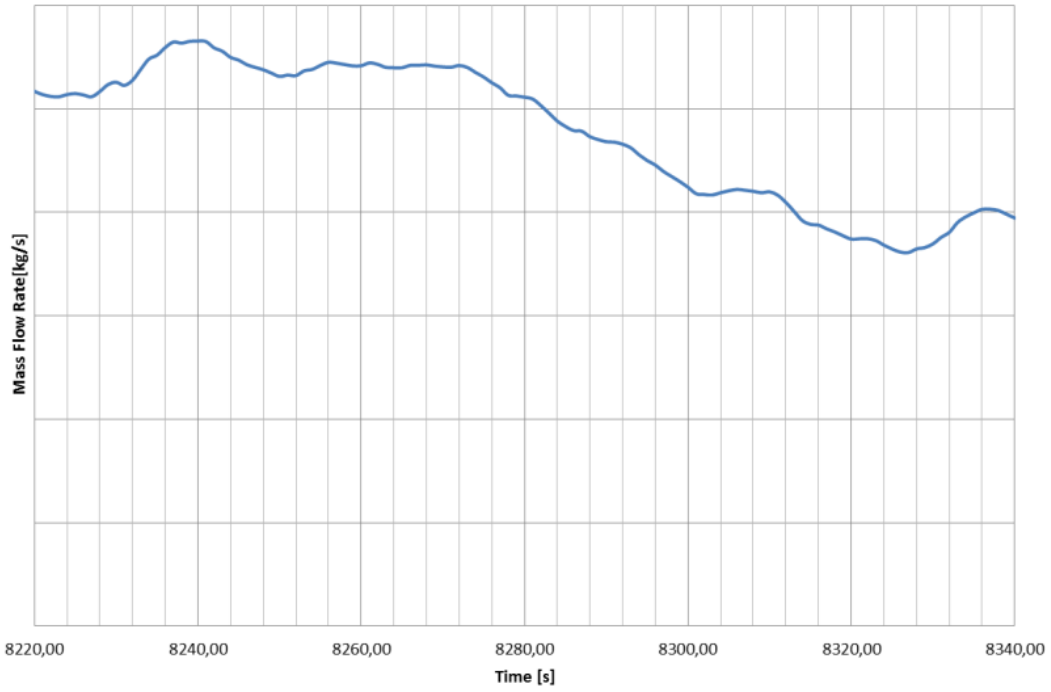

Figure 1: Loop mass flow rate

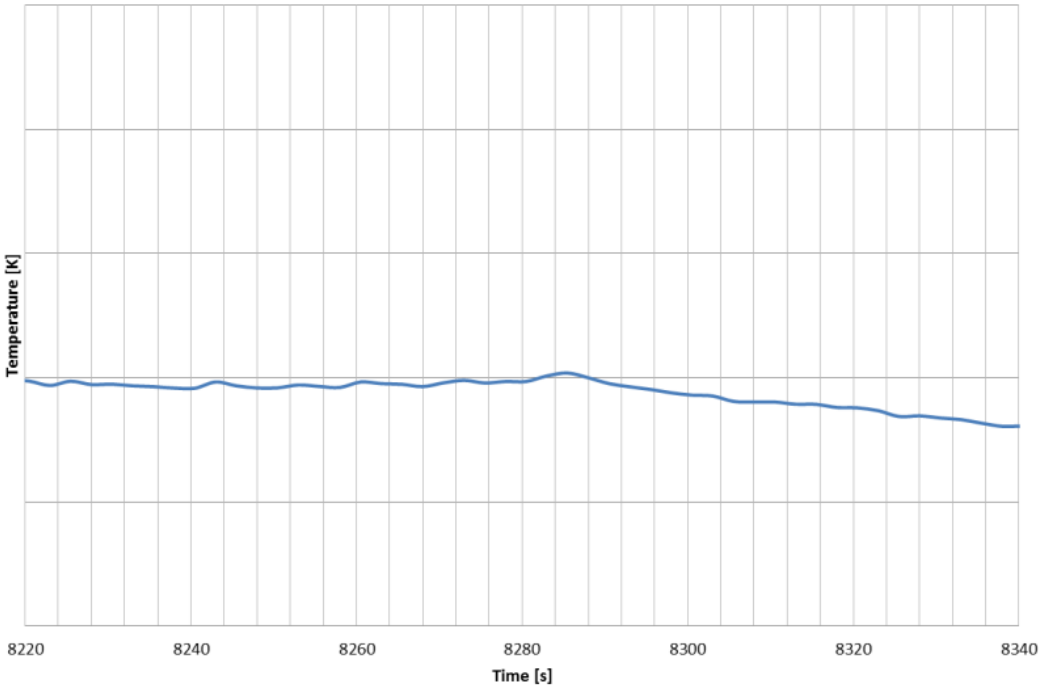

Figure 2: Loop temperature

The ECC mass flow rate and temperature are shown in Figure 3 and Figure 4, respectively. The ECC water reaches a constant value of 1 kg/s and a constant temperature of 300 K.

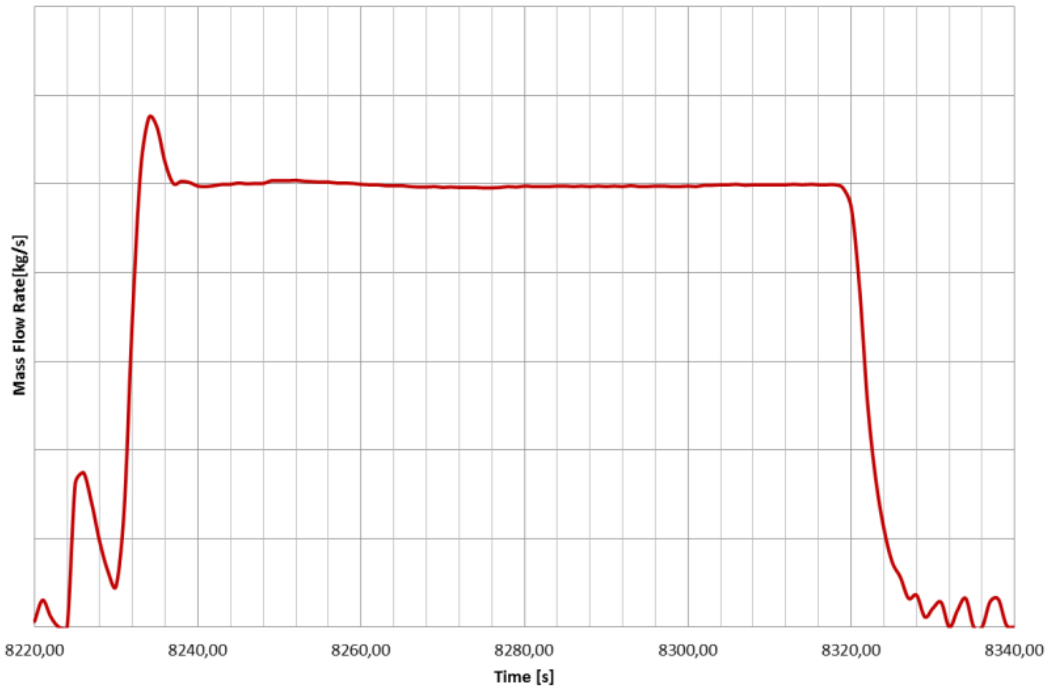

Figure 3: Transient ECC mass flow rate

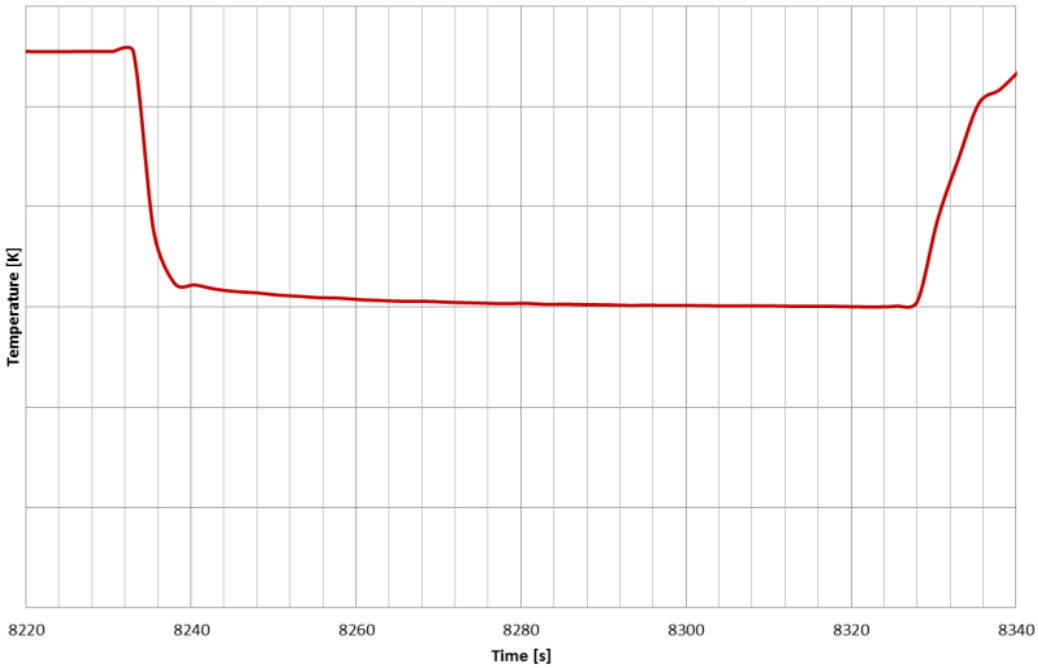

Figure 4: Transient ECC temperature

In the following figures the experimental data are shown in cold leg A (CLA) at thermocouple groups TE1, TE2, and TE3. TE1 is positioned directly below the ECC-injection nozzle. TE3 is located close to the entrance to the downcomer, and TE2 is positioned between injection nozzle and downcomer. At position TE1 three thermocouples are installed (TE1174 – TE1176) in the center of the cold leg. At positions TE2 and TE3, thermocouples are distributed in three columns and seven rows as shown in Figure 5. At position TE2, thermocouples are numbered from TE1177 to TE1197, at position TE3 from TE1198 to TE1216.

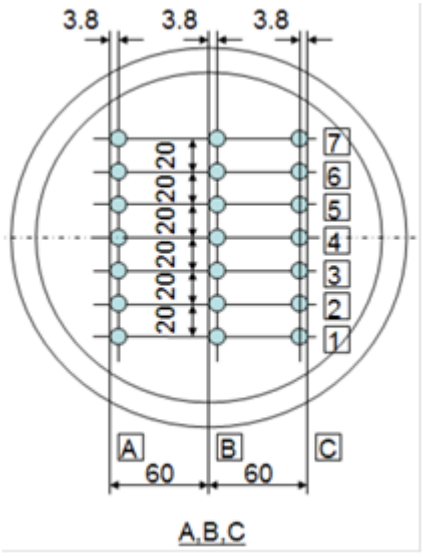

Figure 5: Locations of thermocouples at TE2 and TE3 in CLA

The measured temperature distribution over a time span of 120 s (starting at 8220s, ending at 8340s) is shown at the central positions of TE1 in Figure 6, TE2 in Figure 7, and TE3 in Figure 8. At these positions a comparison is made with the computed temperature data in section 3.4.

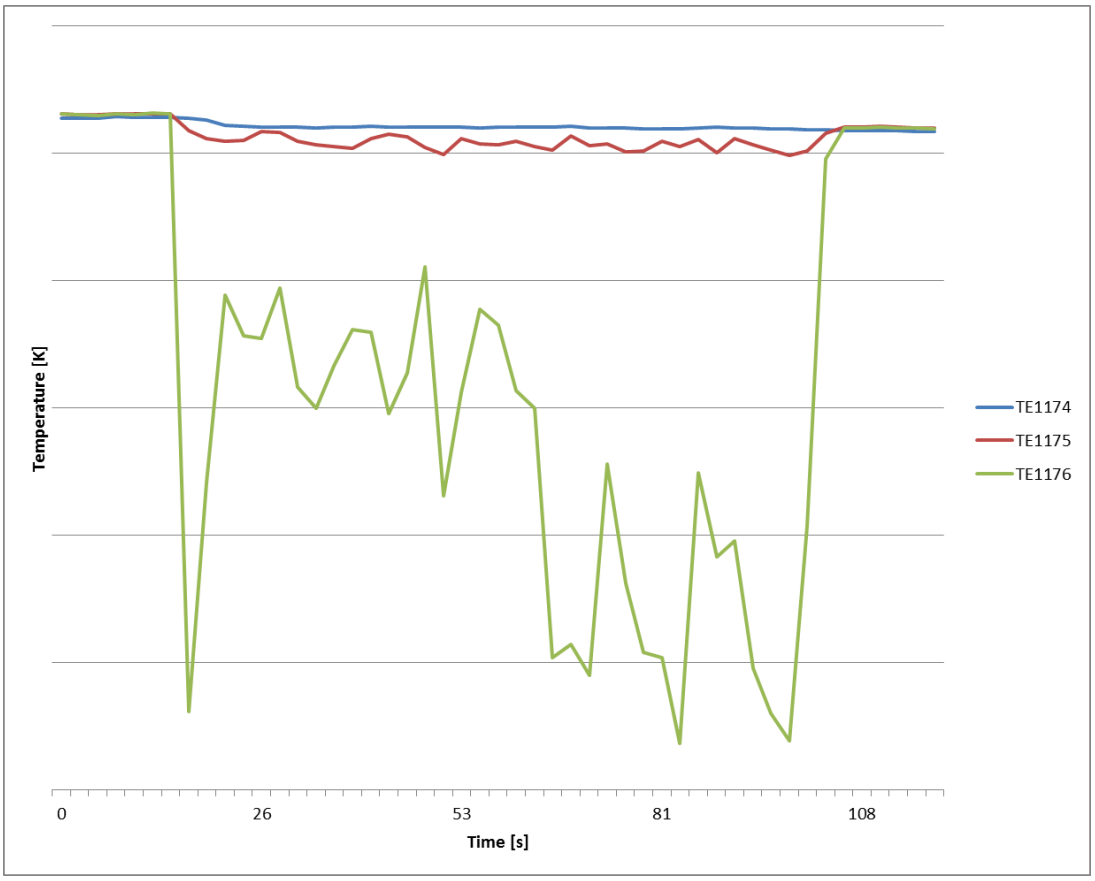

Figure 6: CLA temperature TE1A1 to TE1A3 (TE1174 - TE1176)

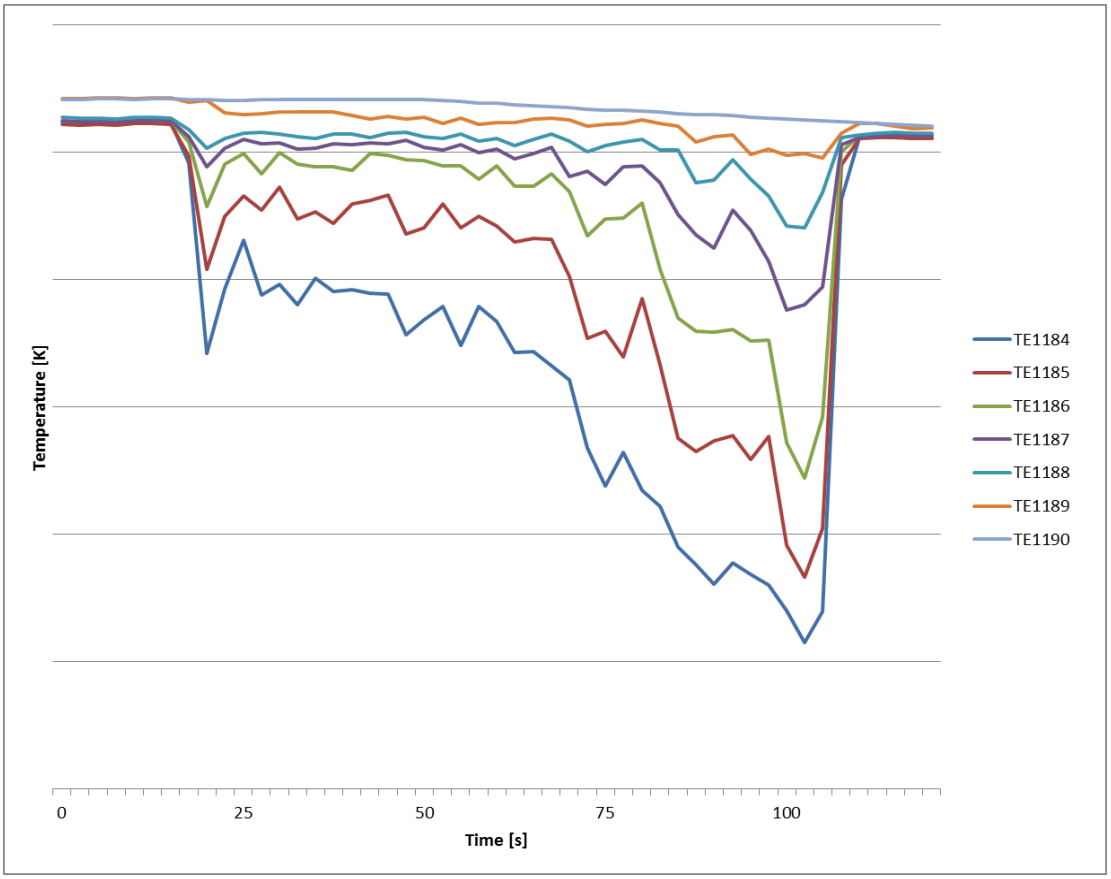

Figure 7: CLA temperature TE2B1 to TE2B7 (TE1184 - TE1190)

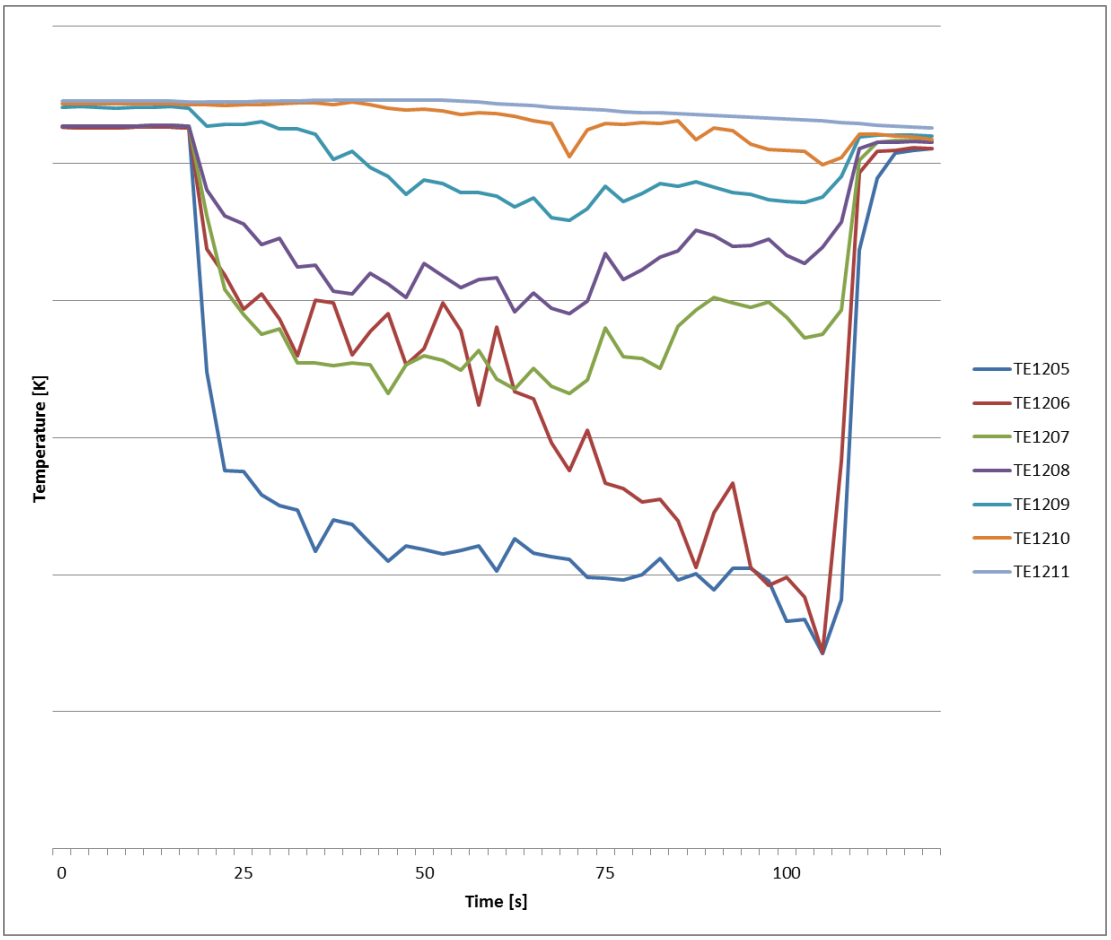

Figure 8: CLA temperature TE3B1 to TE3B7 (TE1205 - TE1211)

3. CFD ANALYSIS

The analysis was performed with ANSYS CFX with the aim to demonstrate the ability of the code to simulate ECC-injection into the cold leg of a PWR at natural circulation conditions when the cold leg is partially filled with steam.

3.1 Geometry and Grid

Geometry and grid were taken from the previous CFD analysis described in the NURISP deliverable (Scheuerer, 2010). For the two-phase flow calculations cold leg A and a 180-degree model of the downcomer were used. The cold leg is connected to the outlet of the pump. It includes the bend upstream of the ECC injection line, and the ECC line and extends to the entrance of the downcomer. The complete length of the downcomer was modelled to avoid feedback of boundary conditions on the flow in the section of interest.

Three systematically refined numerical grids were generated and numerical errors were investigated following OECD Best Practice Guidelines (Mahaffy, 2007) for the single-phase flow calculations described by Scheuerer (2010). The corresponding medium sized grid with 2.5 million nodes was chosen for the two-

phase flow calculations at 80% water inventory. In order to capture the free surface between steam and water the grid was refined at a height of 0.13 m along the horizontal axis of cold leg A, see Figure 9.

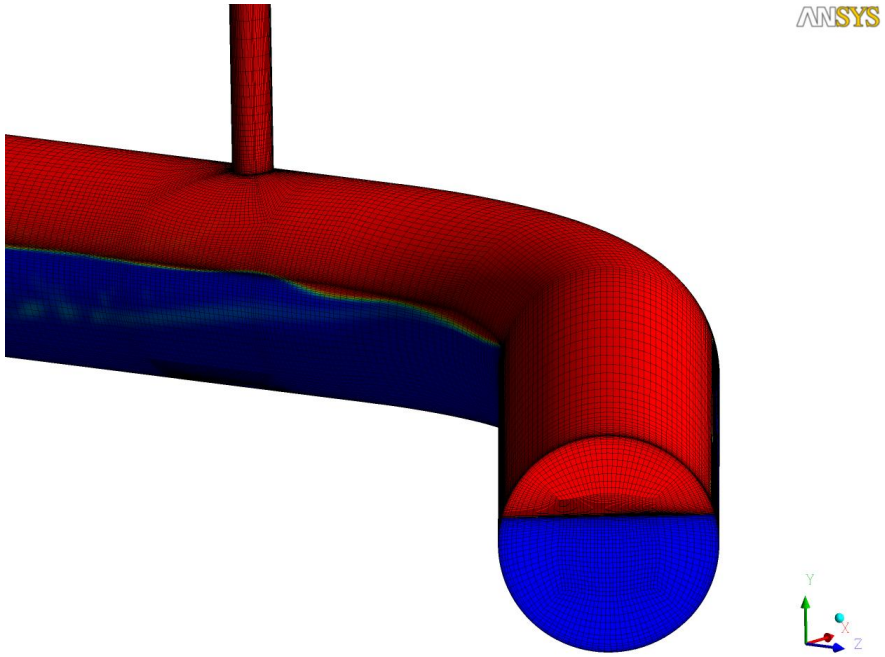

Figure 9: Computational grid in cold leg A

3.2 Mathematical Models

In the ROSA V Test 1-1 the injection of a water jet into stratified flow with a free surface between steam and water is simulated. The temperature differences between the hot water and saturated steam in the primary system and the cold water jet are large. As a consequence, natural circulation is modeled in the CFD calculation by including buoyancy terms in the momentum equations, and in the production terms of the turbulence model equations. The buoyancy terms are driven by the density differences which are calculated as a function of temperature on the basis of IAPWS-IF97 tables (Wagner and Kruse, 1998). The dynamic viscosity and conductivity of the fluids are also derived from the IAPWS-IF97 tables.

The mathematical model for the free surface flow simulation is a so called homogeneous two-phase flow model. It consists of the following transport equations (Ishii and Hibiki, 2006):

- Conservation equation for the mixture mass of steam and water
- Conservation (diffusion) equation for the volume fraction of steam
- Conservation equations for mixture momentum for the three coordinate directions
- Conservation equation for the water enthalpy

In the current set of calculations, the steam phase has been assumed to be isothermal at a constant saturation temperature 553 K. Therefore, the conservation equation for steam enthalpy was not solved.

The conservation equation for the volume fraction of water, α_w, is:

$$\frac{\partial\left(\overline{\overline{\rho_w}}\alpha_w\right)}{\partial t}+\frac{\partial\left(\overline{\overline{\rho_w}}\alpha_w U_{m,j}\right)}{\partial x_j}=\Gamma_{ws}$$

Eq. (1)

The index '*w*' relates to the water phase. ρ_w is the water density; the double-overbar indicates a phase average. $U_{m,j}$ are the velocity components of the water-steam mixture. The diffusion term (see Ishii and Hibiki, 2006) in the conservation equation for the volume fraction of water has been set to zero.

The interfacial mass transfer term, Γ_w, is modelled as the product of an interfacial area density of the water-steam interface and an interfacial mass transfer rate per unit area, as:

$$\Gamma_{ws}=A_{ws}\dot{m}_{ws}$$

Eq. (2)

The calculation of the interfacial mass transfer rate is based on an energy balance at the phase interface as:

$$\dot{m}_{ws}=\frac{q_s-q_w}{H_{sat,s}-H_{sat,w}}$$

Eq. (3)

H_{sat} are the saturation enthalpies. The interfacial heat fluxes, q_s and q_w, are obtained from

$$q_s=h_{sw}\left(T_{sat}-T_s\right)$$

Eq. (4)

and

$$q_w=h_{ws}\left(T_w-T_{sat}\right)$$

Eq. (5)

h_{sw} and h_{ws} are empirical heat transfer coefficients. In the current calculations, steam was assumed to be isothermal and at its saturation temperature. Therefore no heat transfer from steam to water is assumed, $q_s = 0$. The heat transfer coefficient at the water side of the phase interface was assumed to be constant at a value of 100.

The interfacial area density for a free surface flow is calculated as the absolute value of the gradient of the volume fraction, i.e.

$$A_{ws}=\frac{1}{L_{ws}}=\left|\nabla\alpha_w\right|$$

Eq. (6)

L_{ws} is an interfacial length scale.

The low-speed static enthalpy equation for the water phase with energy and mass transfer at the phase interface reads:

$$\frac{\partial\left(\overline{\overline{\rho_w}}\alpha_w H_w\right)}{\partial t}+\frac{\partial\left(\overline{\overline{\rho_w}}\alpha_w U_{m,j} H_w\right)}{\partial x_j}=-\frac{\partial\left[\alpha_w\left(\overline{\overline{q^m_{w,j}}}+\overline{\overline{q^t_{w,j}}}\right)\right]}{\partial x_j}$$
$$+\Gamma^+_{ws}H_{sat,s}-\Gamma^+_{sw}H_w+A_{ws}h_{ws}\left(T_s-T_w\right)$$

Eq. (7)

H_w is the mass-weighted static water enthalpy. The $\overline{\overline{q^m_{w,j}}}$ and $\overline{\overline{q^t_{w,j}}}$ are phase-weighted molecular and turbulent energy fluxes. The turbulent energy fluxes are calculated with the eddy diffusivity hypothesis, i.e. by dividing the eddy viscosity by a constant turbulent Prandtl number. The mass-weighted water and steam

temperatures are denoted by T_w and T_s. Definitions for the mass- and phase-weighted averages are provided by Ishii and Hibiki (2006).

The effects of turbulence on the mean flow and mean enthalpy were simulated with the SST turbulence model (Menter, 1994). The SST turbulence model is an eddy viscosity model whose transport equations are a combination of the *k-ε* and *k-ω* turbulence models, augmented by a special eddy viscosity relation. The turbulent heat fluxes were simulated using the eddy diffusivity assumption. The eddy diffusivity is calculated by dividing the eddy viscosity by a constant turbulent Prandtl number of 0.9. In ANSYS CFX, the SST model is available with so-called 'automatic wall functions'. The automatic wall functions use linear or logarithmic near-wall velocity and temperature profiles, depending on the distance of the first node of the wall.

3.3 Initial and boundary conditions

In the ROSA V Test 1-1, the water level is reduced to 80 % of the water inventory and steady-state two-phase natural circulation is established in the primary loop before ECC injection is started. At the beginning of the CFD calculations, the downcomer and the horizontal cold leg are filled with water and steam at a water level of 0.13 m, see Figure 10. The water and steam velocity is set to zero. Steam and water are at saturation temperature of 552 K. The system pressure is constant at 66.6 bar.

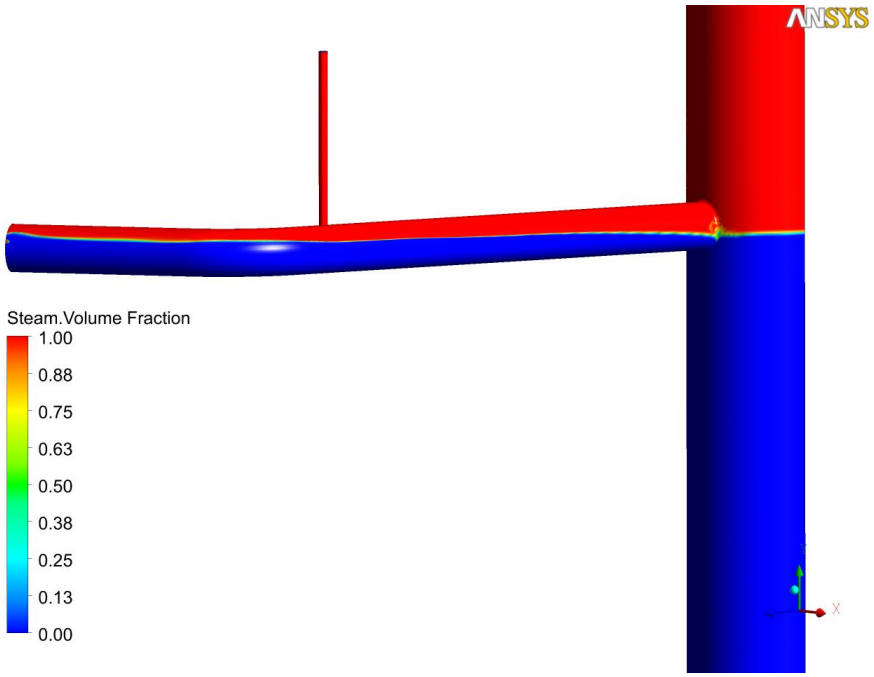

Figure 10: Initial position of free surface (front view)

In order to establish natural circulation conditions and to maintain a free surface between steam and water, the mass flow rate at the pump was linearly increased from 5 kg/s to 10.88 kg/s over a time span of 10 s. The transient calculations were continued until quasi steady-state natural circulation conditions were reached after 50 s. During the initialisation phase, the steam is accelerated by interfacial friction at the free surface and a recirculation zone is established in the downcomer where steam is entrained below the water level, see Figure 11. As observed in the experiment, the liquid level in cold leg A decreases toward the downcomer inlet (JAERI, 2008).

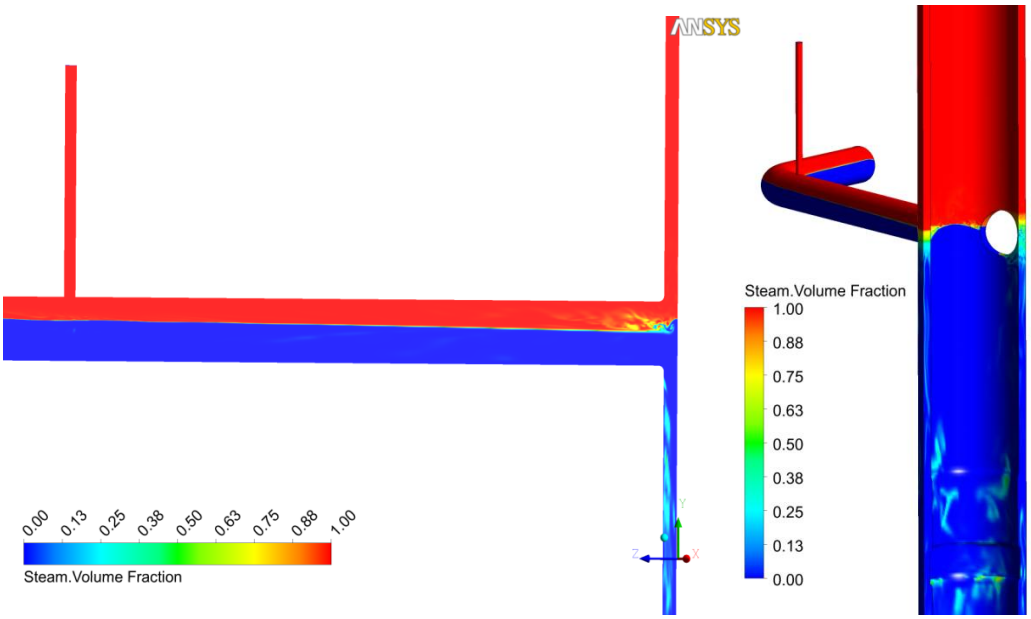

Figure 11: Initial natural circulation condition (left: center view & right: back view)

At the ECC injection nozzle, measured mass flow rates and temperatures were used as inlet boundary condition; see Figure 3 and Figure 4, respectively. The changes in temperature and mass flow rate were specified in tabular form in the ANSYS CFX input deck.

At the outlet, which was positioned at the lower part of the downcomer, a pressure boundary condition is prescribed. At the walls no-slip boundary conditions are used. The walls are assumed to be adiabatic and smooth. The non-modelled half of the downcomer is taken into account by assuming symmetry boundary conditions.

3.4 Results and comparison to data

During the initialisation phase the energy equations were not solved. At the onset of ECC injection heat and mass transfer between steam and water was considered. This type of approximation has also been used by other authors, e.g. Farkas and Toth (2009). During the transient calculation with condensation very small time steps (0.001 s to 0.0005s) had to be used in order to obtain a converged solution within each time step. In order to deliver results within the time frame of the EC-project NURISP the calculations were stopped after reaching 25 s simulation time. In the following the temperature distribution at the thermocouple rakes in cold leg A (TE-1, TE-2, TE-3) will be compared to the CFD calculations. Figure 12 to Figure 14 show the local temperature values at the central positions of the thermocouple rakes as a function of time. Symbols represent the experimental data, while continuous lines show the CFD results.

The measurement rake TE1 is located directly below the ECC-injection nozzle. At this position, the cold water impinges onto the water surface and entrains steam below the water surface. In the experiment, temperature fluctuations between 506 K and 540 K were measured close to the steam water interface. The calculated temperature drops after 8 s as observed in the experiment, however, temperature fluctuations are

stronger and vary between 498 K and 554 K (see, Figure 12). At the measurement rake TE2, which is located between the ECC-injection nozzle and the entrance to the downcomer, qualitatively good agreement is shown in Figure 13 at the onset of the temperature decrease. However, in the calculated temperatures at the bottom of the cold leg (TE-2B1/TE1184 and TE-2B2/TE1185) are lower than in the experiment, while close to the free surface (TE-2B3/TE1186 and TE-2B4/TE1187) the calculated values are higher and reach saturation temperature faster than in the experiment. The measurement rake TE3 is located at the entrance to the downcomer. The onset of cooling at TE3 is calculated in good agreement with the experimental data, see Figure 14. Finally, in Figure 15, the distribution of the void fraction along the central plane in cold leg A is shown after 25 s injection time. Below the ECC injection nozzle, steam is entrained with the impinging cold water jet and the interface between steam and water is disturbed. Steam is entrained, transported towards the downcomer and condensed before reaching the downcomer. At the entrance to the downcomer the free surface remains relatively stable compared to the start of ECC injection in Figure 11.

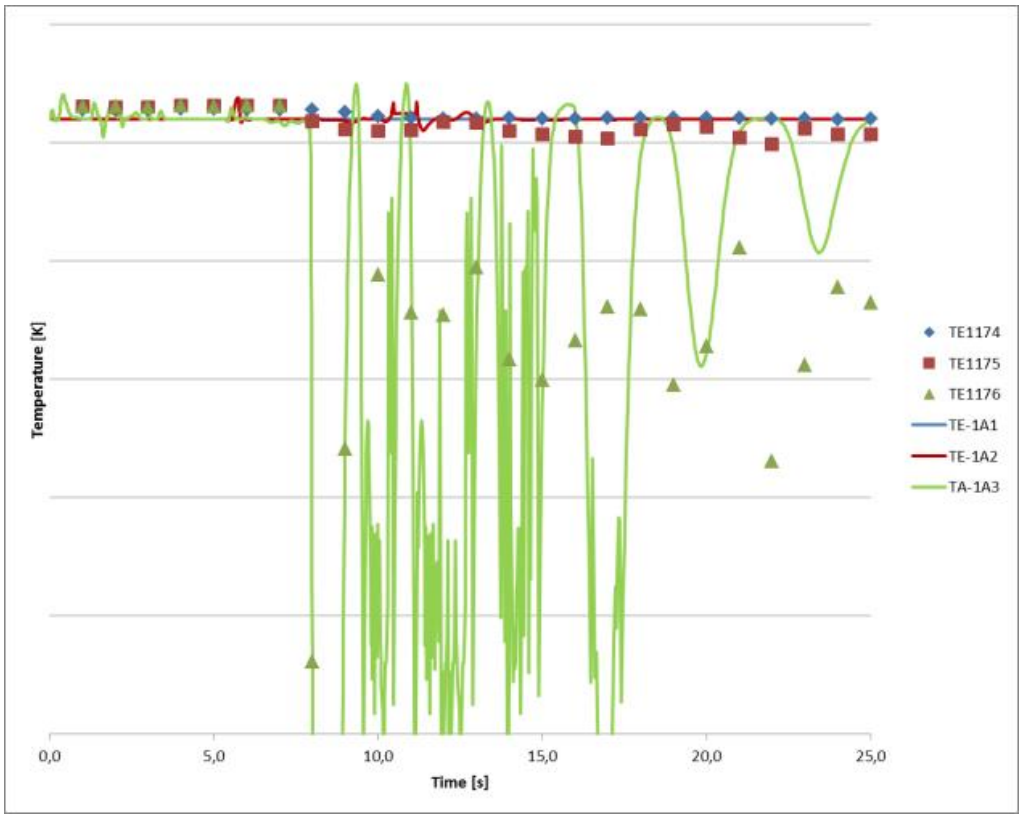

Figure 12: Transient temperature at TE1A1 – TE1A3

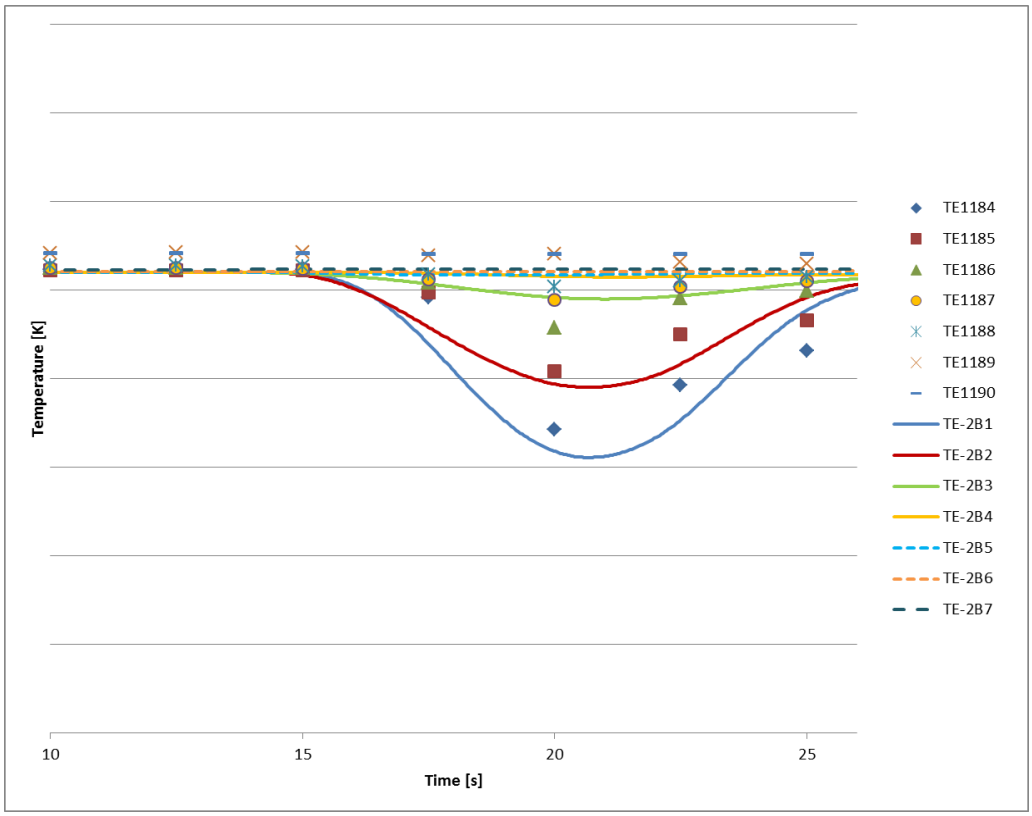

Figure 13: Transient temperature at TE-2B1 – TE-2B7

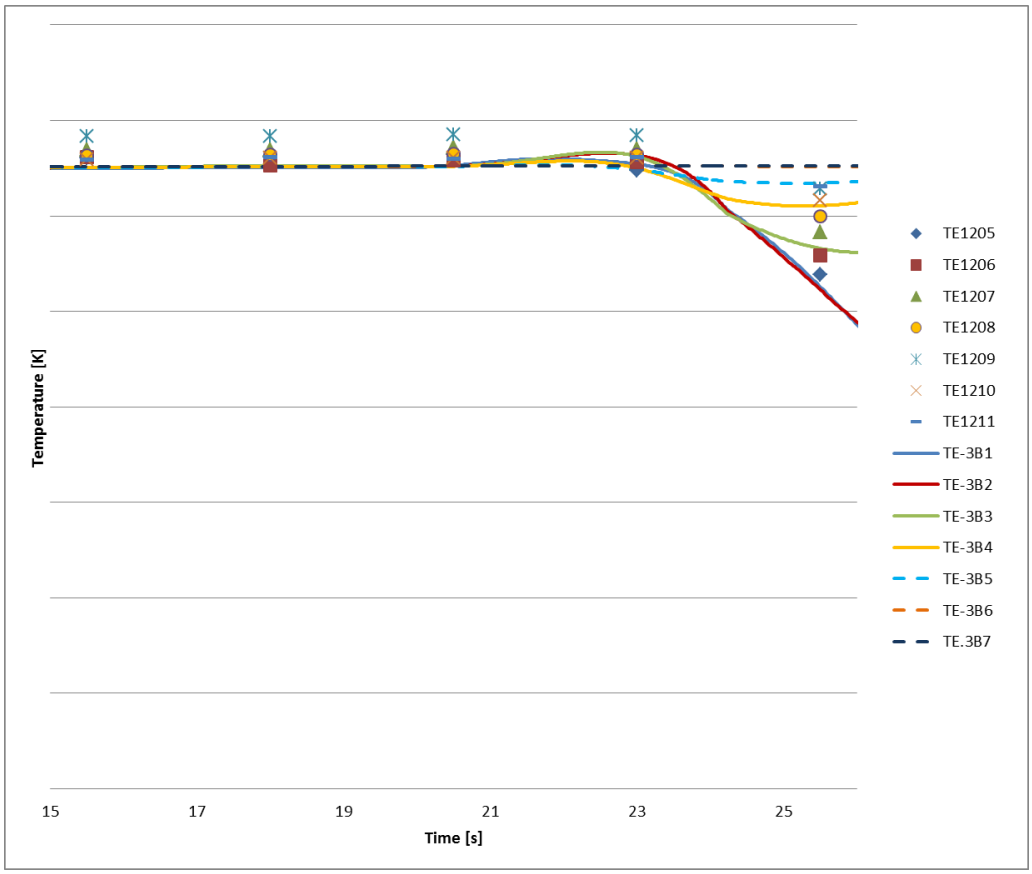

Figure 14: Transient temperature at TE-3B1 – TE-3B7

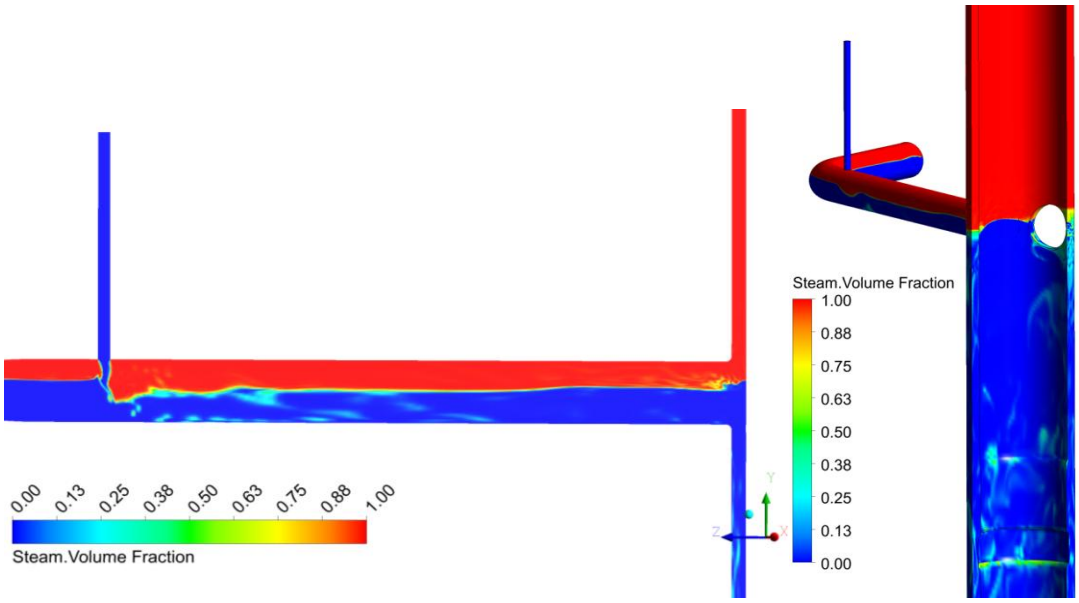

Figure 15: Void fraction distribution along center plane (left: center view & right: back view)

4. SUMMARY AND CONCLUSION

ANSYS CFX calculations were performed for the OECD ROSA V Test 1-1 at two-phase flow conditions. The experiment investigates temperature stratification during ECC-injection into the horizontal cold legs at 80% inventory and at natural circulation conditions. For this purpose thermocouple rakes were installed in the cold legs and the downcomer to measure the local temperature distribution.

The CFD analysis was performed with a structured mesh of 2.5 million nodes modeling one half of the downcomer. A homogeneous two-phase flow model was used to simulate the free surface with condensation between steam and water. Before the start of ECC-injection, the free surface flow between steam and water at quasi steady-state natural circulation conditions is established. A decrease of the liquid level towards the inlet of the downcomer is observed. Similar phenomena are described in the experimental report. The CFD results describe correctly the jet impingement on the water surface, the entrainment of steam and its transport towards the downcomer in the water layer. The comparison with temperature measurements at the central positions of the thermocouple rakes TE2 and TE3 show good agreement with data. At the thermocouple rake TE1 below the injection nozzle, the calculated temperature distribution shows higher frequency fluctuations and larger temperature differences than in the experiment. This could indicate an over-estimation of turbulence around the jet. Further conclusions about turbulent mixing and condensation in the water layer cannot be drawn before an extension of the simulation time.

5. REFERENCES

ANSYS-CFX User's Manual; http://www.ansys.com/Support/Documentation (2010)

T. Farkas, I. Tóth, "FLUENT Analysis of a ROSA Two-Phase Stratification Test", Proceedings of the 17th International Conference of Nuclear Engineering (ICONE-17), Brussels, Belgium, 12-16 July 2009, Paper 76012, (2009)

M. Ishii, T., Hibiki, Thermo-Fluid Dynamics of Two-Phase Flow, Springer Science+Business Media, New York, (2006)

JAERI, "ROSA V Large Scale Test Facility (LSTF) System Description for the Third and Fourth Simulated Fuel Assemblies", Tokai Research Establishment, Japan Atomic Energy Research Institute (2003)

JAERI, "Final Data Report of OECD/NEA ROSA Project Test 1-1", Thermohydraulic Safety Research Group, Nuclear Safety Research Centre, Japan Atomic Energy Agency (2008)

J. Mahaffy, "Best Practice Guidelines for the Use of CFD in Nuclear Reactor Safety Applications", NES/CSNI/R 5 (2007)

F. R. Menter, "Two-Equation Eddy-Viscosity Turbulence Models for Engineering Applications", AIAA-Journal, Vol. 32, pp. 269 – 289 (1994)

M. Scheuerer, J. Weiss, "CFD Calculations of OECD/NEA ROSA Test 1-1", NURISP report, EC-deliverable D2.1.2.4a (2010)

W. Wagner, and A. Kruse, "The Industrial Standard IAPWS-IF97: Properties of Water and Steam", Springer-Verlag, Berlin (1998)

6. ANNEX 1: DOCUMENT APPROVAL BY BENEFICIARIES' INTERNAL QA

Fill involved beneficiaries as appropriate (mandatory for Milestones and Deliverables, but optional for other document type)

#	Name of beneficiary	Approved by	Function	Date
1	GRS	M. Scheuerer	Author	28-03-2012
2	HZDR	P. Apanasevich	WP coordinator	12-04-2012
3	CEA	D. Bestion	SP2 coordinator	11-04-2012

EUROPEAN COMMISSION

Community Research

EURATOM

NURISP

NUclear Reactor Integrated Simulation Project

Collaborative Project (Large – scale Integrating Project)

Seventh Framework Programme EURATOM

Contract Number: 232124

Start date: 01/01/2009 Duration: 36 Months

Coupled ATHLET – ANSYS CFX Calculations of the OECD/NEA Large Scale Test Facility ROSA V Test 1-1

A. Papukchiev, G. Lerchl, M. Scheuerer (GRS, Germany)

NURISP – Contract Number: 232124

NUclear Reactor Integrated Simulation Project

Document title	***Coupled ATHLET - ANSYS CFX Calculations of OECD/NEA Large Scale Test Facility ROSA V Test 1-1***
Author(s)	Angel Papukchiev, Georg Lerchl, Martina Scheuerer
Number of pages	26
Document type	Deliverable
Work Package	WP3.3
Document number	XXXXX
Issued by	Gesellschaft für Anlagen- und Reaktorsicherheit mbH (GRS)
Date of completion	15/10/2011
Dissemination level	Public

Summary

This deliverable documents the next step of the validation process of the developed coupled code ATHLET – ANSYS CFX. The selected experiment was ROSA V Test 1-1 and within NURISP SP3 it was simulated with ATHLET - ANSYS CFX and separately with the ANSYS CFX software in order to compare the coupled results with the 3D solution and the experimental data. The test series were performed within the OECD ROSA V project in the Large Scale Test Facility. The test rig is a 1:48 volume scaled model of a four loop Westinghouse pressurized water reactor. The ROSA V Test 1-1 investigates the temperature stratification under natural circulation conditions in LSTF primary circuit during cold water injection in the cold legs.

The coupled 1D-3D and the stand alone 3D simulations were performed for single phase, natural circulaiton flow conditions. A hexagonal ANSYS CFX mesh representing part of the LSTF cold leg A with the injeciton nozzle was generated. Cold leg A is instrumented with 3 different measurement rakes with 45 thermocouples and provides enough data for the validation process of the coupled code. The final grid selected for the simulations consisted of 1.3 M elements. The transient calculations started at natural circulation conditions and a steady-state solution was used for the initialisation of the calculations. For the 3D stand alone simulations, measured mass flow rates and temperatures were used, while in the coupled simulations these were provided by ATHLET.

The comparison with experimental data showed good agreement in the TE3 and larger deviations in the TE2 measurement rake, which is close to the ECC injection nozzle. Possible reasons for these are insufficient geometry modeling or inadequacy of the turbulence models to simulate the combination of impinging jet flows with strong buoyancy effects. Nevertheless, a very good agreement between stand-alone calculations with ANSYS CFX, and coupled 1D-3D ATHLET – ANSYS CFX calculations has been observed, proving the consistency of the new coupling methodology.

Approval

Rev.	Date	First author	WP leader	SP or Project Coordinator
0	10/2011	A. Papukchiev (GRS)	P. Emonot (CEA)	M. Zimmermann (PSI)
		15/10/2011	XXXX	XXX

Distribution list

Name	Organisation	Comments
Michel HUGON	EC DG RTD	
All beneficiaries	NURISP	Through NIWS

Abbreviations

ECC	emergency core cooling
CAD	computer aided design
CFD	computational fluid dynamics
LES	large eddy simulation
LOCA	loss of coolant accident
LSTF	large scale test facility
NPP	nuclear power plant
OECD	organisation for economic cooperation and development
PP	primary coolant pump
PWR	pressurized water reactor
RMS	root mean square
RPV	reactor pressure vessel
ROSA	rig of safety assessment
BSL RSM	baseline Reynolds stress model
SAS	scale adaptive simulation
SST	shear stress transport
SBLOCA	small break loss of coolant accident
SG	steam generator
TH	thermal-hydraulic
VVER	water water energy reactor (Russian PWR design)

Contents

1 Introduction 6

2 Large Scale Test Facility ROSA V Experiment 7

2.1 Upgrades for ROSA Test 1-1 10

2.2 ROSA V initial conditions 13

3 Pressurized Thermal Shock Simulations 14

3.1 Initial and boundary conditions 14

3.2 1D simulations with the system code ATHLET 15

3.3 3D simulations with the CFD program ANSYS CFX 15

3.3.1 Grid generation 15

3.3.2 Mathematical models 17

3.4 Coupled 1D-3D simulations with ATHLET - ANSYS CFX 17

4 Analysis and Comparison of the Results with Experimental Data 19

5 Conclusions 26

6 References 27

7 Annexes 28

7.1 Annex 1: Document approval by beneficiaries' internal QA 28

1 Introduction

Thermal-hydraulic (TH) system codes are being successfully used in the last decades for the analyses of the physical behavior of nuclear power plants (NPPs) under off-normal or accidental conditions to evaluate and improve the design, operation and safety of current nuclear installations. These codes are extensively validated against experiments and provide reliable results at comparatively low computational cost. Nevertheless, such programs use simplifications in the mathematical models describing the simulated systems. Balance equations for mass, momentum and energy for the two phases are obtained by averaging local basic flow equations over coarse meshes in space and solved mostly in 1D direction. As a result, mean values for relevant physical parameters are calculated, which in reality are spatially distributed fields. However, for specific nuclear reactor safety problems with well pronounced 3D mixing effects, like boron dilution, pressurized thermal shock, and main steam line break, a high spatial resolution and 3D flow modeling is needed.

Computational fluid dynamics (CFD) codes are capable to predict three-dimensional fluid flow behavior in complex geometries and can provide detailed distributions of the physical parameters in space and time. Such programs are already widely used in the oil, automotive, power generation, marine, aviation and other industries. Unfortunately, CFD simulations require very high computation time so that a full CFD representation of the primary circuit of a NPP is currently not feasible. Therefore, stand-alone 3D CFD simulations are performed only for certain parts of the primary circuit where 3D phenomena occur (e.g. the downcomer).

In order to perform advanced best-estimate analyses and overcome the deficiencies of CFD and system codes at the same time, a direct coupling of these simulation tools is pursued. A new methodology for the coupling of the GRS TH system code ATHLET with the commercial CFD software package ANSYS CFX is currently being developed at GRS. Main efforts are related to the implementation of explicit and semi-implicit schemes, to the simulation of different test configurations as well as to the validation on large scale experiments. First verification calculations have already been reported in [1, 2]. Within the framework of this European Nuclear Reactor Integrated Simulation Project (NURISP), ATHLET – ANSYS CFX validation activities for the new coupled code have been carried out. The selected experiment was dedicated to the pressurized thermal shock (PTS) phenomenon and performed within the OECD/NEA Rig of Safety Assessment (ROSA) V project in the Japanese Large Scale Test Facility (LSTF). It deals with flow mixing and temperature stratification during emergency coolant injection in the primary circuit of a pressurized water reactor (PWR). Pressurized thermal shock may occur when cold water is injected in the primary circuit filled with hot coolant. The cold water might rapidly cool down the reactor pressure vessel (RPV) wall when entering the downcomer. This greatly increases the potential for RPV failure by cracking. Due to the 3D nature of the stratification and mixing phenomena, such reactor safety problems need to be simulated with advanced 3D tools. In this report, coupled ATHLET - ANSYS CFX simulations and data for the ROSA V Test 1-1 are compared and assessed. As the experimental data is proprietary, absolute temperature values could not be provided.

2 Large Scale Test Facility ROSA V Experiment

The LSTF was designed in Japan to simulate thermal-hydraulic phenomena which occur during small break loss of coolant accidents (SBLOCAs) and operational transients. It has prototypical component elevation differences, large loop piping diameters, prototypical primary pressure levels, simulated system controls, and core power level sufficient to simulate the core power decay heat starting from a few seconds after SCRAM [3]. The reference reactor for the LSTF is Tsungura-2, a 3423 MW_{th} (1100 MW_e) 4 loop Westinghouse type pressurized water reactor. Figure 1 shows a picture of the LSTF on the left side and in comparison a scheme of a Westinghouse type PWR to the right.

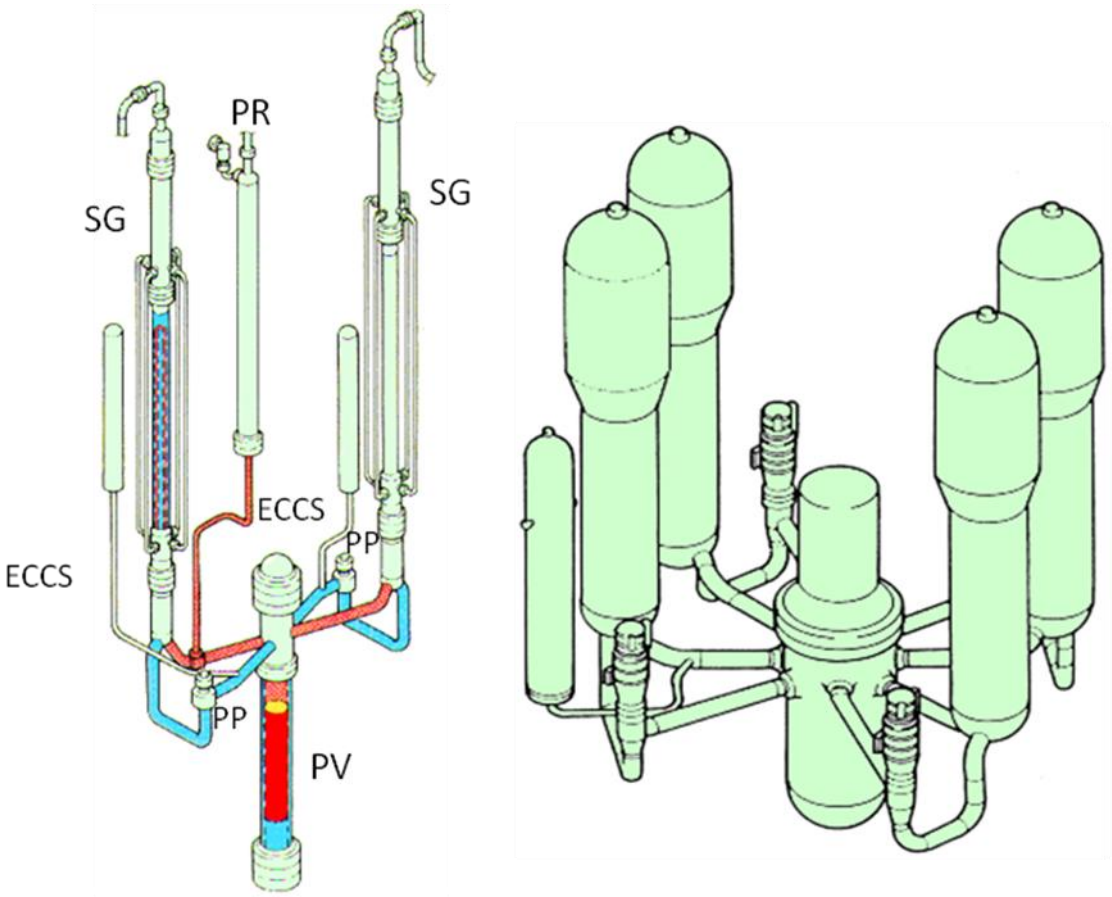

Figure 1: Large Scale Test Facility and scheme of a Westinghouse PWR

The LSTF was constructed with two loops (loop A and loop B), including the steam generators (SG), the primary coolant pumps (PP), one hot and one cold leg in each loop. These two loops are nearly identical, the only differences are related to the inclination of the emergency core cooling (ECC) injection line to the cold leg pipe and the pressurizer connected to the hot leg of loop A. In loop A, the ECC line is perpendicularly attached to the cold leg, which represents the Russian VVER design. In loop B the ECC line is attached to the cold leg with an angle of 45°, which is similar to the European and American PWR designs.

The LSTF is volume scaled at 1/48 of its reference reactor, but it has the same heights (approx. 30 m). The pressure level which can be reached is also similar to the nominal pressure in current PWRs. (approx. 16 MPa). The LSTF core is equipped with 1008 electrical heater rods with a total thermal power of 10 MW. In the whole facility, approx. 2500 instruments are installed to measure different parameters [4].
Figure 2 shows the plan view of the pressure vessel and the two loops. In cold leg A, the coolant flows after the PPs through an elbow part before it enters the straight part of the cold leg A attached to the pressure vessel. The length and the diameter of the cold legs A and B are identical. In cold leg A, the ECC line is located behind the elbow part and is connected perpendicularly to the cold leg, as already explained. In loop B, the ECC line is inclined and located between the primary pumps and the elbow junction.

Figure 3 shows a comparison between the dimensions of the pressure vessels of a real PWR and the LSTF. The heights of the pressure vessels are comparable (PWR: ~12.5m; LSTF: ~11m) and the hot and cold legs are attached at the same levels. However, the diameter of the LSTF pressure vessel is much smaller (PWR inner diameter: 4.4 m; LSTF inner diameter: 0.6 m), which led to the volumetric scaling ratio of 1/48.

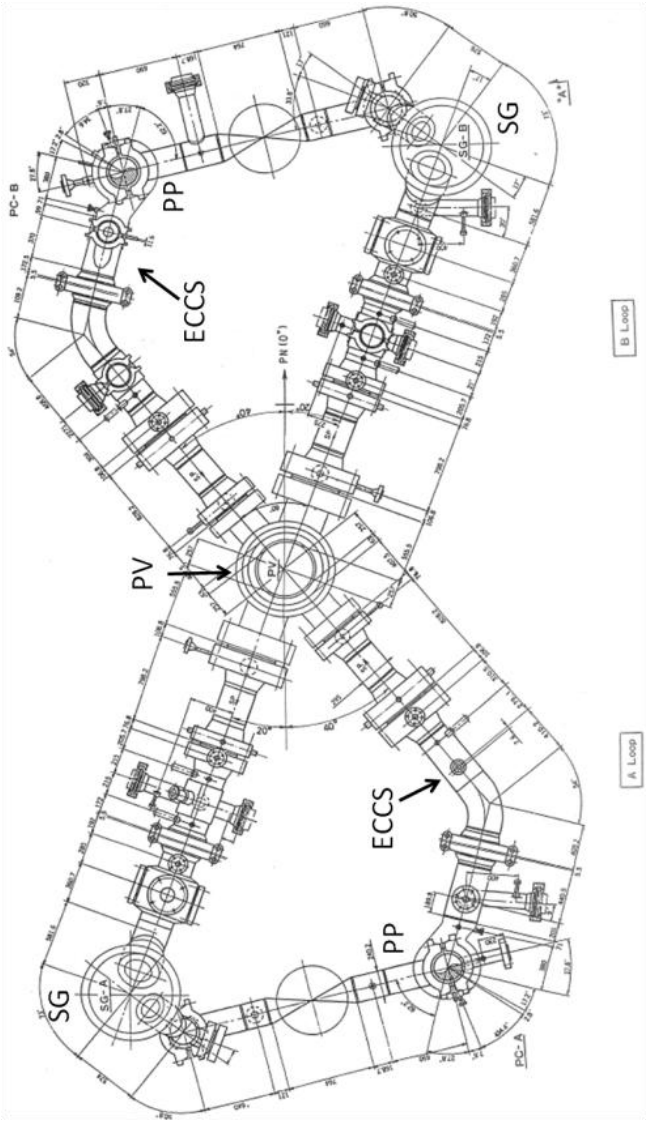

Figure 2: Primary Loop Dimensions (Plan View)

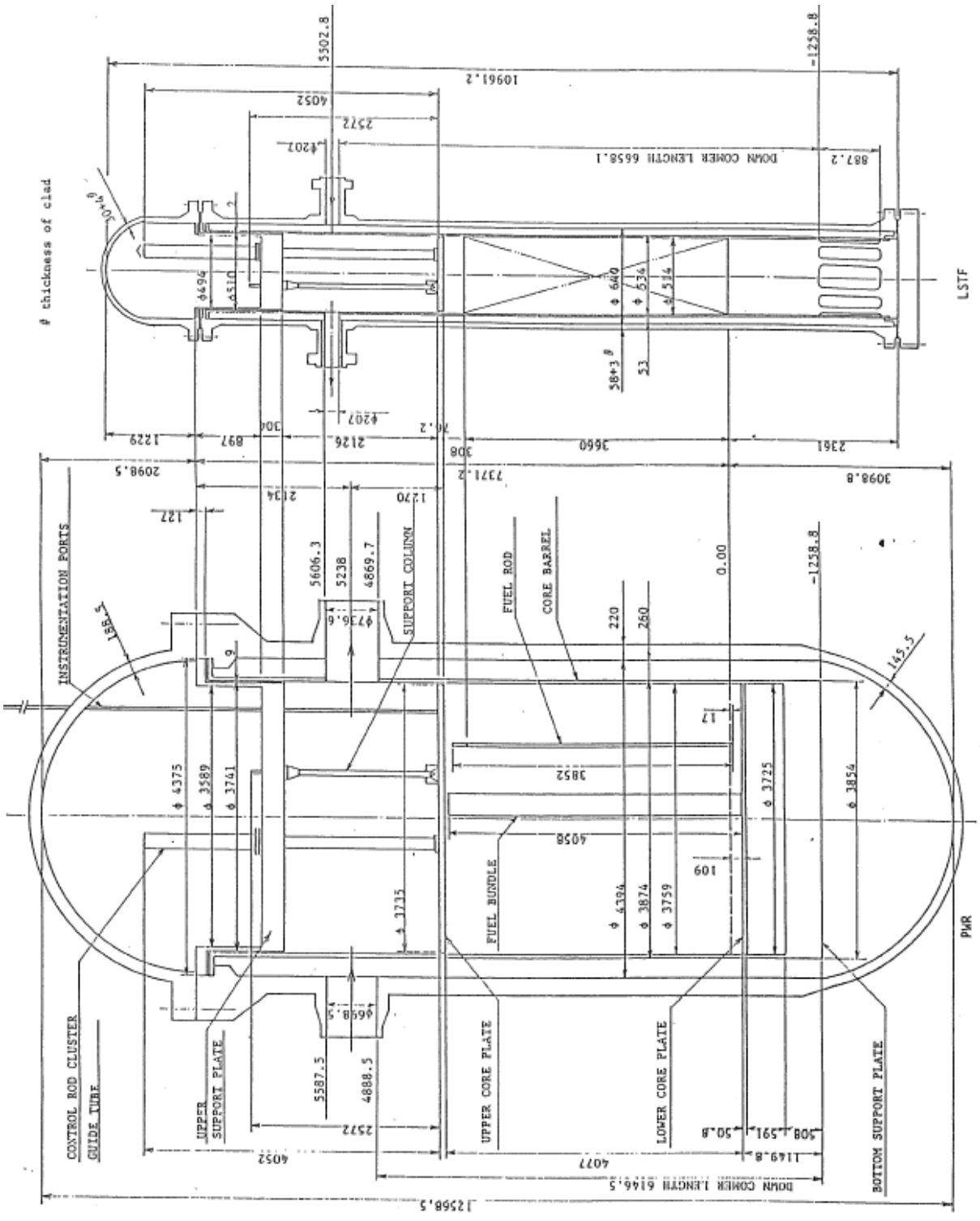

Figure 3: Comparison of PWR and LSTF pressure vessel dimensions

2.1 Upgrades for ROSA Test 1-1

On October, 26th and 27th, 2006 the OECD/NEA ROSA Project Test 1-1 was conducted at the LSTF. Its objective was to simulate PTS phenomena in reactor primary circuit and to obtain the multidimensional temperature distributions in cold legs and downcomer during ECC water injection for validation of computer codes and models [5]. For these measurements, the equipment of the LSTF had to be upgraded. The locations of the 144 new thermocouples, which were installed for this test, are explained in Fig. 4.

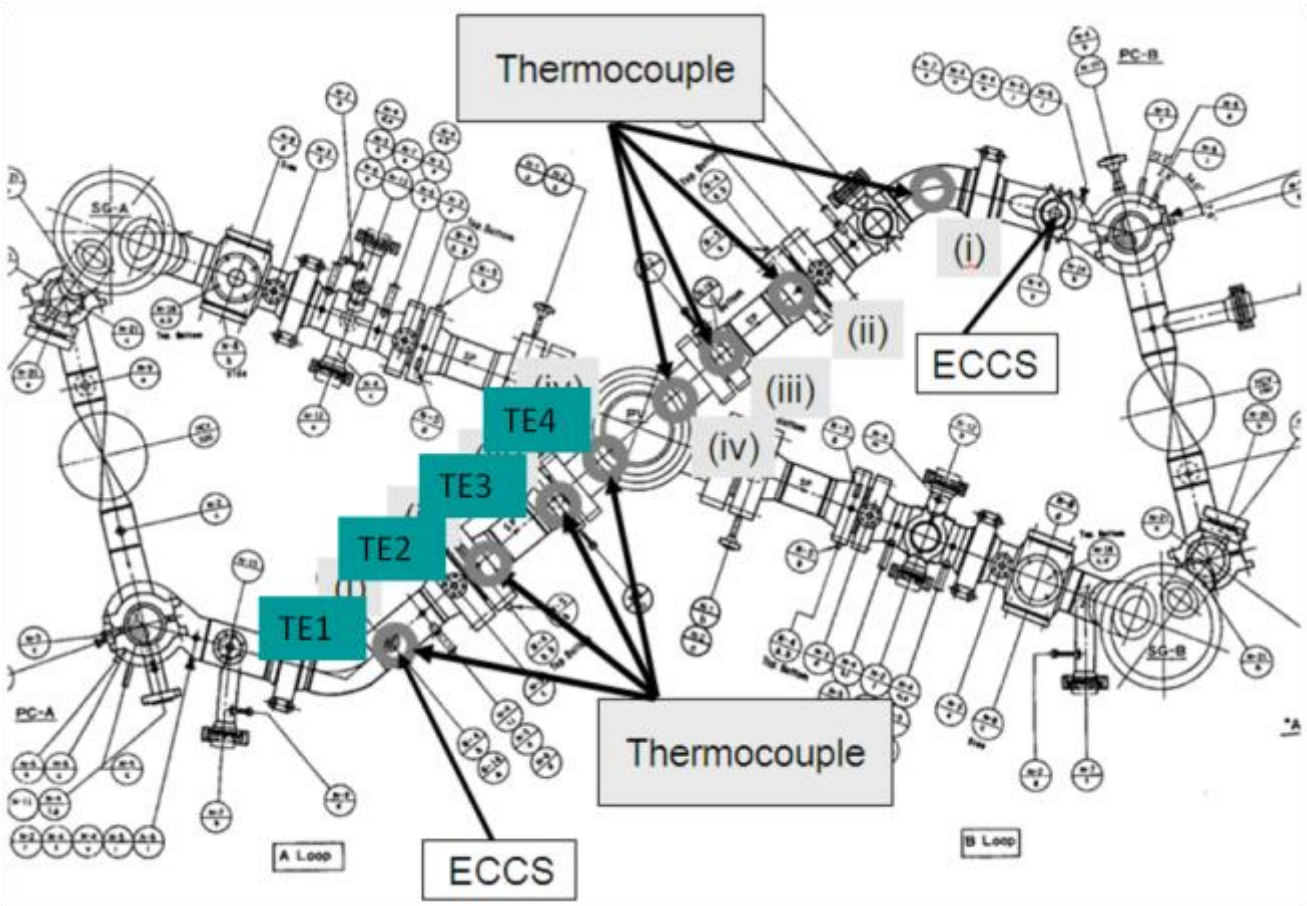

Figure 4: Location of new thermocouples in cold legs and downcomer

The newly installed thermocouples have an uncertainty of +/- 2.75 K and provide data in the range between 270 K and 720 K. There are 3 positions in cold leg A where rakes with thermocouples are installed. The first rake, which is called TE1, consists of three thermocouples located just under the ECC line (see Fig. 5).

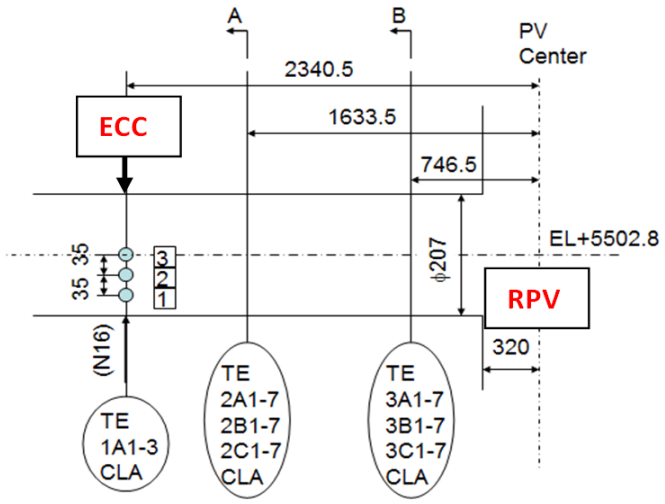

Figure 5: Locations of new thermocouples in cold leg A

It is located directly under the injection nozzle of the ECC line which center is placed at a distance of 2340 mm from the center of the pressure vessel. The picture in Fig. 6 shows the installed thermocouples of rake TE1 in the cold leg and also the ECC nozzle can be seen. The support rod for the TE1 thermocouples is 8 mm in diameter and is inserted from the bottom to the center of the cold leg A.

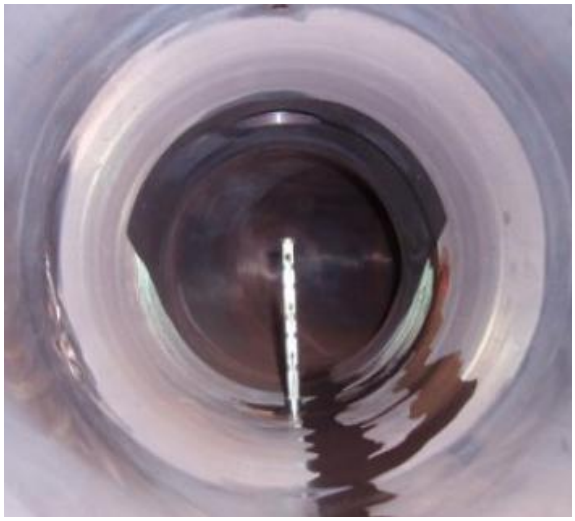

Figure 6: Thermocouples of group TE1 and ECC nozzle

The positions of rakes TE2 and TE3 are located further downstream (TE2: 0.7 m; TE3:1.6 m downstream of the ECC nozzle, Fig. 5) in the cold leg and consist of 21 thermocouples each. The cross-section A and B of Fig. 5 is shown in Fig. 7:

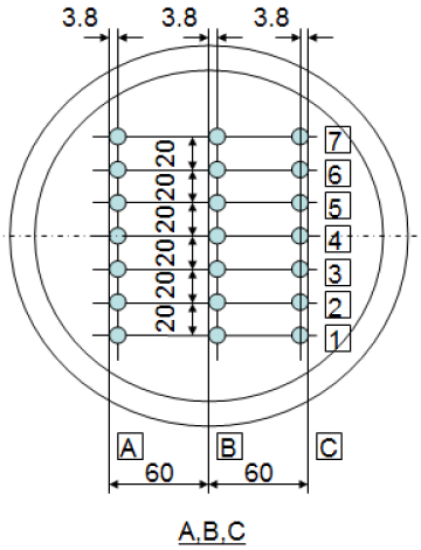

Figure 7: Locations of new thermocouples of rakes TE2 and TE3 in CLA

The thermocouples are distributed in three columns and seven rows and were placed at the ends of a spool piece flange which is shown in Fig. 8:

Figure 8: Thermocouples in spool piece flange

The support rods for the thermocouple rakes TE2 and TE3 are 6 mm thick and are inserted from the bottom to the top of the cold leg. The experimental data from these two rakes was used for comparison with the results from the performed calculations within this NURISP work package.

2.2 ROSA V initial conditions

Table 1 summarizes the LSTF steady-state, nominal, operating parameters, used as initial conditions for the experiment. These initial conditions (except the core power) were used for the SBLOCA experiments, where temperature stratification phenomena at high pressure and high temperature were of interest [5].

Table 1: Initial conditions of the ROSA V Test 1-1

Pressurizer pressure	15.5 MPa
Pressurizer liquid level	7.2 m
Core Power	~6 MW
SG pressure	6.5 MPa
SG secondary side liquid level	9.1 m
Primary loop flow rate	24.3 kg/s
Primary coolant pump speed	800 rpm
Hot leg temperature	598.0 K
Cold leg temperature	562.0 K

After reaching these parameters, the core power is reduced to 1.4 MW, which corresponds to 2% of the scaled nominal power, and the primary coolant pumps are stopped. Steady-state natural circulation is then established in the primary loop. A loop flow rate of 5.8 ~ 6.0 kg/s was measured in the loop-seal section. This steady-state natural circulation is a single-phase natural circulation at 15.5 MPa with 100% primary inventory. The ECC water is injected separately into the cold leg A and B. The injection flow rates are 0.3 kg/s and 1.0 kg/s and the temperature of the ECC water is approx. 300 K.

The simulation results presented in this work are focused only on the first phase of Test 1-1, where ECC water was injected for about 110 s in the cold leg A at these conditions. The temperature difference between the hot water in the primary system and the cold ECC water is almost 250 K resulting in density differences greater than 200 kg/m^3.

3 Pressurized Thermal Shock Simulations

Pressurized thermal shock may occur when cold water is injected in the primary circuit filled with hot coolant. The cold water may rapidly cool down the RPV wall when entering the downcomer. This greatly increases the potential for RPV failure by cracking. The cool down process can be even intensified by a thermal stratification in the cold leg. Thermal stresses are more dangerous for the RPV downcomer compared to the cold leg structures because of its thick walls and the presence of welds. Due to the 3D nature of the stratification and mixing phenomena, such reactor safety problems need to be simulated with advanced 3D CFD tools. This experiment is challenging for any thermal-hydraulic program and even more for coupled codes because strong buoyancy and mixing effects at natural circulation conditions have to be addressed in a proper manner. The next paragraphs describe the simulation setups, while final results are discussed in chapter 4.

3.1 Initial and boundary conditions

In this work, three different simulations were performed – ATHLET stand alone, ANSYS CFX stand alone and a coupled ATHLET – ANSYS CFX calculation. The transient ANSYS CFX stand-alone and the coupled calculations were started from a steady-state solution of the natural circulation part of ROSA Test 1-1, while ATHLET stand-alone calculations involved also the simulation of the transition from forced to natural circulation in LSTF. For the CFD stand-alone simulations, time-dependent measured mass flow rates and temperatures were specified at the inlet boundaries. At the outlet, a constant pressure boundary condition was prescribed and at the walls, no-slip boundary conditions for smooth surfaces were used.

In the coupled 1D-3D calculations the transient mass flow rates and temperatures were calculated by ATHLET – ANSYS CFX, because in this case the thermal-hydraulic configuration is not an open system (like the stand-alone CFD calculations with the cold leg A), but a closed system representing the complete LSTF. Table 2 shows the initial values of the main thermal-hydraulic parameters.

Table 2: Initial conditions.

Parameter	Initial value
Fluid temperature at pump exit	553.7 [K]
Mass flow rate at pump exit	5.9 [kg/s]
Fluid density at pump exit	764 [kg/m^3]
Fluid velocity at pump exit	0.24 [m/s]
Pressure at cold leg outlet	15.5 [MPa]

3.2 1D simulations with the system code ATHLET

For the 1D system code calculations, detailed 1D ATHLET input deck for the LSTF was used. Both loops A and B were modeled and connected to a RPV with two-channel downcomer and core representation. The pressurizer has been simulated with five nodes and connected via the surge line to the hot leg of loop A. Fine nodalization scheme with three different heat exchanger U-tube bundles (short, medium and long) has been developed for the modeling of the steam generators' primary sides (Fig. 9). The secondary side is also modeled in detail. With this input deck several ATHLET stand-alone calculations have been performed not only for the single phase, but also for the two-phase part of Test 1-1. The calculated averaged thermal-hydraulic parameters were in good agreement with experimental data.

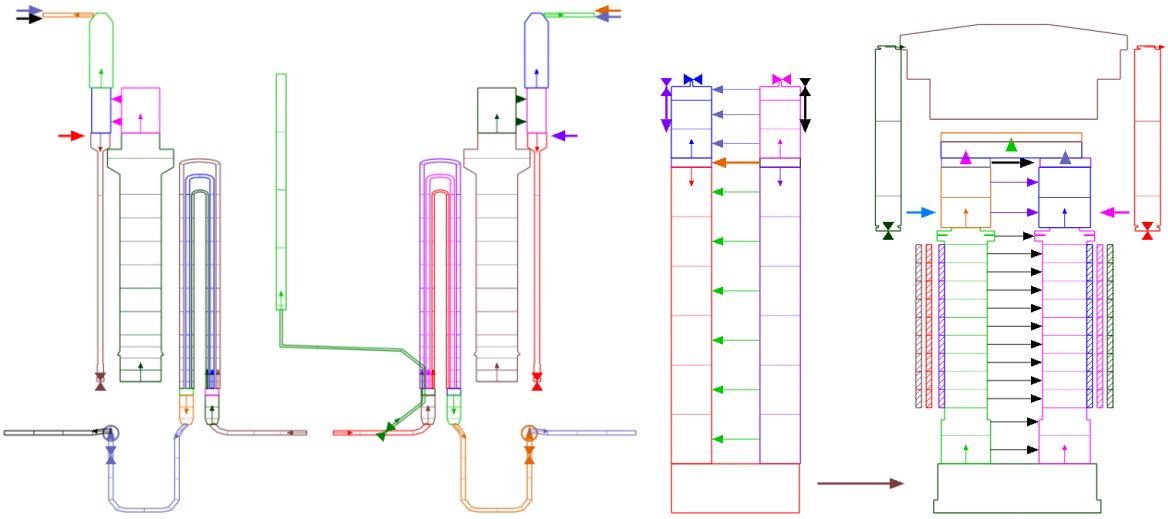

Figure 9: ATHLET model of LSTF.

3.3 3D simulations with the CFD program ANSYS CFX

3.3.1 Grid generation

A CAD model of the LSTF cold legs, ECC lines, and downcomer was generated on the basis of the available drawings (Fig. 9). This geometry served as an input for the ICEM CFD software, which has been used to prepare systematically refined hexahedral grids. Careful grid sensitivity studies [6] were performed in accordance with the OECD/NEA Best Practice Guidelines [7].

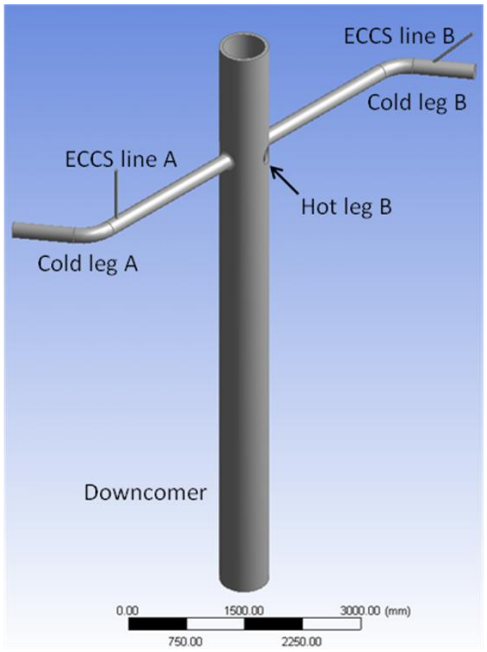

Figure 9: ANSYS CFX model of LSTF.

Since the main objective of this coupling study was to validate the ATHLET-ANSYS CFX coupling methodology and to investigate the thermal mixing and subsequent stratification in the cold leg A, it was decided to accelerate the calculations by “cutting” the 4 m long section of the LSTF cold leg A between the main coolant pump and the RPV downcomer (which includes the ECC injection nozzle) and to use it for the ANSYS CFX stand-alone and coupled calculations. This part of the cold leg is well instrumented with measurement rakes TE2 (close to the ECC injection) and TE3 (close to the RPV downcomer) which results in 2x21 thermocouples in total. Additional thermocouples are positioned under the ECC injection line (TE1). After refinement, the final mesh of the cold leg A consisted of 1.13 million elements (Fig. 10). Figure 11 gives an impression how in reality a measurement rake with 21 thermocouples looks like. The geometry of the rakes was not resolved in the numerical grid.

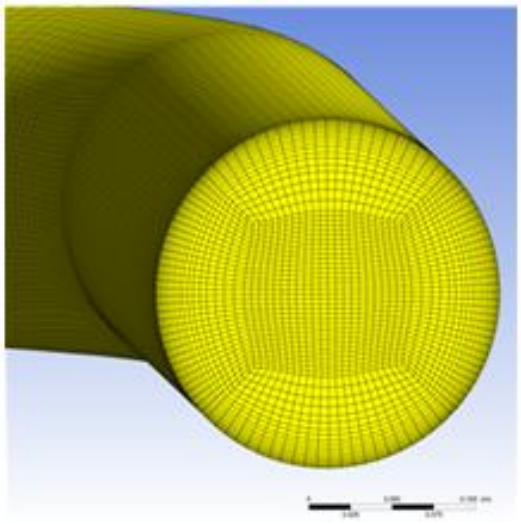

Figure 10: ANSYS CFX grid.

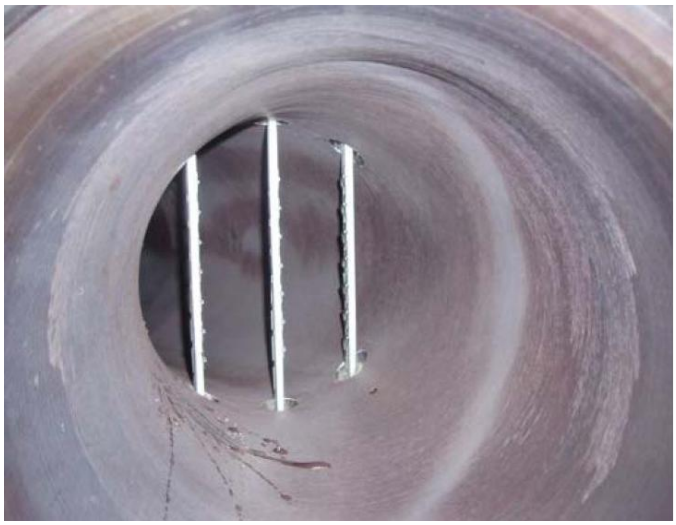

Figure 11: Rake with thermocouples.

3.3.2 Mathematical models

For the correct modeling of the buoyant flows in the LSTF, buoyancy terms in the momentum equation and in the production terms of the turbulence model equations have been included. These are driven by the density difference between the hot and cold water, while water density is calculated as a function of temperature on the basis of IAPWS-IF97 tables [8]. Dynamic viscosity and heat conductivity of the fluid are also derived from these tables.

Preliminary calculations with two turbulence models were carried out - the Shear Stress Transport (SST) model of Menter [9] and the Baseline Reynolds Stress turbulence model (BSL RSM) [10]. The simulations with the more complex BSL RSM showed slightly better agreement with experimental data, and therefore it was selected for the coupled 1D-3D calculations. Both models were combined with 'automatic' wall functions in which the near-wall fluxes are derived from either linear or logarithmic wall laws, depending on the position of the wall-adjacent grid point.

In a next step, the numerical and model errors have been assessed. The ANSYS CFX convergence criteria have been set to root mean square (RMS) residual target 1.E-4 and the mass conservation target was set to 1.E-3. A first order upwind advection scheme was used in the simulations, because the second-order high resolution scheme predicted, as expected, more oscillatory flow behavior. Constant 0.05 s time steps have been selected for both ANSYS CFX stand-alone and the coupled ATHLET - ANSYS CFX calculations.

3.4 Coupled 1D-3D simulations with ATHLET - ANSYS CFX

For the simulations with ATHLET - ANSYS CFX, a coupled 1D-3D model of the LSTF has been developed. In the first step, the 1D ATHLET pipe section in the cold leg A between the main coolant pump and the RPV downcomer, was "replaced" with the same 3D ANSYS CFX pipe section (as described in chapter 3.3.1). For this purpose, the thermal-hydraulic parameters were exchanged after each time step between the programs. The ATHLET - ANSYS CFX model of the LSTF can be seen in Fig. 12. In this way, the part of the primary circuit with complex 3D phenomena is treated with ANSYS CFX (cold leg A), and ATHLET is used to provide fast solution for the flow behavior in those areas where 1D simulation is adequate (the rest of the system). The coupled calculation was started two seconds before the injection of the cold water in order to allow both codes to find a stable solution for the natural circulation conditions.

The 3D CFD and the coupled 1D-3D calculations were performed with the ANSYS CFX software (Version 11) and ATHLET Mod. 2.2 Cycle A. These were run on eight Intel Woodcrest 3.0 GHz CPUs integrated in a Sun Blade X6250 cluster system. Both ANSYS CFX and ATHLET - ANSYS CFX calculations of 125 s transient time and 0.05 s time step size run approximately five days. In the coupled simulations, ATHLET CPU time is so small that it can be neglected.

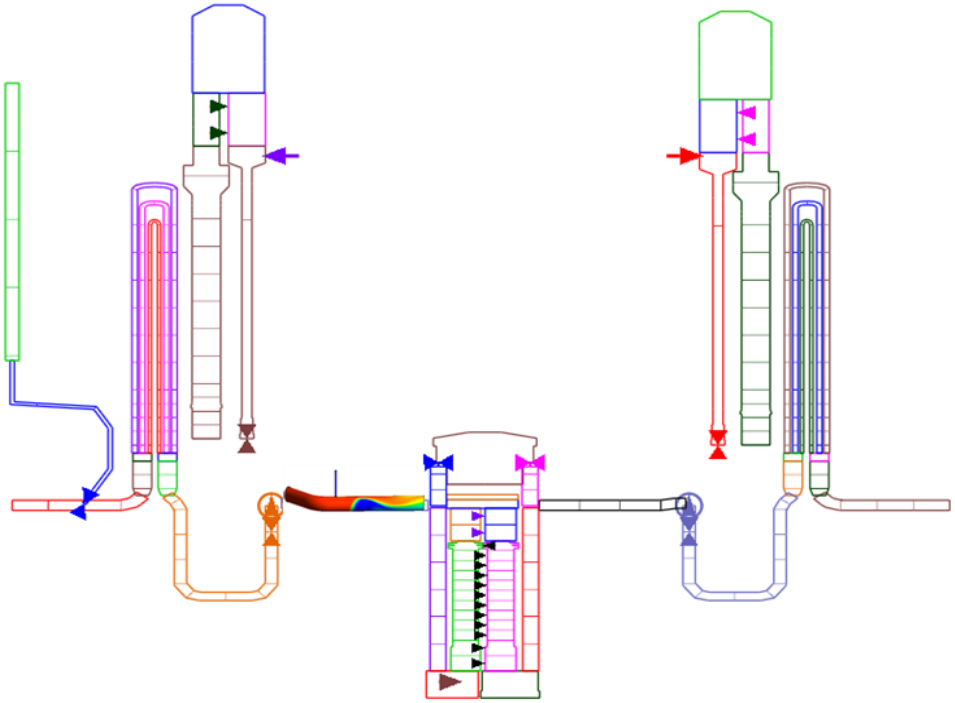

Figure 12: ATHLET – ANSYS CFX model of the LSTF RPV and loop A.

4 Analysis and Comparison of the Results with Experimental Data

As already mentioned, the simulation results of the ATHLET-ANSYS CFX calculations were not only compared with LSTF ROSA V experimental data, but also with ANSYS CFX stand-alone results. In this chapter, multiple plots are exposed, where blue color is always used to present the experimental data, green - the ANSYS CFX stand-alone results, and red – the coupled ones.

In the first step of the comparative analysis, the results from the coupled 1D-3D simulations were visualized with the help of ANSYS CFX Post software. Figure 13 shows the calculated temperature distribution during ECC injection at the wall (left picture) of the cold leg A and its central longitudinal section (right picture). The vertically downwards injected cold ECC water hits the bottom of the cold leg and then swashes to the left and right pipe walls. Due to its higher density, the cold water pushes the lighter hot water to the top and gradually stratifies at the bottom of the cold leg. This can be also observed in Fig. 14 which shows the temperature distribution in the cross-section planes 0.45 (top, left), 0.90 (top right), 1.35 (bottom left) and 1.80 m (bottom right) from the ECC injection nozzle in the direction of the RPV inlet. One sees that horizontally shaped and stratified temperature layers build up approx. 0.3 m away from the RPV entrance (bottom right picture). The maximum temperature difference between top and bottom of the pipe in this cross-section is 12 K.

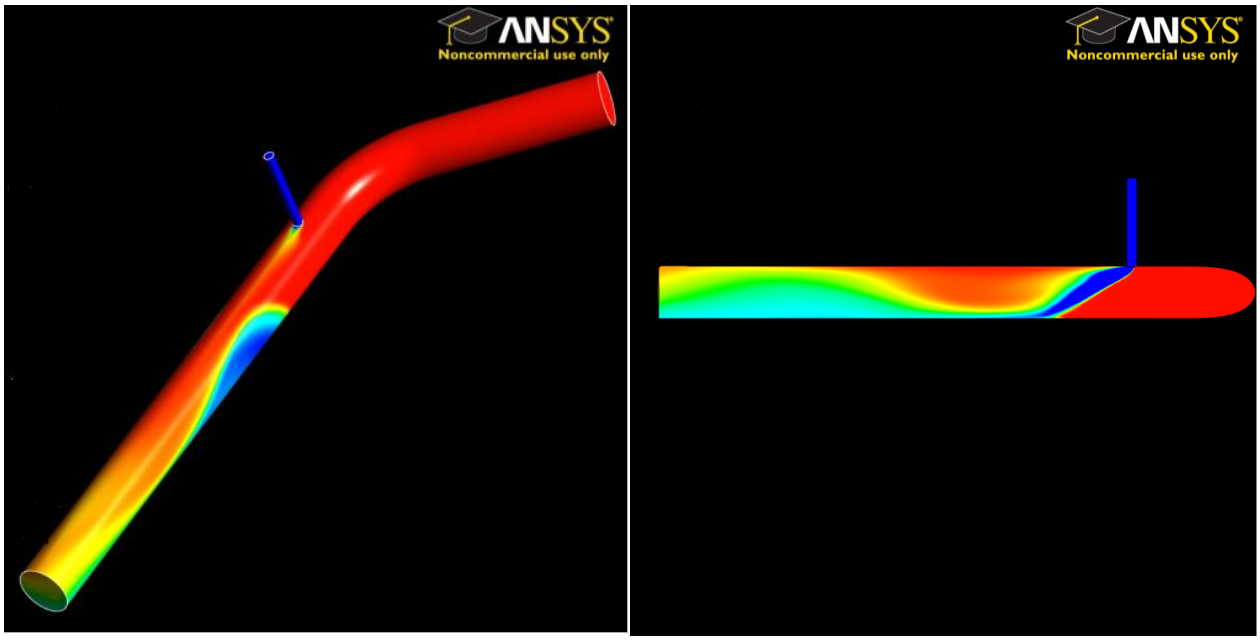

Figure 13: Calculated temperature distribution in the cold leg A.

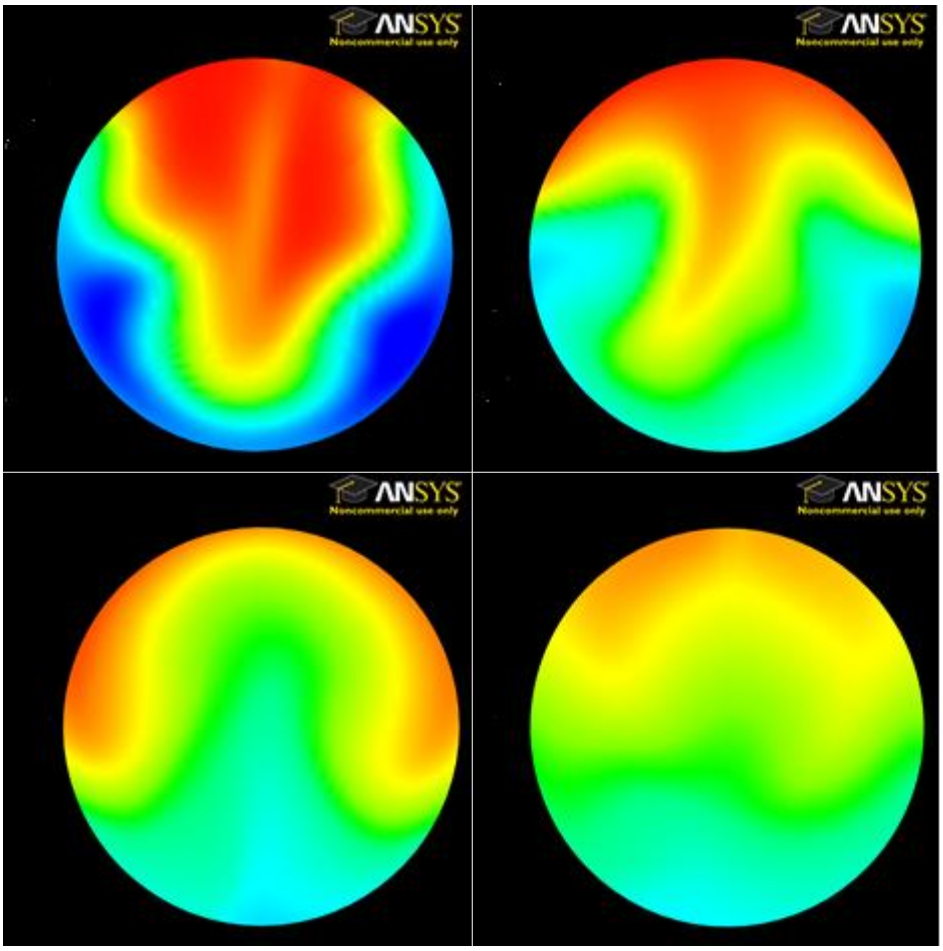

Figure 14: Temperature distribution 0.45 (top left), 0.90 (top right), 1.35 (bottom left) and 1.80 m (bottom right) from the ECC injection nozzle.

Figure 15 shows the comparison to data for the thermocouple TE1205 (rake TE3) which is situated centrally at the bottom of the cold leg A, 1.59 m from the ECC injection nozzle and close to the LSTF pressure vessel entrance (Fig. 5). Since the OECD ROSA data are restricted, no absolute numbers can be shown. Nevertheless, one still can see the very good agreement between experiment and both calculations. Generally, the results in the measurement rake TE3 compare good to the experimental data.

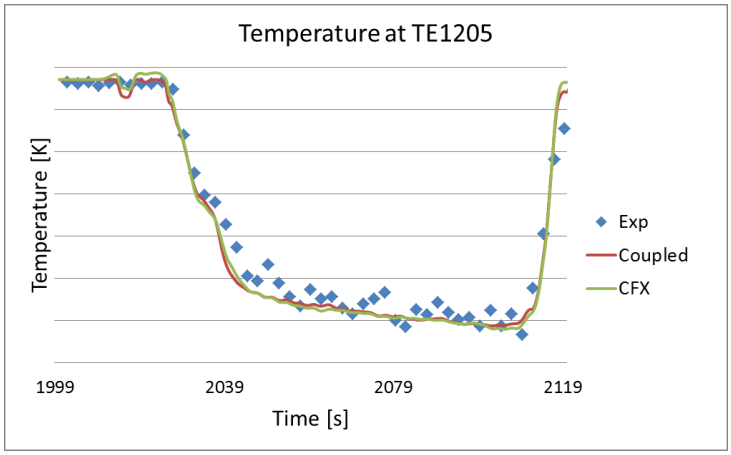

Figure 15: Local temperature at TE1205 (TE3).

Thermocouple TE1184 is located at the same bottom position (like TE1205), but in the TE2 measurement rake, which is situated just 0.7 m away from the ECC injection nozzle. In this case, the distribution of the cold water in the pipe cross-section is not predicted correctly by the code and the temperature in the bottom part of the cold leg A is higher than the measured one (Fig. 16). The maximum temperature deviation from the experimental data for this thermocouple is almost 8 K.

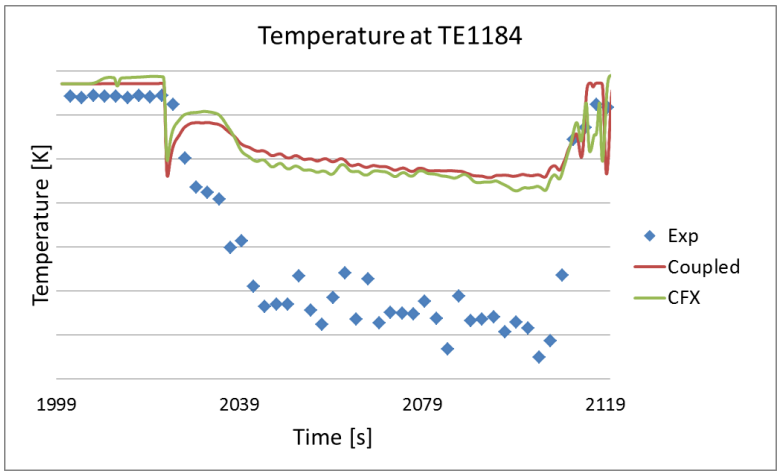

Figure 16: Local temperature at TE 1184 (TE2).

Figures 15 and 16 are representative for the results in the two rakes – TE2, which is close to the ECC nozzle and TE3 which is close to the RPV downcomer. Nevertheless, in order to better assess the performance of ANSYS CFX and the coupled code, it should be investigated if the 3D solver was able to capture the temperature distribution over the entire pipe cross-section. For this reason, nine plots for each instrumentation rake (positioned in its top, middle and bottom parts) were generated. Figures 17 and 18 show the exact positions of the thermocouples, which data was used for the analyses. The comparison with the calculation is presented in Fig. 19 and 20.

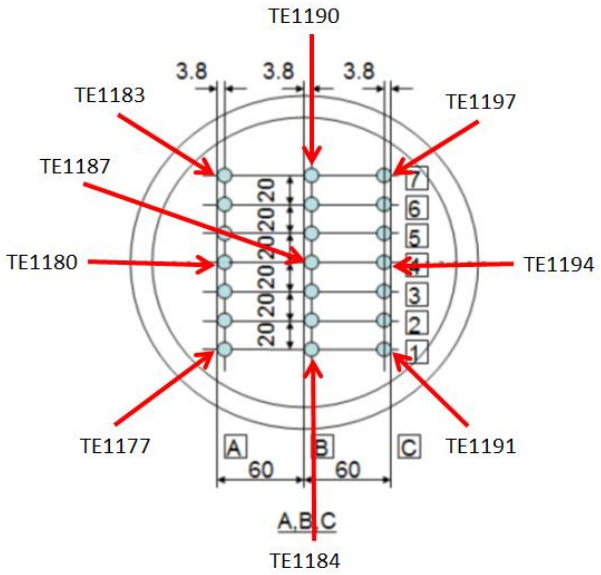

Fig. 17: Thermocouples in rake TE2

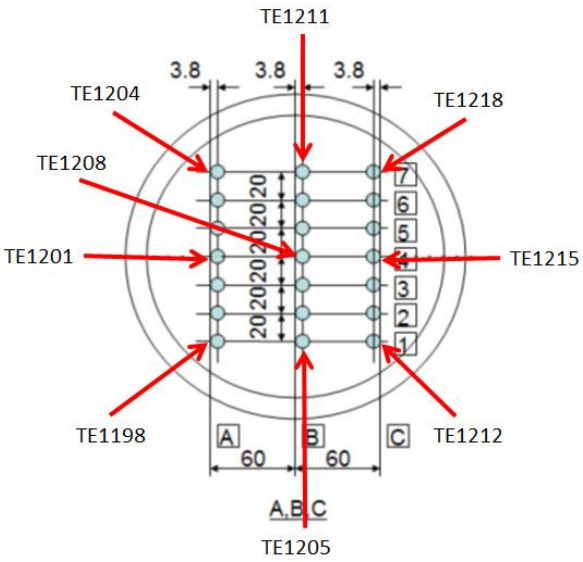

Fig. 18: Thermocouples in rake TE3

Figure 19 shows, that the swashing of the cold water to the left and right pipe walls in the vicinity of TE2, predicted by the ANSYS CFX and ATHLET – ANSYS CFX (Fig. 13 and Fig. 14) can not be seen in the experiment. For TE2, both ATHLET - ANSYS CFX and ANSYS CFX codes over-predict the temperature in the middle of the cold leg over its whole height. Furthermore, large over-estimation of the fluid temperature can be observed also for thermocouple TE1177. Better agreement between experimental and calculated data can be observed for the rake TE3, which is close to the dowcomer (see Fig. 20). The largest deviations from the experiment can be seen for the thermocouple TE1211, which is situated in the top, central part of the pipe.

It is interesting that good agreement between experiment and calculation is found in TE3 measurement rake (downstream), although these results are affected by the temperature distribution in TE2 (upstream), which was not predicted correctly by the CFD code. One should not forget, that both fluids mix and downstream the temperature distribution over the pipe cross-section gets more and more homogeneous (compare the first and the last picture in Fig. 14). Sharp density and temperature gradients are no longer present and the correct prediction of the fluid temperature is probably not that challenging for the RSM turbulence model.

There are several possible reasons for the large deviations in the TE2 measurement rake. The first one is that the experimental flow might be influenced by the relatively large fixtures of the thermocouples (Fig. 11) which have not been modelled with Design Modeller and hence are not present in the current model. Main reason for this is that the significance of their influence on the flow behaviour is questionable [11].

Another reason for the large deviations from experimental data for the measurement rake TE2 could be inadequate turbulence modeling. In these calculations, two-equation turbulence models like SST and even more complex Reynolds Stress models were used. The calculations with the BSL RSM turbulence model provided better agreement (and were thus selected as final ROSA Test 1-1 results). These are considered to be more suitable for the simulation of buoyant flows [12]. Nevertheless, the measurement rake TE2 is very close to the location where the cold ECC water jet impinges on the bottom of cold leg A. In this area, complex mixing phenomena occur which are strongly influenced by the momentum of the impinging jet and the buoyancy effects due to the large density differences between both streams (>200 kg/m^3). This might be too challenging for the two-equation and RSM turbulence models. Further calculations with the same CAD model and more sophisticated turbulence resolving approaches like scale adaptive simulation (SAS) or large eddy simulation (LES) could give an answer to the question if the poor results for TE2 are due to insufficient geometry or turbulence modeling.

The main objective of the presented work was to validate the ATHLET – ANSYS CFX coupling methodology. Generally, even if the agreement of the results with experimental data for rake TE2 can be considered as poor, the agreement between ANSYS CFX stand alone and coupled ATHLET - ANSYS CFX calculations is very good. This proves the consistency of the methodology developed for the coupling of both thermal-hydraulic codes. Larger deviations are observed only for thermocouples TE1183, TE1197 and TE1112. These can be explained with the different boundary conditions used both 3D and 1D-3D calculations. In the ANSYS CFX stand-alone simulations, experimental temperature and mass flow rate values are applied as boundary conditions. In the case of the coupled solution, the boundary conditions for ANSYS CFX are calculated by the system code ATHLET.

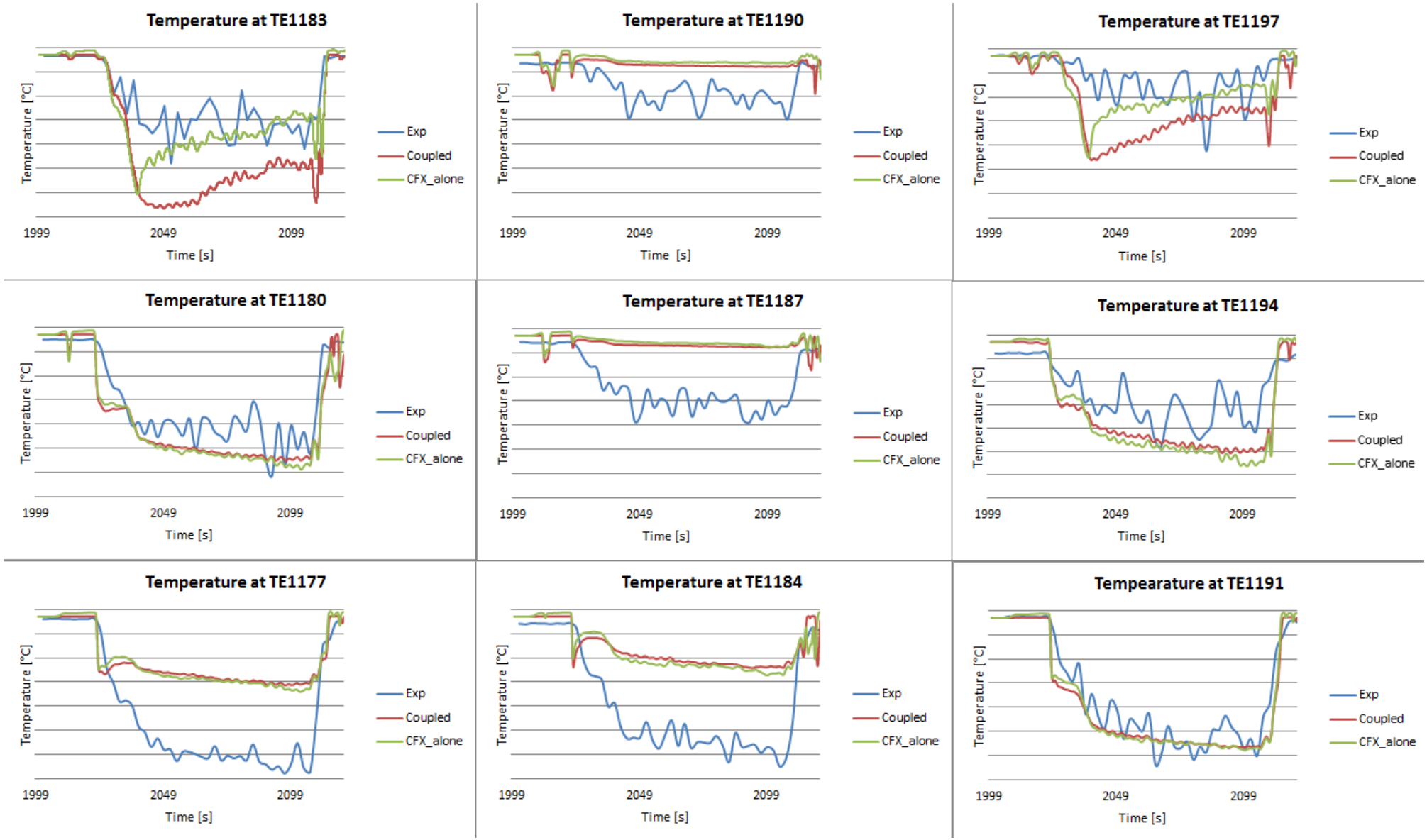

Figure 19: Temperature distribution in rake TE2.

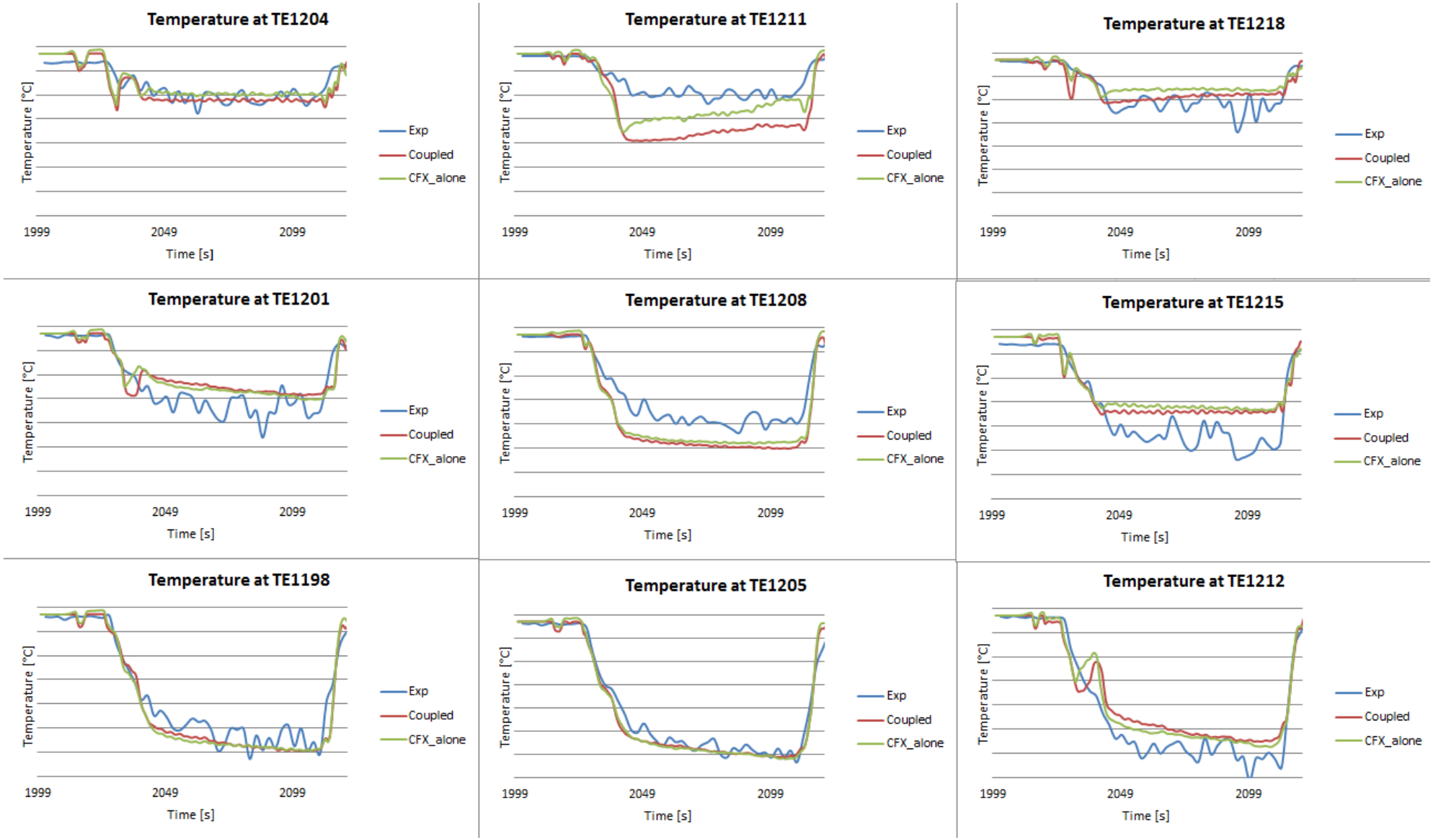

Figure 20: Temperature distribution in rake TE3.

Figure 21 compares ATHLET stand-alone and coupled ATHLET - ANSYS CFX results for the average pipe cross-section temperatures in the ATHLET control volume downstream of the ANSYS CFX domain near the RPV downcomer inlet. The good agreement between ATHLET stand-alone and ATHLET - ANSYS CFX demonstrates that the coupled code system successfully accomplishes the transition from spatially distributed to lumped parameter approximation schemes. The comparison with the measured temperature averaged over 21 thermocouples distributed across the pipe cross section (actually located 0.4 m upstream of the RPV downcomer inlet) shows that the end of the injection phase is predicted slightly better by the coupled codes due to the reduced numerical diffusion in the ANSYS CFX domain of the cold leg A.

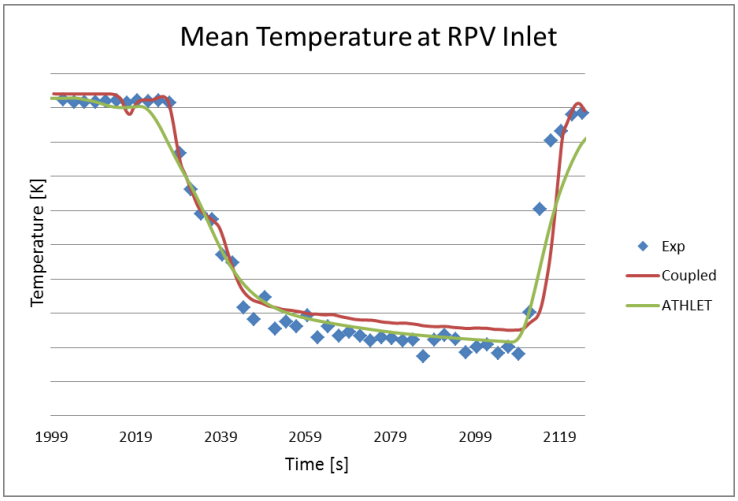

Figure 21: Temperature distribution in rake TE3.

5 Conclusions

System codes like ATHLET are based on one dimensional models and these have only limited capabilities to predict in detail 3D flows and coolant mixing processes being important for certain classes of transients and accidents. In order to overcome these limitations and extend the capabilities of ATHLET, explicit and semi-implicit schemes have been developed and implemented to couple the GRS best estimate code with the commercial CFD tool ANSYS CFX. Within the European project NURISP, development and validation activities for the 1D-3D code ATHLET - ANSYS CFX were performed for the OECD ROSA V Test 1-1 dedicated to the PTS phenomena in PWR. The ROSA V experiment investigates thermal stratification at single-phase natural circulation conditions and cold ECC injection in the cold leg of a PWR. The coupled results were compared with temperature measurements at two rake positions in cold leg A, and with ANSYS CFX stand-alone simulations. The comparison with experimental data showed good agreement in the TE3 and larger deviations in the TE2 measurement rake, which is close to the ECC injection nozzle. Possible reasons for these are insufficient geometry modeling or inadequacy of the turbulence models to simulate complex mixing phenomena which are strongly influenced by the momentum of an impinging jet in combination with buoyancy effects due to large density differences. Nevertheless, a very good agreement between coupled 1D-3D ATHLET – ANSYS CFX and stand-alone ANSYS CFX calculations has been observed, proving the consistency of the coupling methodology.

6 References

[1] A. Papukchiev, G. Lerchl “Development of an Interface with Different Schemes for the Coupling of the 1D System Code ATHLET with the 3D CFD Software Package ANSYS CFX”, GRS NURISP SP3 deliverable GRS_D02, GRS (2010)

[2] A. Papukchiev, G. Lerchl “Assessment of the Performance of the 1D-3D Code System ATHLET – ANSYS CFX with Explicit and Semi-Implicit Coupling Schemes”, GRS NURISP SP3 deliverable GRS_D03, GRS (2010)

[3] Japan Atomic Energy Research Institute (JAERI): ROSA IV, “Large Scale Test Facility (LSTF), System Description”, Tokai Research Establishment, (1985)

[4] T. Yonomoto, “ROSA/LSTF Tests on PWR Natural Circulation and RELAP5 Validation”, Oregon State University, Corvallis, Oregon, (2005)

[5] JAERI, ”Final Data Report of OECD/NEA ROSA Project Test 1-1”, Thermohydraulic Safety Research Group, Nuclear Safety Research Centre, Japan Atomic Energy Agency (2008)

[6] J. Weis “Computational Fluid Dynamics Analysis of a ROSA Cold Leg Stratification Test”, Diploma Thesis, Lehrstuhl für Nukleartechnik, Technische Universität München (2009)

[7] J. Mahaffy, “Best Practice Guidelines for the Use of CFD in Nuclear Reactor Safety Applications”, NES/CSNI/R 5 (2007)

[8] W. Wagner, and A. Kruse, The Industrial Standard IAPWS-IF97: Properties of Water and Steam, Springer-Verlag, Berlin (1998)

[9] F. R. Menter, “Two-Equation Eddy-Viscosity Turbulence Models for Engineering Applications”, AIAA-Journal, Vol. 32, pp. 269 – 289 (1994)

[10] B. E. Launder, G. Reece, W. Rodi, “Progress in the development of a Reynolds stress turbulence closure”, J. Fluid Mech. 68:537-66 (1975)

[11] A. Papukchiev, discussion with ANSYS Germany, ANSYS Germany (2010)

[12] ANSYS CFX 11.0 User’s Manuals, ANSYS Germany (2006)

7 Annexes

7.1 Annex 1: Document approval by beneficiaries' internal QA

#	Name of beneficiary	Approved by	Function	Date
1	GRS	A. Papukchiev	Author	15-10-2011
2	GRS	G. Lerchl	Author	15-10-2011
	GRS	M. Scheuerer	Author	15-10-2011
3	CEA	P. Emonot	WP3.3 coordinator	
4	PSI	M. Zimmermann	SP3 coordinator	

Verteiler

		Exemplare: gedruckt	Exemplare: pdf	CD-ROM
BMWi				
Referat III B 4		1 x		
GRS-PT/B				
Internationale Verteilung	(FIZ)	10 x		30 x
Projektbegleiter	(wei)	2 x	1 x	1 x
GRS				
Geschäftsführung	(wep, stj)		je 1 x	
Bereichsleiter	(erv, paa, prg, rot, stc, ver, zir)		je 1 x	
Abteilungsleiter	(luw, poi, som, vek)		je 1 x	
Projektleitung	(bam)	1 x		
Projektbetreuung	(wal, bna)		je 1 x	
Informationsverarbeitung	(nit)		1 x	
Bibliothek	(Köln)	1 x		
Autor(en)	(bam)	2 x	je 1 x	
Gesamtauflage	**Exemplare**	**17**		**31**

Gesellschaft für Anlagen- und Reaktorsicherheit (GRS) mbH

Schwertnergasse 1
50667 Köln
Telefon +49 221 2068-0
Telefax +49 221 2068-888

Forschungszentrum
85748 Garching b. München
Telefon +49 89 32004-0
Telefax +49 89 32004-300

Kurfürstendamm 200
10719 Berlin
Telefon +49 30 88589-0
Telefax +49 30 88589-111

Theodor-Heuss-Straße 4
38122 Braunschweig
Telefon +49 531 8012-0
Telefax +49 531 8012-200

www.grs.de